DLC1 AS A COMPARATIVE EPIGENETIC BIOMARKER FOR RADIOTHERAPY OF NON-HODGKIN'S LYMPHOMA

A Dissertation presented to the Faculty of the Graduate School
University of Missouri-Columbia

In Partial Fulfillment
Of the Requirements for the Degree

Doctor of Philosophy

---

by

JEFFREY N. BRYAN

Dr. Michael R. Lewis, Dissertation Supervisor

AUGUST 2007

The undersigned, appointed by the dean of the Graduate School, have examined the dissertation entitled

DLC1 AS A COMPARATIVE EPIGENETIC BIOMARKER FOR RADIOTHERAPY OF NON-HODGKIN'S LYMPHOMA

presented by Jeffrey N. Bryan,

a candidate for the degree of doctor of philosophy,

and hereby certify that, in their opinion, it is worthy of acceptance.

Professor Michael R. Lewis

Professor Charles W. Caldwell

Professor Carolyn J. Henry

Professor Wynn A. Volkert

Professor Jeff W. Tyler

DEDICATION

I wish to express my gratitude to four groups of individuals who have given me the assistance, insight, inspiration, and energy necessary to complete this dissertation. I want to first thank my mentors, Dr. Mike Lewis, Dr. Bill Caldwell, and Dr. Carolyn Henry. The productivity of the research relationship between Mike Lewis and me has been tremendous. He taught me the bench skills, mentored me as new faculty, honed my writing skills, and encouraged my vision and focus in research. On top of that, he has been a fantastic, and life-long, friend to me. I look forward to many years of fruitful collaborations. Bill Caldwell generously took me under his wing and helped turn a veterinary oncologist into an informatician and molecular biology researcher. He has been encouraging, supportive, and an excellent mentor. I look forward to many future collaborative discoveries with him and his group as well. Carolyn Henry inspired me to pursue a PhD, and encouraged me along the way. She has been a fantastic mentor in oncology, on faculty, and in career development. She is also a fantastic, life-long friend. Our bond of Liberian children will give us many years of laughter ahead. Our many projects yet to be completed will ensure regular communication. I look forward to continuing the great work in veterinary oncology she began in the Pacific Northwest so many years ago. I also want to thank my committee members Jeff Tyler and Wynn Volkert for their guidance and support. The two of you have been a tremendous help to me throughout my career here at MU.

The second group I must thank are my lab partners and collaborators. Fang Jia has been helping and mentoring me from the beginning. Her skill,

knowledge, and sense of humor have always made my time in the Lewis lab fun and productive. I appreciate all of the help she has given me over these past five years. Kristen Taylor has been an amazing help and mentor in genetics and bench techniques. I truly could not have made the progress that I have without her guidance and assistance. Her friendship and sense of humor has made challenging days in the lab much easier to bear. I appreciate all she has given me. Farah Rahmatpanah has provided invaluable guidance, assistance, and camaraderie. Her technical abilities and knowledge of epigenetics are truly outstanding, and she made a tremendous effort to share those things with me. Jenny Guo has assisted me with techniques and provided materials, for which I am very grateful. It has been fun sharing stories about our training and our experiences. I am grateful for her help. Both the Lewis and the Caldwell lab groups are truly unique collections of individuals doing tremendous work with a great camaraderie. I will take the lessons learned from them forward in my career.

I dedicate the new knowledge that has come from this work to my patients. To Buddy, Pooh, Mr. Kitty, Lucky, Wolf, Izzie, Isis, Godzilla, and all the others who have been such brave patients in the face of such terrible disease, I pledge to continue to work to ease the comfort, extend the quality of life, and seek a cure for the affliction that is cancer.

I dedicate the hours that have gone into this work to my family. To my beautiful, brilliant wife Peggy and my wonderful children Christina, Claire, Darius, Ruth, and Bobby, I extend my love and gratitude. All of you have supported me

with humor and patience while we lived the life of grad students for a while longer. I learn from each of you every day what it is that is important in life. I love you all completely, and love the laughter, chaos, and excitement with which you fill our house and lives. Now that the training is over, I look forward to starting a new adventure with all of you in Pullman. Whatever the future holds, we all get to face it together, which always gives me great hope of good things. Kids, never forget that education is vitally important and must continue your whole life.

.

ACKNOWLEDGEMENTS

This research was funded in part by the University of Missouri College of Veterinary Medicine, Department of Veterinary Medicine and Surgery Committee on Research. I am grateful to the National Library of Medicine Biomedical Informatics Research Training grant LM07089 for financial and resource support. This work was also supported by NIH Grants CA103130 and CA10005. Production of ^{177}Lu was performed at the University of Missouri Research Reactor. I want to thank West Flamingo Animal Hospital and Dr. Kim Selting for canine lymphoma samples for the first investigation.

TABLE OF CONTENTS

LIST OF ILLUSTRATIONS

LIST OF TABLES

Table Page

LIST OF ABBREVIATIONS

5-Aza	5-azacytidine
5'RACE	Five prime rapid amplification of cDNA ends
^{90}Y	Yttrium-90
^{111}In	Indium-111
^{176}Lu	Lutetium-176
^{177}Lu	Lutetium-177
^{177m}Lu	Metastable Lutetium-177m
ALL	Acute lymphoblastic leukemia
bp	Base pair
Bq	Becquerel
CD3	Cluster of differentiation 3
CD4	Cluster of differentiation 4
CD19	Cluster of differentiation 19
CD21	Cluster of differentiation 21
CD79a	Cluster of differentiation 79a
CLL	Chronic lymphocytic leukemia
COBRA	Combined bisulfite restriction analysis
CpG	Cytosine followed by guanosine

DAPK1	Death associated protein kinase
DLBCL	Diffuse large B-cell lymphoma
DLC1	Deleted in liver cancer
DMH	Differential methylation hybridization
DNA	Deoxyribonucleic Acid
DNMT	DNA methyl transferase
DOTA	1,4,7,10-tetraazacyclododecane-*N*,*N'*,*N''*,*N'''*-tetraacetic acid
DOTA-TATE	DOTA-Tyr^3-octreotate
DTPA	Dimethyl-triamine-phosphoric acid
EC	Electron capture
EGCG	Epigallocatechin gallate
FAK	Focal adhesion kinase
FDA	Food and Drug Administration
FL	Follicular lymphoma
GAPDH	glyceraldehyde-3-phosphate dehydrogenase
GDP	Guanosine diphosphate
GTP	Guanosine triphosphate
Gy	Gray, a unit of absorbed radiation dose
HCC	Hepatocellular carcinoma
HDAC	Histone deacetylase inhibitor
hTERT	Telomerase reverse transcriptase
IGF1	Insulin-like growth factor 1
IGF2	Insulin-like growth factor 2

IL-6	Interleukin 6
JAG2	jagged 2
keV	Kiloelectron volts
LHX2	Lim homeobox 2
Le^y	The ceramide variant of the internalizing $Lewis^y$ antigen
mAb	Monoclonal antibody
mb	millibarns
MBq	Megabecquerels
µCi	Microcurie
µM	Micromolar
mCi	Millicurie
MCL	Mantle cell lymphoma
MeV	Megaelectron volts
mRNA	Messenger RNA
MSP	Methylation specific PCR
MZL	Marginal zone lymphoma
NCBI	National Center for Biotechnology Information
NHL	Non-Hodgkin's lymphoma
NOTCH	Notch homolog 1
NSCLC	Non-small cell lung cancer
PCR	Polymerase chain reaction
PET	Positron emission tomography
PLCδ	Protein lipase c delta

POU3F3	POU domain, class 3, transcription factor 2
PRKCE	Protein kinase C epsilon
QMSP	Quantitative MSP
Ras-MAPK	RAs mitogen-activated pathway kinase
RASSF1A	Ras association domain family 1
RIT	Radioimmunotherapy
RLGS	Restriction landmark genomic scanning
RNA	Ribonucleic acid
ROI	Region of interest
RP_HPLC	Size-exclusion high performance liquid chromatography
Sp1	Sp1 transcription factor
SAM2	Sterile α motif
SH2	Src homology 2 domain
SOS	Son of sevenless
SPECT	Single photon emission computed tomography
SRE	Serum response element
START	Steroidogenic acute regulatory-related lipid transfer
TIMP2	Tissue inhibitor of metalloproteinase pathway 2
TSP2	Thrombospondin 2
UCSC	University of California at Santa Cruz
V-D-J	Variable, diversity, joining
VEGF	Vascular endothelial growth factor
ZAP70	zeta-chain (TCR) associated protein kinase 70kDa

ABSTRACT

The American Cancer Society estimates that 58,870 people were diagnosed with non-Hodgkin's lymphoma (NHL) in 2006, and 18,840 people died of the disease. Recent advances in chemotherapy, monoclonal antibody (mAb) therapy, and radioimmunotherapy (RIT) have improved the manageability, but not the curability of indolent forms of NHL in humans. In the search for understanding of the root mechanisms of this disease, covalent DNA modification patterns have been identified that result in epigenetic gene silencing, yet leave the sequence of the genetic code intact. Termed DNA methylation, the addition of a methyl group to cytosine bases in cytosine followed by guanine dinucleotides persists from generation to generation of cells, often silencing the expression of the gene. However, this addition is also chemically reversible, allowing the silenced gene to be re-expressed. Such hypermethylated genes may serve as markers of disease, markers of prognostic groups, or targets for therapy. The causes of the observed patterns of methylation are not yet clear, and models are necessary for preclinical evaluation of diagnostic and therapeutic strategies. In this series of experiments, evidence of DNA hypermethylation was identified in the gene *Deleted in Liver Cancer 1* (*DLC1*), a tumor suppressor gene, in canine NHL as it is in humans. The structure of the canine form of this gene was further characterized *in silico* and biologically, and the methylation patterns surrounding its promoter region were defined in 21 cases of naturally occurring NHL. The comparative evaluation of the human and canine promoter regions revealed

similarity between Sp1 transcription factor binding sites that are known to be modulated by hypermethylation. Although the presence of hypermethylation did not result in silencing of the gene in the majority of the dogs, methylation patterns were statistically associated with NHL compared to normal lymphoid tissue. Further experiments discovered a significant synergistic interaction between external irradiation or ^{177}Lu-labeled 1,4,7,10-tetraazacyclododecane-*N*,*N'*,*N''*,*N'''*-tetraacetic acid (DOTA)-tyrosine^{3}-octreotate (TATE) treatment and zebularine, a demethylating agent. Finally, ^{111}In-DOTA-TATE was successfully used to image somatostatin receptors of NHL lesions in three dogs with naturally occurring disease. The comparative evaluation of the *DLC1* gene identified important similarities in methylation boundaries between humans and dogs. The presence of hypermethylation and somatostatin receptors in canine NHL, both characteristics of human NHL, suggest that dogs may serve as a pre-clinical model for evaluation of epigenetic modification therapy and targeted imaging and radiotherapy designed for eventual human use. The results of these studies will form the underpinnings of future canine clinical trials, modeling markers for diagnosis, prognosis, and therapy of NHL.

Chapter 1

Introduction and literature review

This project was aimed at developing the comparative examination of canine and human non-Hodgkin's lymphoma (NHL). It began with the examination and characterization of the DNA methylation patterns of a previously unexamined canine tumor suppressor gene orthologous to a gene silenced in human NHL. It then moved into *in vitro* studies of the effect of modulating DNA methylation on response to radiation delivered by external source and radiopharmaceutical preparation. It finished with a translational study of a radiopharmaceutical imaging agent that may be a precursor platform to future imaging and therapy. To set a foundation for the experiments that follow, this introduction will describe the mechanisms of epigenetic modification, some of the known effects of those changes, the drugs that may modify DNA methylation, the comparative examination of canine and human NHL, and targeted imaging and radiotherapy of NHL. Although broad in scope, this project was intended to carry a future therapy concept from computer to lab bench to clinic, underpinning future investigations for translational therapy.

In 1948, a DNA chromatogram, run by Rollin Hotchkiss, revealed the presence of a fifth base in the mix.[1] Subsequently identified as 5-methylcytosine, a modification of the standard base, its role in eukaryotic cells was largely unexplored for decades. In 1993, the contribution of DNA methylation to the neoplastic phenotype was postulated.[2] Subsequent research is identifying the mechanisms of Dr. Hotchkiss' contribution at an increasing rate. Epigenetic changes are covalent modifications of DNA bases, particularly cytosine, or histones that alter the tertiary structure of chromatin, the binding of transcription

factors, and, ultimately, the expression patterns of genes within a cell. In human cell lines and primary tumors, abnormal DNA methylation has now been demonstrated to contribute to cancer of the breast, colon, stomach, kidney, prostate, skin, hemolymphatic organs, and other tissues.[3-9] The presence of aberrant methylation patterns in neoplastic tissues offers the promise of novel markers for diagnosis and prognosis, as well as untapped therapeutic targets.

Methylcytosine serves multiple important functions in the normal cell. These include transcriptional silencing of transposons, the imprinted silencing of genes on the X chromosome of females and other somatic genes in the genome, and the identification of self versus invading DNA from pathogens.[10;11] Most commonly, cytosine in a C followed by G (CpG) dinucleotide is methylated by enzymes called DNA methyltransferases (DNMT) (Figure 1.1). These enzymes are responsible for either maintenance (DNMT1) or *de novo* methylation (DNMT3a, DNMT3b), using S-adenosyl methionine as the methyl donor. Maintenance methylation, occurring shortly after DNA replication, serves the purpose of conserving patterns of methylation that silence transposons and maintain monoallellic expression of genes imprinted during development.[10]

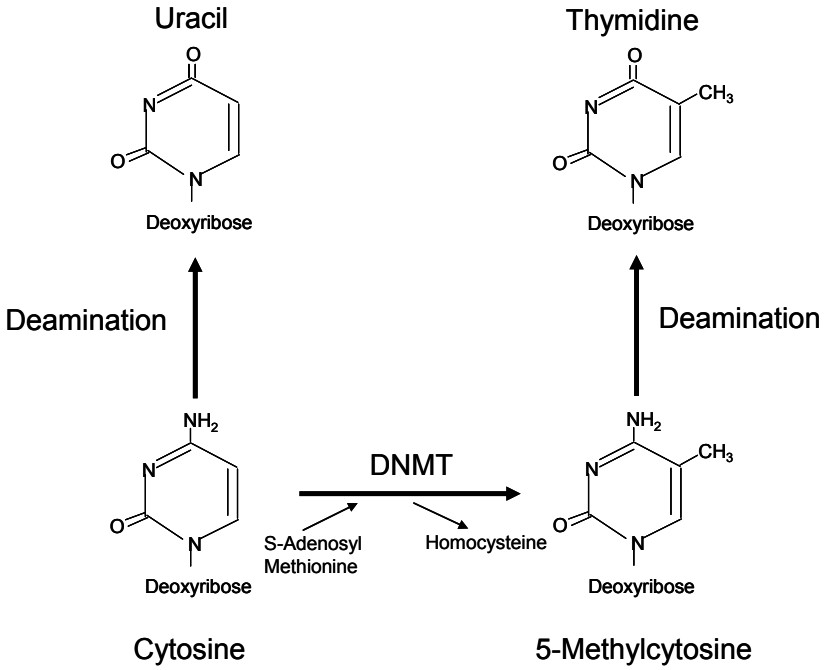

Figure 1.1: Cytosine becomes 5-methylcytosine by an electrophilic methyl substitution at the 5 position catalyzed by DNA methyltransferases. A deamination event results in transformation of cytosine to uracil and methylcytosine to thymidine as illustrated.

De novo methylation allows the dynamic modulation of gene expression through novel methylation of CpG dinucleotides in the promoter and first exon regions of genes, events critical to normal embryogenesis and *in utero* development.[12;13] These methylation events are mitotically heritable for generations.[14] Across the genome, CpG dinucleotides are statistically relatively scarce. This is likely because methylcytosine that undergoes spontaneous deamination becomes thymidine, and the change is inefficiently corrected. As a result, most genomic CpG dinucleotides are low density and are methylated.[10] Regions with higher density of CpG dinucleotides are referred to as CpG islands. These are functional units defined by a mathematical construct rather than well-defined physical boundaries. CpG islands are regions of DNA spanning at least 500

bases with a G + C content > 55% and an observed/expected ratio of CpG > 0.6.[15] In most cases, CpG islands are associated with the promoter and first exon regions of genes, and are largely unmethylated.[10;15] When these regions are predominantly methylated, as in imprinted genes or parasitic DNA sequences, histone modifications occur, chromatin compaction occurs, transcription factors no longer bind, and transcription is silenced (Figure 1. 2).[12]

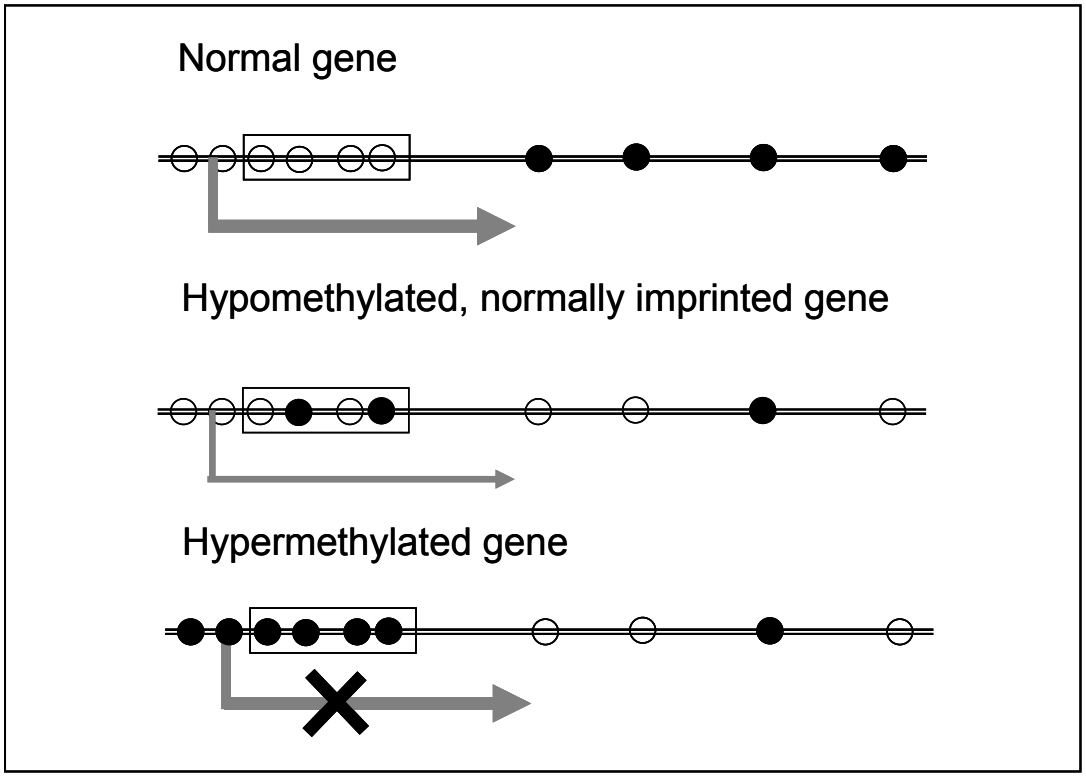

Figure 1.2: Cytosine methylation patterns of DNA in normal cells, cells expressing normally imprinted alleles due to hypomethylation, and cells with silencing of tumor suppressor genes due to hypermethylation. Circles represent CpG dinucleotides along the DNA (double lines) with black representing the methylated condition and white the unmethylated condition. Boxes represent the promoter/first exon regions of the gene. The region containing more densely spaced CpG dinucleotides represents a CpG island. The grey arrows represent the activity of transcription.

Often this change is associated with modifications of histone tails as well. The order of events in silencing has not been entirely elucidated. Open,

transcriptional chromatin typically contains histone H3 with acetylated tails, phosphorylation of Serine 10, and a methyl group added to lysine-4, as well as acetylation of lysine 8 of histone H4.[12] Condensed, transcriptionally silenced chromatin, however, generally lacks acetylation and methylation of lysine-4 on histone H3, and demonstrates methylation of histone H3 lysine-9. It appears that the presence of DNA hypermethylation can attract methylcytosine binding proteins, which recruit histone deacetylases (HDAC) and histone methyltransferases.[12] Recent research has demonstrated that histone modification events may occur in the absence of promoter methylation as well.[3;16] These modifications of histone tails have been dubbed the "histone code."[17]

In human cancers, results of recent studies have begun to elucidate the contribution of DNA methylation to the neoplastic phenotype. Early studies identified a global loss of methylation in cancer cells. This was shown to lead to hypomethylation of *Ras* oncogenes, among others, that could result in overexpression of growth factors participating in neoplastic transformation.[18] Global genomic hypomethylation appears to contribute to genomic instability and the acceleration of the accumulation of genetic abnormalities that characterize cancer cells.[12] Concurrently, cancer cells exhibit hypermethylation of CpG islands in promoter regions, leading to the silencing of tumor suppressor genes.[12] The DNA methylation changes typical of cancer cells are illustrated in Figure 1. Methylation is a post-replicative event. As such, the standard polymerase chain reaction (PCR) adds cytosine, not methylcytosine to the growing DNA strand. To preserve information about methylcytosine bases, several techniques have been

employed. Large-scale information about methylation of CpG dinucleotides can be determined by the use of methylation-sensitive restriction enzyme digestion with a restriction landmark genomic scanning technique (RLGS).[19;20] In this procedure, genomic DNA is digested, and methylated targets will not be cut. Analysis of the fragments generates a pattern which reveals the overall degree of methylation present at restriction sites in the sample.

Bisulfite conversion: To understand the precise pattern of cytosine methylation, DNA may be treated with bisulfite to convert unmethylated cytosine to uracil. This, in turn, becomes thymidine in subsequent PCR amplification of the bisulfite converted DNA. When compared to the original sequence, the presence of a thymidine, instead of a cytosine, prior to a guanosine indicates the presence of unmethylated cytosine in the original DNA strand. Preservation of a cytosine is evidence that methylcytosine was present originally.

Combined bisulfite restriction analysis (COBRA): This assay uses bisulfite converted DNA as the template for PCR. A specific region of a gene, usually in the promoter region, is amplified with primers designed to avoid CpG dinucleotides. Thus, the DNA will be amplified whether the CpG island is hypermethylated or not. Between these primers will have been identified restriction enzyme sites that contain CpG dinucleotides. When treated with methylation sensitive enzymes such as Hpy99I, HpyCH4IV, TaqaI, and BstUI, sequences that originally contained methylcytosine will be cut, whereas those with unmethylated cytosine will have been converted to thymidine and not be recognized (See Figure 1.3). Some idea of the density of methylation can be

gleaned by including multiple cut-sites within the sequence to be studied. Greater numbers of fragments positively correlate with a greater degree of methylation.[21]

Methylation Specific PCR (MSP): Using bisulfite converted DNA, PCR is performed with primers designed to include at least two CpG dinucleotides in each forward and reverse primer. Two sets of primers are designed: One, for methylated sequences, that retains the CpG complementarity; a second, for unmethylated sequences, that is complementary to a TpG sequence. The presence of a band using the methylated primers is evidence for methylation in the original sequence(Figure 1.3).[22] This technique is sensitive, but does not convey information about the density of methylation.

Quantitative MSP (Q-MSP): Similar to MSP, this is performed using a real-time PCR machine. Using the TaqMan technology, a probe containing a fluorophore is designed complementary to the PCR amplicon. The relative intensity of fluorescence between the methylated and unmethylated primers allows quantification of the degree of methylation in the sample.[22]

Differential Methylation Hybridization Microarray (DMH): Genomic DNA from a tumor is digested using restriction enzymes to 200 base fragments, leaving CpG islands relatively intact. Methylation-sensitive restriction enzymes are then used to digest the fragments that are CpG rich. Cut sites that are methylated are ignored by the restriction enzyme, leaving those sequences intact. The resulting fragments, both methylated and unmethylated are tagged with a fluorophore different from that used to tag normal genomic DNA from a

similar tissue. The two tagged samples are co-hybridized on a microarray chip containing sequences from regions of interest that span the cut sites of the restriction enzyme used. Those experimental sequences that remain intact will hybridize to the chip, and those that have been cut will not. The resulting fluorophore intensity correlates to the degree of methylation in the tumor sample relative to the normal tissue. This is a discovery tool for candidate methylated sequences. Validation is required by other described techniques. No canine chip exists.[23]

Bisulfite sequencing by cloning: Fragments of bisulfite treated DNA amplified for COBRA or MSP analysis are cloned by phage into bacteria. The resulting colonies are harvested and submitted for sequencing with universal primers. The resulting sequence is compared to the original sequence to determine the degree of methylation in that region of the gene.

High-throughput bisulfite sequencing: Current research is utilizing high-throughput sequencing methods to bisulfite sequence PCR product to evaluate the methylome. A limitation of this technique is the conversion of much of the genome to a nearly three base, rather than a four base, system. This can make alignment with the complete sequenced genome a bioinformatics challenge, as statistical uniqueness declines significantly.

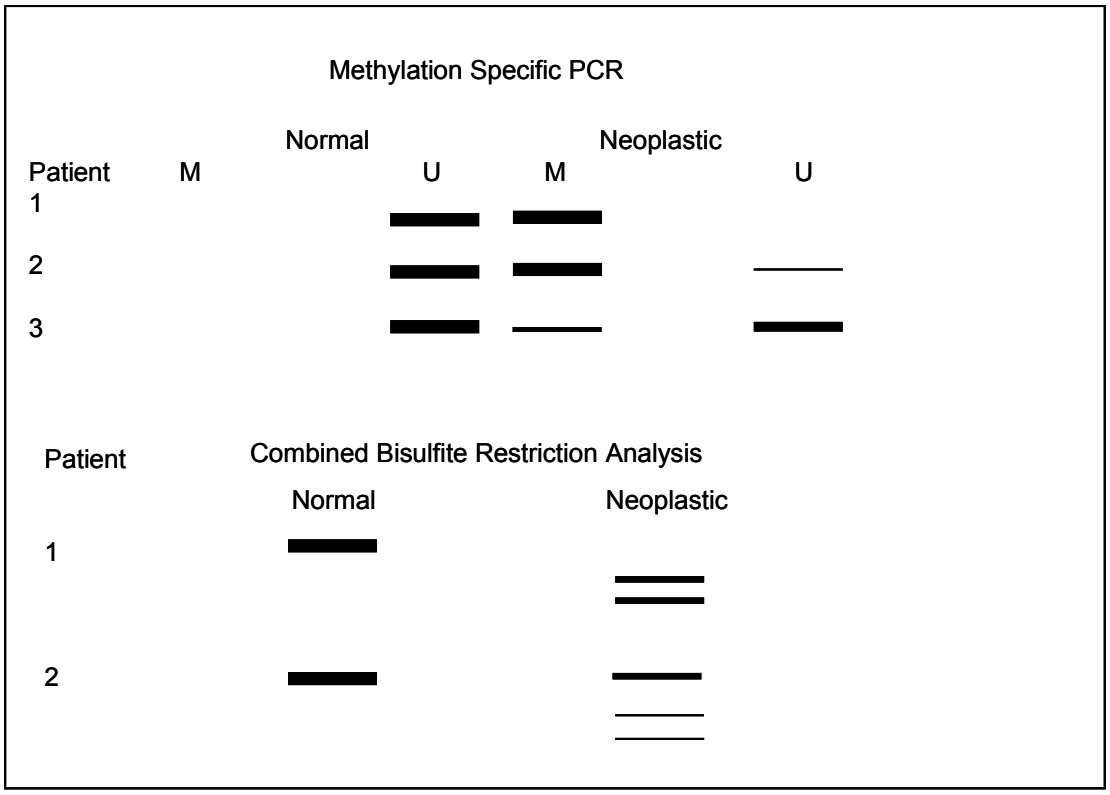

Figure 3: The top panel represents the gel results for MSP. Unless imprinted, normal tissue will rarely yield a methylated band (column M) and will display an unmethylated band (column U). Neoplastic cells that contain a hypermethylated gene of interest will yield a methylated band, and possibly unmethylated bands of varying size as well. The combination may be due to heterogeneity of the tumor, heterozygosity within tumor cells, or a mixed tumor/normal cell population. This can occur with COBRA as well (lower panel). Normal samples will not demonstrate digestion with the restriction enzyme, whereas the hypermethylated gene will be digested, resulting in two smaller bands. An unmethylated band may be seen for the aforementioned reasons.

Loss of imprinting or normal methylation of a gene promoter can lead to overexpression of that gene's product, contributing to the neoplastic phenotype. An example of this is the overexpression of the NOTCH ligand, JAG2, in malignant human plasma cells. Houde and others demonstrated that hypomethylation of the promoter region of this gene in malignant cells, compared to normal cells, resulted in higher levels of expression of the JAG2 protein.[24] This induced the secretion of interleukin-6 (IL-6), vascular endothelial growth

factor (VEGF), and insulin-like growth factor-1 (IGF-1). Secretion of IL-6 could be blocked by inhibition of the NOTCH pathway, confirming the mechanism.[24] It is likely that such alterations exist in many other human and canine cancers. As a potential diagnostic screening test, the loss of imprinting of the *IGF2* gene was examined in colon cancer. [9] The investigators identified an odds ratio for loss of imprinting in peripheral blood lymphocytes of 21.7 for patients with colorectal carcinoma. Such screening techniques could lead to much less invasive, and potentially more cancer-specific, tests for markers of risk for disease, of early disease, or the presence of residual disease.

Promoter hypermethylation has been demonstrated to silence many tumor suppressor genes in human cancers and cancer cell lines.[12] The gene *RASSF1A* is frequently silenced in head and neck carcinoma.[25] In one study the silencing of the gene was inversely associated with the presence of human papillomavirus infection, a common predisposing infection for these carcinomas.[25] Such differentiation among etiologies could inform therapeutic decisions for clinical patients. *In vitro* studies have demonstrated that the gene could be demethylated and re-expressed by treatment with 5-aza-2'-deoxycytidine, making methylated *RASSF1A* a potential therapy target.[25] The presence of methylated *RASSF1A* has also been evaluated as a diagnostic test in urine samples of humans with urinary transitional cell carcinoma.[26] The test was more sensitive than cytology for detecting low-grade and early cases. This demonstrates the potential utility of DNA methylation as a method of specific

primary diagnostic screening. This would also yield a marker to be followed throughout therapy to determine efficacy and detect early relapse.

Occasionally, aberrant promoter methylation may result in a beneficial change for cells. The gene coding O^6-methylguanine-DNA methyltransferase (*MGMT*) is an important DNA repair enzyme that can lead to chemotherapy resistance by removing potentially lethal DNA adducts that form after chemotherapy exposure. In human diffuse large B-cell lymphomas (DLBCL) lack of expression of *MGMT* due to DNA methylation has been shown to be positively prognostic for chemotherapy response and outcome.[27] The same has been shown to be true in glioblastoma, in which methylated *MGMT* can be used to predict a positive response to temozolamide chemotherapy.[28;29] Discovery of more such markers in cancer would help categorize patients into useful therapeutic subgroups.

Genomic hypomethylation has been identified in canine lymphoproliferative disease.[30] Using RLGS, investigators demonstrated differences in methylation between normal and neoplastic lymphoid tissue.[30] Further, they demonstrated that the normal pattern of methylation was preserved in peripheral lymphocytes of dogs with lymphoma.[30] This was the first paper to demonstrate the similarity of methylation change between human and canine neoplastic disease. This underscores the potential for companion animal cancer to be instrumental as a clinical model for diagnosis and therapy of similar diseases in humans. Recently, promoter hypermethylation was reported by Chuammitri and others in abstract form at the Genes, Dogs, and Cancer: Fourth

Annual Canine Cancer Conference, 2006-Chicago, IL. This group identified promoter hypermethylation in the E-cadherin gene in canine mammary tumors, and in the *TIMP3* and *DAPK1* genes in a small number of canine lymphomas. No methylation was demonstrated in the *RASSF1A* gene in canine lymphomas. To date, no peer-reviewed literature exists that documents the presence of promoter hypermethylation in dogs.

Numerous inhibitors of DNA methylation have been examined, both *in vitro* and *in vivo*. Cytidine analogs that inhibit DNMT are diagrammed in Figure 4. The drug 5-azacytidine (5-Aza) is a false base that is incorporated into DNA during replication. When encountered in the DNA sequence, it binds covalently with DNMT enzymes, but electrophilic substitution at the 5 position cannot proceed.[31;32] This causes the enzyme to be degraded.[33] 5-aza, having a component ribose group, is not specific for DNA and is incorporated into RNA in the cell, potentially decreasing its specificity and potency as a DNMT inhibitor.[33] This drug has been approved by the FDA for use in the treatment of myelodysplastic syndrome of humans.[34] A deoxy analog of this drug, 5-aza-2'-deoxycitabine (decitabine) contains a deoxyribose sugar base. This makes the compound specific to DNA incorporation. Its mechanism of action is similar to 5-aza after incorporation into DNA. This compound has also shown promise in clinical trials of myeloid leukemias.[32] The compound zebularine functions similarly to the azacytidine compounds, lacking an amine group at the 4 position which prevents electrophilic substitution at the 5 position. Zebularine has shown significant demethylating activity *in vitro*, but has not been pursued clinically.[32]

Drugs commonly used in both human and veterinary cardiology, procainamide and hydralazine, also have DNMT inhibiting effects, although the mechanism is not clearly defined.[32] Green tea extract, which contains several polyphenol compounds, particularly epigallocatechin-3-gallate (EGCG), is being evaluated in clinical trials after demonstrating potential therapeutic benefit in humans with chronic lymphocytic leukemia.[35] A small molecule inhibitor of DNMT, RG108, has recently been developed through rational drug design.[36] This molecule blocks the active site of DNMT1, preventing maintenance methylation of DNA.[36] The clinical use of these drugs has not, yet, been reported in dogs.

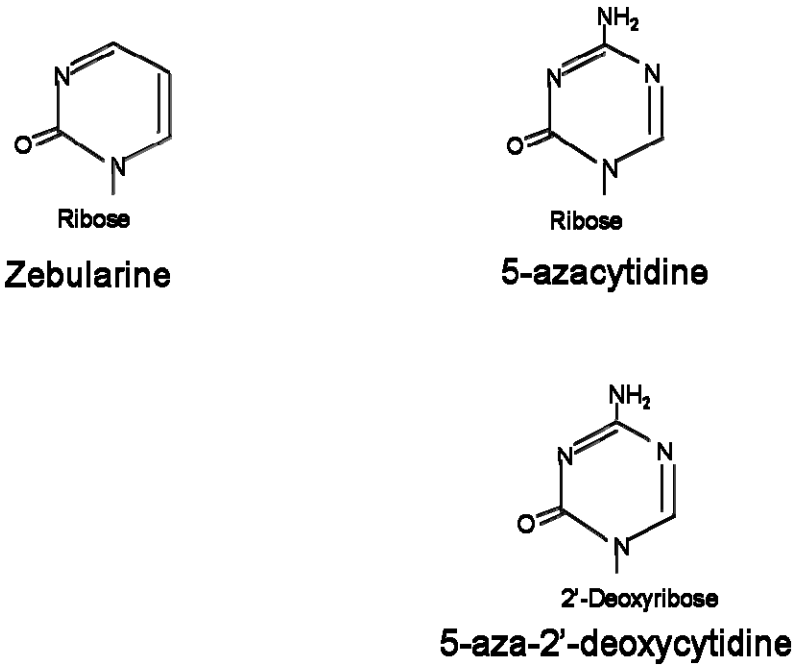

Figure 1.4: Cytidine analogs that inhibit DNMT. Loss of the amine group, for zebularine, and substitution of a nitrogen for carbon in the others result in an inability to receive the methylat substitution at the 5 position.

Deletion of chromosome region 8p21.3-22 was observed to be causally related to the formation of hepatocellular carcinoma (HCC) in humans.[37] Examination of this region for potential tumor suppressor genes revealed the presence of a gene orthologous to the rat gene *p122-RhoGAP*.[37] It has been demonstrated that this is the functional tumor suppressor gene in this chromosomal region, and was named Deleted in Liver Cancer (*DLC1*).[37] Subsequent to this discovery, investigators identified cases of HCC in which the deletion was not present, but *DLC1* was not expressed.[37;38] These cases had hypermethylated promoter regions that appeared to silence the expression of the gene.[37] Subsequently, cell lines and primary tumors of non-small cell lung (NSCLC), neuroectodermal, breast, colon, prostate, gastric, renal, uterine, esophageal, naspharyngeal, and rectal cancers, as well as NHL have shown decreased or absent *DLC1* mRNA when the gene promoter region was hypermethylated.[12;38-44] Re-expression of the *DLC1* gene by treatment with a demethylating agent, alone or in combination with an HDAC inhibitor, has been demonstrated in HCC, breast cancer, and NSCLC, as well as NHL cell lines.[39;45;46] Expression of *DLC1* has also been upregulated in breast cancer cell lines by treatment with flavone.[47]

The *DLC1* gene possesses tumor suppressor gene function.[37] The coded protein is a Rho-GTPase Activating Protein (RhoGAP) that counteracts the feed forward signaling of RhoA and Cdc42 among other Ras signaling proteins.[38] The RhoGAP protein causes catalysis of GTP to GDP when bound to the Rho proteins, causing them to become inactive.[38] Loss of this function results in

unconstrained growth signaling from the surface of the cell to the nucleus, changes in cell mobility, and signaling between the cell and its extracellular environment.[37;38;48] Transfection of *DLC1 in vitro* caused decreased proliferation and colony forming potential of NSCLC cells and breast carcinoma cells.[39;46] Stable transfection of *DLC1* in a mouse model of metastatic NSCLC halted tumorigenicity of the cell line and resulted in decreased invasiveness of the cells into normal tissue.[39] Expression microarray analysis of the transfected cells revealed transcriptional upregulation of thrombospondin 2 (*TSP2*), a tumor growth inhibitor, acting principally through counteracting angiogenesis.[46] The rat orthologue, *p122-RhoGAP*, has been shown to interact directly with phospholipase Cδ (PLCδ).[49] This interaction mediates the stimulation of PLCδ resulting in cytoskeleton rearrangement through the actin binding proteins gelsolin and profilin.[49] The human DLC1 protein contains three recognized functional domains: a sterile α motif (SAM), a steroidogenic acute regulatory-related lipid transfer (START) domain, and a RhoGAP domain.[50] The START and RhoGAP domains have been shown to be necessary for the tumor-suppressor function of the protein.[51] At points of focal cellular adhesion, the tumor suppressor gene product, and tensin family member, cten interacts with DLC1 through a Src homology 2 (SH2) region present on each protein.[50] This interaction was confirmed by mutation of the SH2 regions of both *DLC1* and *cten*, resulting in a loss of both interaction and localization at the plasma membrane. DLC1 also interacts with tensin2 in caveolae, contributing to the organization of the local actin cytoskeleton and inhibition of the formation of stress fibers.[52] The

interacting DLC1 and tensin2 suppress activity of the serum response element (SRE), a Ras cytoskeleton effector.[52] Also at focal adhesion sites, DLC1 induces the dephosphorylation of focal adhesion kinase (FAK), resulting in interaction with Grb2 and recruitment of son of sevenless (SOS), activating the Ras-MAPK pathway.[45] Loss of such function could confer significant growth advantages to preneoplastic or neoplastic cells, contributing to the initiation, promotion, or progression of cancer, as well as metastasis. Indeed, *DLC1* silencing has been demonstrated to be a significant contributor to many human cancers as described above. However, this gene and its protein have not yet been characterized in the dog.

The presence of a hypermethylated promoter region of the *DLC1* gene has been demonstrated in humans with NHL.[53] Shi and colleagues examined NHL cell lines and patient samples for hypermethylation of CpG islands with DMH using a CpG island microarray.[53] The *DLC1* gene was found to be hypermethylated in all six NHL cell lines examined, with concomitant silencing of transcription. In several lines, expression could be upregulated by treatment with a combination of a demethylating agent and a histone deacetylase inhibitor. Seventy-five NHL patient samples were examined for methylation of several candidate genes, including *DLC1*. Of these, 87% demonstrated hypermethylation of *DLC1*.[53] Overall, expression of mRNA for this gene was significantly downregulated in tumor tissue compared to normal tissue.[53] A subset of 15 patients with banked tumor and plasma samples was evaluated for the presence of DNA containing the methylated *DLC1* gene in both tumor and

plasma.[53] These samples yielded concordant results in 12 of 15 cases. Of these, 10 demonstrated methylation in both tumor and plasma, and two demonstrated methylation in neither.[53] The three remaining patients had methylated *DLC1* DNA present in the tumor sample with none in the plasma.[53] This preliminary data offers the tantalizing possibility of developing screening tests to monitor for the presence of minimally residual disease and detection of early relapse. This has been evaluated in 27 patients with B-cell acute lymphoblastic leukemia (ALL).[54] Methylated DNA from dried slides was detected in 18 of 27 patients (67%).[54] This is a promising beginning. However, the utility of such a test could only be established through large-scale clinical trials. Development of such screening tests in dogs would allow the preclinical evaluation of this novel approach at a cost far below human trials, but with data of far more relevant content and quality than mouse studies.[55]

The American Cancer Society estimates that 58,870 people were diagnosed with NHL in 2006, and 18,840 people died of the disease. This group of diseases is the third most common cancer that occurs in companion dogs.[56] Neoplastic transformation of lymphocytes may occur in the bone marrow prior to differentiation, in the germinal center of lymph nodes, or in the post-germinal phase of B-cell biology.[57] To facilitate comparative examination of the diseases that arise from these various stages of development, the human Kiel and Working Formulation classification systems have been applied to canine NHL.[58;59] The Kiel classification is based on cytological criteria defining cell size, nuclear morphology, cytoplasmic characteristics, and degree of cellular

variability.[59] Immunophenotype further subdivides lymphomas in this system, but is difficult to identify based on cytological criteria alone.[59] The Working Fomulation is a histologic system classifying lymphomas using their location of origin within the node, cellular morphology, degree of differentiation, and mitotic rate.[59;60] See Table 1.1 for classification categories. This system has been found adequate to grade canine NHL with few modifications.[59;60] In a study of 134 canine lymphomas, Fournel-Fleury and others found that approximately 26% met the criteria for low-grade malignancy and 74% intermediate to high-grade malignancy in the Kiel system.[59] Using the Working Formula in the same cases, 20% of the cases were low-grade and 80% intermediate to high-grade.[59] Carter and others found only 5% of 285 cases of lymphoma to be low-grade, with 28% intermediate and 67% high-grade using the Working Formula.[60] With the advent of immunohistochemistry, veterinary pathologists could identify T-cell lymphomas using anti-CD3, CD4, CD5, and CD8 polyclonal antibodies and mAbs.[59] However, anti-CD19 and CD20 pan-B antibodies that are in wide use in humans do not react with the canine antigens.[59] As such, development of anti-B cell antibodies anti-CD21, anti-immunoglobulin, and, most recently, anti-CD79a antibody have allowed the reliable identification of B-cells.[59;61] In the Fournel-Fleury study, a subset of 92 cases was evaluated histologically and immunohistochemically. Of these cases, 24 (26%) were found to be of T-cell origin, of which 15 were low-grade lymphomas.[59] The frequency of T-cell disease in dogs prompted the investigators to identify the centrocytic designation as problematic in a comparative study, as human centrocytic disease is of B-cell

origin.[59] Carter also noted hypercalcemia and a mediastinal location associated with lymphoblastic lymphomas, evidence that they were of T-cell origin.[60] Valli and others, examining exclusively low-grade canine NHL, found only 10 of 66 cases to be of T-cell origin, however.[62] Additionally, those tumors identified as immunoblastic demonstrated nuclear size smaller than that typical of human immunoblastic forms.[60] The category of small noncleaved lymphomas is also problematic, in that the Burkitt's form, common in this class of human NHL, is extremely rare in dogs, without a causal virus like Epstein-Barr.[60;63] This led to a modified subtype of plasmacytoid or clear cell that is not commonly employed in the human classification of this form of lymphoma.[60] Intermediate to high-grade lymphomas occur most frequently in mature dogs, with diffuse large cell being the most common, followed by immunoblastic lymphoma.[59]

Grade	Working Formulation	Kiel Formulation
Low	Diffuse, small lymphocytic Follicular, predominately small cleaved cells Follicular, mixed	Lymphocytic Lymphoplasmacytic Lymphoplasmacytoid Centrocytic, follicular
Intermediate	Follicular, predominately large Diffuse, small cleaved Diffuse, mixed Diffuse, large cleaved Diffuse, large noncleaved	Centoblastic/centrocytic, follicular, small cells Centrocytic, diffuse Centroblastic/centrocytic, diffuse, small cells Centrocytic, diffuse, large cells Centrocytic monomorphous Centroblastic polymorphous
High	Immunoblastic Lymphoblastic Small noncleaved	Immunoblastic Lymphoblastic

Table 1.1: Classification categories of the Working Formulation and Kiel Formulation adapted for canine lymphoma. The Working Formulaton is the best classification system currently available for the comparative evaluation of human and canine lymphomas.

Since the publication of the comparative papers described, few veterinary pathologists have adopted the practice of classifying canine NHL. The prevailing

view appears to be that the subtle differences do not alter therapy, and only immunophenotype and grade alter prognosis.[64] From a comparative perspective, however, it is difficult to fully characterize the dog as a model for human disease without large-scale categorization of the forms of disease. Further development of the understanding of mechanistic and biological differences among forms of NHL are necessary to develop the dog as a model for human disease.

Several critical events in the biology of B-cells appear to be pivotal in their neoplastic transformation. The first process is that of V(D)J recombination in the bone marrow, in which multiple double-strand DNA breaks occur.[57] Inappropriate rejoining may result in chromosomal translocations that can lead to transformation.[57] The second series of events occurs in the germinal center of the lymph node after antigen stimulation. Immunoglobulin class-switching and somatic hypermutation to respond to a variety of antigens are processes which also result in double-strand DNA breaks, risking incorrect rejoining.[57] Each process leaves new combinations of surface markers on the cells allowing identification of the stages of B-cell differentiation at which neoplastic transformations occurred.[57] Lymphoblastic lymphoma and acute lymphoblastic leukemia represent neoplastic transformation of the B-cells in the pre-germinal phase, usually prior to undergoing V-D-J rearrangement of the antigen receptor genes.[57] Pre-germinal forms of indolent NHL include pre-germinal marginal zone (MZL) mantle-cell (MCL) NHL, and chronic lymphocytic leukemia (CLL). Forms of post-germinal NHL include CLL, follicular NHL (FLL) and some diffuse large B-cell lymphomas (DLBCL). [57;62] Some DLBCL and all intermediate to high-grade

lymphomas follow a more aggressive course, but may be cured in humans.[59] Methylation changes have been shown to be more frequent in post-germinal center NHL than pre-germinal NHL.[53] Such changes may be integrally related to the events in normal B-cell biology. To date, evaluation of both genetic and epigenetic events in canine B-cells has been minimal.[30;65]

The indolent forms of NHL have a protracted course of disease that ultimately leads to therapy resistance and intractability.[62;66] While the protracted course is associated with a more positive prognosis in dogs, relative to high-grade NHL, the lack of curability remains an important focus of research in humans. As such, the dog has been proposed as a model for preclinical evaluation of novel diagnostics and therapeutics intended for human use.[55;58] Although classic indolent disease is rarer in dogs than in people, the clinical course of canine NHL, response followed by chemotherapy resistant relapse, is similar. Furthermore, it is shorter than the human course of the disease, allowing evaluation of novel therapies or molecular markers over a much shorter span of time at lower cost than human trials.[55] The recent evaluation of DNA hypermethylation in human NHL has no such corollary in canine NHL that has been reported at this time.[30;53;67;68] In order to characterize more fully the relationship between human and canine NHL, particularly the underlying epigenetic changes associated with developmental lineage, epigenetic similarities and differences must be identified. Ultimately, the model must be deemed appropriate based on similarities of molecular mechanisms and alterations.

Canine models of disease hold great promise for radiopharmaceutical therapy research .[69;70] This is true for the canine forms of NHL. For humans with indolent forms of the disease, recently approved radioimmunotherapy (RIT) utilizing mAbs offers higher rates of complete response and longer disease-free intervals than traditional therapy and immunotherapy alone, but the diseases remain essentially incurable.[71-73] Furthermore, the response to therapy diminishes with successive treatments.[72] This phenomenon can be attributed to decreased target antigen density and also progressive radioresistance of the disease.[72] This resistance arises from accumulation of genetic, and likely epigenetic, changes promoting an anti-apoptotic state within the cell.[74-77] There is a need to develop novel approaches of maximizing tumor dose, combining tolerable radiopharmaceutical therapy with chemotherapy, and administering radiopharmaceuticals that have different dose-limiting tissue than potential concurrent chemotherapy. Diminishing resistance may render radiotherapy curative.

While RIT offers exquisite specificity of targeting B-cells, the plasma kinetics of mAbs result in prolonged exposure of the bone marrow to radioactivity.[78] Marrow exposure is the dose-limiting toxicity of radiolabeled mAbs, including both FDA-approved products.[79;80] Tumor-absorbed dose is limited by marrow tolerance, with calculated median tumor doses in patients with NHL treated with ^{90}Y-ibritumomab tiuxetan (Zevalin®) of 17.0 Gy (range 5.8-67.1) achieving an objective response rate of 67%.[80] The cure rates with radioimmunotherapy, however, are no better than chemotherapy or mAb

therapy.[66;72;73] Dose-fractionation schemes, re-treatment, combination therapy, and dose-intensification have been investigated to enhance cure rates with no dramatic advances currently identified.[81-83]

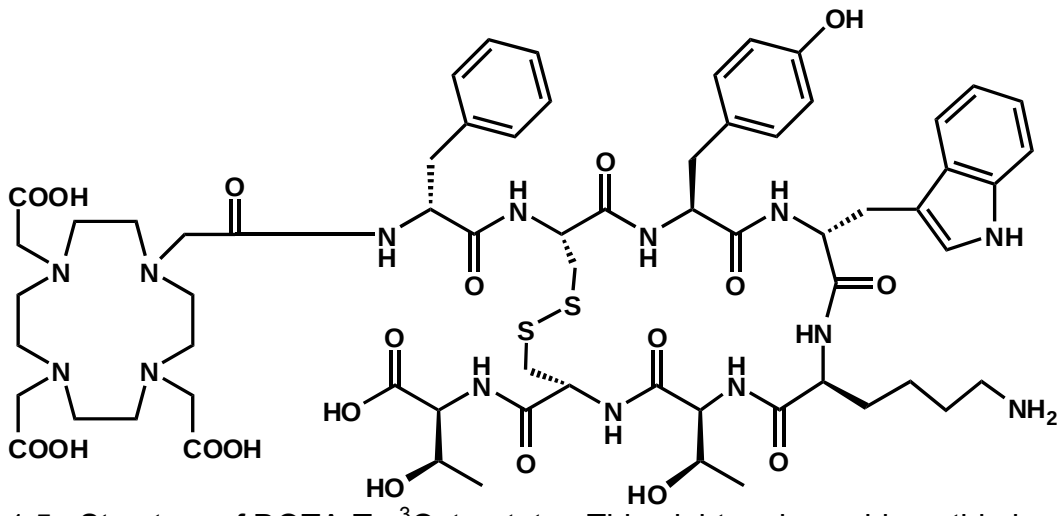

Figure 1.5: Structure of DOTA-Tyr^{3}Octreotate. This eight amino acid peptide is a hydrophilic agonist with high affinity for somatostatin 2 and 5 receptors.

The chelator-conjugated peptide 1,4,7,10-tetraazacyclododecane-*N*,*N'*,*N''*,*N'''*-tetraacetic acid (DOTA)-tyrosine-3-octreotate (TATE) is a small peptide that binds type 2 and type 5 somatostatin receptors with high specificity (See Figure 1.5). [84-86] It is similar to the product Octreoscan®, an FDA approved agent for imaging neuroendocrine tumors. Eliminated rapidly in the urine, the dose-limiting organ of radiolabeled DOTA-TATE is the kidney which tolerates a greater than 10-fold higher dose than marrow.[87] Human NHL expresses somatostatin receptors in approximately 80% of cases.[88] Somatostatin analogues have been used to image NHL in adults and children.[89-93] While the imaging agent was supplanted by the advent of FDG-PET imaging, the targeting properties could be exploited to deliver a payload of radioactivity or molecular therapy for NHL. Certain questions must first be answered to determine whether

this is feasible. Somatostatin analogues have been imperfect in lesion detection.[90] It is not clear if this lack of sensitivity was a property of the agent or the imaging system utilized. Human xenograft models of indolent NHL in SCID mice have been shown to accumulate sufficient radiometal-labeled DOTA-TATE to be imaged by PET and SPECT technology.[94;95] A large animal model would be extremely useful for investigating the utility of these under-explored delivery agents in NHL. This would allow tolerability studies to determine true dose-limiting organs and overall dose-tolerance. However, canine lymphoma has not, yet, been demonstrated to be a suitable model in which to evaluate these compounds.

Dogs have been shown to express suitable somatostatin type 2 receptors (SSTR2) in endocrine and gastrointestinal tissues. Using ^{111}In-DTPA-D-Phe^{1}-octreotide, an SSTR2- and SSTR5-specific agent, investigators performed biodistribution studies in normal beagles as a preclinical evaluation for imaging endocrine disease.[96] Receptor-mediated uptake was shown to exist in the stomach, intestinal tract, gall bladder, pancreas and kidneys.[96] Germinal follicles of Peyer's patches in the intestines showed significant uptake, suggesting lymphoid accumulation of the agent, but specific cellular accumulation could not be demonstrated .[96] Similar agents have been used successfully in dogs to image endocrine inflammatory diseases and neoplasia.[97-99] Substitution of radiometals from imaging to therapy nuclides would allow this specific targeting to be utilized in a therapeutic manner.

The decay properties of ^{177}Lu are listed in Table 1.2. The long half-life of this radionuclide emits low dose-rate radiation exposure to the targeted tissue. The medium-energy β- particle results in localized energy deposition.[86] The γ emission can be imaged with standard scintigraphy equipment, but is of low abundance, minimizing non-therapeutic dose.[86] Mouse studies of solid-tumor xenografts found ^{177}Lu to be superior to other radiolanthanides in effecting tumor control with pretargeted therapy, an approach that results in similar plasma kinetics of the radiolabeled compound as would ^{177}Lu-DOTA-TATE.[100] In an intra-patient comparison of ^{177}Lu-DOTA-TATE to ^{177}Lu-DOTA-Tyr^3-octreotide with endocrine cancer, tumor residence was judged superior for the TATE compound, resulting in a 50% higher tumor dose.[101] An increased renal residence time accompanied this, but was judged to be within acceptable clinical limits.[101] The kidney and, to a lesser extent, the bone marrow are the dose-limiting organs for radiolabeled peptides.[86] Lysine or arginine-lysine infusions are administered to decrease renal accumulation.[86] Although more effectively decreasing this accumulation, lysine infusion is more likely to induce hyperkalemia, nausea, and vomiting.[86;102] In one study, cumulative doses of up to 800mCi of ^{177}Lu were administered to humans with endocrine cancer, resulting in only two of 131 manifesting renal disease, and the rest maintaining normal creatinine clearance.[103] These patients experienced an objective response rate of 28%, with a further 44% having disease stabilization.[103] Since the kidney is not particularly dose-limiting with any of the traditional chemotherapy drugs used to treat NHL in dogs and humans, the possibility of combination chemotherapy with

a ^{177}Lu-containing compound is attractive. In fact, a case series was reported in which two human patients with SSTR-positive cancer were treated with a combination of ^{177}Lu-DOTA-TATE, doxorubicin, cyclophosphamide, and vincristine or etoposide sequentially with good tolerance.[104] In this series, humans with paragangliomas and meningiomas had reasonable rates of response to ^{177}Lu-DOTA-TATE, but those with NSCLC and melanoma responded poorly.[104] No such evaluation has been performed in humans with NHL. Companion dogs with NHL may serve as a suitable model for such a trial.

	^{177}Lu	^{111}In
$T_{1/2}$	6.71d	2.83d
β-	497keV	None
Imaging emission	113, 208keV	171, 245keV

Table 1.2: Decay properties of ^{177}Lu for imaging and therapy

There are important practical considerations for dog studies using ^{177}Lu-labeled peptides. The radiometal ^{177}Lu is reactor produced in a thermal neutron reaction by the following: $^{176}Lu + n \longrightarrow {}^{177}Lu + \gamma$. Lutetium-176 has a cross-section of 1639mb, yielding efficient conversion to ^{177}Lu. This reaction also results in production of the metastable product ^{177m}Lu with a half-life of 160 days, a functional contaminant that must be managed in the waste stream. Fortunately, the reaction produces less than 0.4kBq ^{177m}Lu per MBq of ^{177}Lu produced.[105] Typically, radionuclides of similar half-lives, such as ^{131}I and ^{177}Lu, may be decayed in the same waste containers. However, the contamination with ^{177m}Lu requires separating ^{177}Lu waste from that of ^{131}I.[105] Appropriate waste-handling must be pre-planned for veterinary and human radiation facilities intending to handle these radionuclides for therapy. The metastable contaminant

can be avoided through production of high specific-activity ^{177}Lu using a ^{176}Yb target, as described by Ketring and others.[106] This production is limited and not commercially available at this time.

What follows is a series of experiments to further characterize the dog as a model for comparative evaluation of the etiology, pathobiology, and therapy of NHL. Specific Aim One was to identify the genomic features common to epigenetically regulated genes in humans. A comparative bioinformatics examination of an extensive list of genes resulted in four that were of biological and structural interest. Computer modeling identified CpG islands and promoter regions to serve as the basis for further evaluation of the control regions of these genes. Assays were developed, and one optimized to examine the predicted canine *DLC1* gene. Evidence of a CpG island, hypermethylated in naturally occurring canine NHL relative to normal lymph node DNA, was discovered.

Specific Aim Two was to examine the relationship between methylation and expression of the *DLC1* gene in biopsy samples of canine NHL, with the intention of characterizing this predicted canine gene. Further promoter analysis revealed important similarities and differences between the human and canine gene. Methylation patterns were identified that appear unique to the neoplastic phenotype. Expression patterns were established for normal and canine NHL samples. Cloning of portions of the cDNA confirmed the validity of the expression study and identified the functional unit of the canine RhoGAP gene, *DLC1*.

Specific Aim Three was to evaluate the effects of DNA demethylation on radiosensitivity of a human NHL cell line. Evidence of a synergistic effect between radiation and DNA demethylation was observed. The effect was demonstrated to differ as a result of the quality of the radiation employed. The methylation patterns of four genes potentially involved in mechanistic pathways were established.

Specific Aim Four was to characterize the somatostatin receptor expression in canine NHL through a pilot imaging trial of dogs with naturally-occurring disease. Clear evidence of SSTR expression will serve as the basis for further investigation of peptide radiotherapy and molecular imaging of canine NHL. Together, the results of these investigations will advance the understanding of the common molecular contributors to NHL in dogs and humans. This will be used as a platform for future clinical trials to evaluate novel radiopharmaceutical imaging and therapy agents and demethylating drugs in dogs for translation into human patients.

Chapter 2

In Silico and *in Vivo* Identification of a Novel Hypermethylated Canine Tumor Suppressor Gene

Introduction

As no published examination of promoter region hypermethylation exists in dogs, it was necessary to develop a robust assay to begin this study. This required first an exhaustive evaluation of canine genes with potential for epigenetic control. A list of genes examined is presented in Appendix 1. This list was generated from DMH data to identify differentially methylated CpG islands in human NHL cell lines and samples.[68] The NCBI codes for each gene were manually entered into the NCBI BLAST website and the results evaluated. The majority of the genes identified code for predicted proteins, with few representing sequenced genes. The 5' region of each gene was screened for the presence of a CpG island and a promoter region. From the resulting list of genes with a predicted CpG island corresponding with a predicted promoter region, the genes *DLC1*, *PRKCE, POU3F3* (*BRN1*), and *LHX2* were selected for their relevant biological functions. As discussed, the presence of CpG dinucleotides is statistically rare in much of the mammalian genome.[11] Criteria for determination of a CpG island used by Methprimer were: Island size >100bp, G+C content: >50%, and CpG observed to expected ratio > 0.6. While these conditions resulted in a strong association with the promoter region of the genes examined, the definition given in the introduction, which is in general use at this time, is stricter.[15] It should be noted that the CpG island identified for *PRKCE* did not meet the 500bp minimum of the strict criteria.

The discovery and function of *DLC1* is described in the Introduction. Protein Kinase C ξ (PRKCE) is a novel class of PKC that is activated by

phosphatidylserine and diacyl glycerol, but not calcium, which is required for the classical PKCs. This gene has been identified to play a role in carcinogenesis of carcinomas through its activity in chronic inflammation.[107] It has also been shown to be methylated in human B-cell NHL.[68] The gene *POU3F3*, or *BRN1*, is a member of the class III group of transcription factors. It has important regulatory functions in the development of neural structures and renal distal tubules.[108] It has also been identified to be hypermethylated in human NHL.[68] The gene product of *LHX2* is a zinc-binding protein mediating, through protein-protein interactions, B-cell, brain, and retina development.[109] Like the others, it is hypermethylated in B-cell NHL.[68]

An initial study was planned using cell samples collected by lymph node aspiration to evaluate canine DNA for the presence of hypermethylation of CpG islands. This method of collection was chosen to facilitate rapid material collection and case accrual. As some of the samples were collected in a private referral hospital and shipped to the University of Missouri-Columbia, preservation of RNA in the samples could not be assured. As such, all samples were processed for DNA harvest with no attempt to collect the message of any of the genes involved. Normal lymph node samples collected by biopsy were shared with a concurrent proteomics research protocol.[110] The dogs in the proteomics study were treated in accordance with a protocol approved by the institutional animal care and use committee. No normal samples were collected by lymph node aspirate.

The purpose of the present study was to evaluate clinical lymphoma samples for the presence of hypermethylation. Companion dogs with NHL have been suggested to be appropriate, naturally occurring clinical models of human NHL.[55;58] To date, no research has identified the presence of DNA hypermethylation in canine NHL as has been demonstrated in human NHL. Confirmation of this potential therapeutic, diagnostic, and prognostic target would establish the dog as a pre-clinical model for manipulation of epigenetic modification before and after the development of NHL. The hypotheses of this study were:

1) Canine orthologs of human genes regulated by methylation will have similar 5' CpG islands and regulatory factors in the promoter region.

2) Canine orthologs of human genes regulated by methylation will show evidence of CpG island hypermethylation by bisulfite-based analysis.

Results

Searching the canine genome using the reference number NM_182643 for *DLC1* yielded a highly significant similarity with a canine sequence in chromosome 16 a mid-sized, 64Mb chromosome (score 1328, Expect Value 0.0). This region is part of a predicted RhoGAP protein. The sequence of the canine 5' region corresponding to the human *DLC1* promoter was retrieved (Figure 2.1). This sequence yielded two CpG islands in the MethPrimer analysis (Figure 2.1). These islands are large, 1,065 and 556 bp, respectively. The PromoterScan analysis of the reverse strand yielded an extremely high promoter score of

260.20 with a minimum promoter cutoff of 53.00 from bases 39,535,766 to 39,536,015. This identified promoter region corresponds highly to the reported human gene promoter region.[37] The promoter analysis identified 16 Sp-1 binding sites in close proximity with proper orientation to gene transcription (Figure 2.2). The transcription factor binding sites identified by Promoterscan in dogs and humans are listed in Table 2.1. The predicted promoter region does not correspond to the full-length predicted Rho-GAP gene in the NCBI database, but appears orthologous to the human splice variant that has tumor-suppressor function. Furthermore, no promoter region with a CpG island could be identified upstream of the database sequence.

Analysis of the sequence downstream of the predicted promoter region using the InterProScan web-tool, revealed the presence of code for all the major functional units of the human *DLC1* protein. These include the Rho-GAP active site, a lipid binding steroidogenic acute regulatory protein (START) site, and a sterile alpha motif homology 2 (SAM2) unit. This lends further support to the location of the promoter being in the proposed location, rather than the longer gene predicted in the database. Recently, gene prediction software has been added to the UCSC genome browser.[111] The algorithm N-Scan predicts the location of the *DLC1* gene of dogs to be similar to the location predicted above with all functional subunits included.

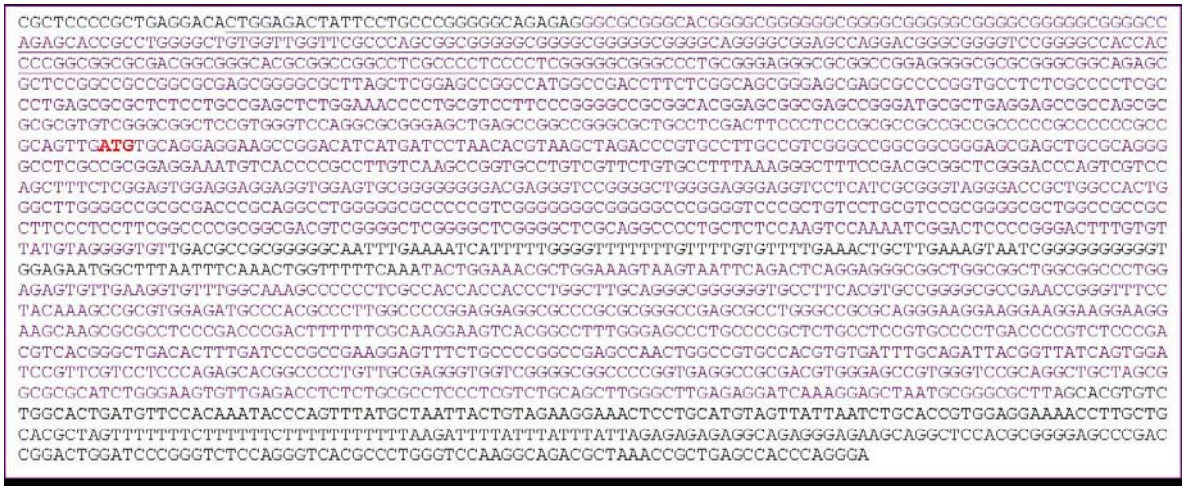

Figure 2.1: Canine DNA sequence for the 5' end of the gene encoding the putative promoter and first exon. The predicted promoter sequence is underlined and the CpG islands are in purple type.

CGCTCCCCGCTGAGGACACTGGAGACTATTCCTGCCCGGGGGCA
GAGAGGGCGCGGGCACG**GGGCGG**G**GGGCGG**GGCGG**GGGCGG**GGC
GGGGGCGGGGCCAGAGCACCGCCTGGGGCTGTGGTTGGTTCGCC
CAGCGGCGG**GGGCGG**GGCGG**GGGCGG**GGCAG**GGGCGG**AGCCAGG
AC**GGGCGG**GGTCCGGGGCCACCACCCCGGCGGCGCGACGGCGGG
CACGCGGCCGGCCTCGCCCCTCCCCTCGG**GGGCGG**GCCCTGCGG
GAGGGCGCGGCCGGAGGGGCGCGC**GGGCGG**CAGAGCGCTCCGGC
CGCCGGCGCGAGCGGGGCGCTTAGCTCGGAGCCGGCCATGGCCG
ACCTTCTCGGCAGCGGGAGCGAGCGCCCCGGTGCCTCTCGCCCC
TCGC

Figure 2.2: Sequence of the predicted promoter region of the gene. The promoter region is underlined, the CpG island is in purple type, and nine of the identified SP1 binding sites are bolded.

Dog		Human	
Trans Factor	Number	Trans Factor	Number
Similar Factors			
Sp1	16	Sp1	8
JCV_repeated_seq	2	JCV_repeated_seq	1
T-Ag	2	T-Ag	1
GCF	2	GCF	1
Differing Factors			
AP-2	2	AP-2	0
NGFI-C	1	NGFI-C	0
KROX24	1	KROX24	0
UCE.2	0	UCE.2	1
MRE_CS6	0	MRE_CS6	1
JunB-US2	0	JunB-US2	1

Table 2.1: Transcription factors identified by Promoterscan in orthologous dog and human promoter regions of *DLC1*.

Primer	**Sequence**
Unmethylated F	TGGTTTTAAGTTTAGTGGTTAGTGG
Unmethylated R	CCTTATCAAACCAATACCTATCATT
Methylated F	GCGGTTTTAAGTTTAGTGGTTAGC
Methylated R	CCTTATCAAACCGATACCTATCGT
COBRA F	GAGAGGTTTTAATATTTTTTAGATG
COBRA R	ACCTTTAAAAACCCTACCCC

Table 2.2: Primer sequences for MSP and COBRA for the canine RhoGAP gene *DLC1*.

Primers used for MSP and COBRA are listed in Table 2.2. A complete description can be found in Appendix 2. Examination of the CpG island containing the promoter region by MSP demonstrated the presence of bands from methylated primers in six of 13 NHL samples and two of three CLL samples (Table 2.3, Figure 2.3). The primers designed for this assay amplify a 183bp

region in the proximal predicted first intron, located between bases 39,535,120-39,535,307 of chromosome 16. Nine of 13 NHL samples and two of three CLL samples demonstrated bands from unmethylated primers. Three NHL samples did not amplify with either primer set. Examination of the second CpG island by COBRA demonstrated methylation in nine of 13 samples with the same three samples failing to amplify (Table 2.3). The primers designed for this assay amplify a183bp region in the proximal predicted first intron, located between bases 39,534,203-39,534,496 of chromosome 16.

Immunophenotype was determined for six of the dogs with four B-cell and two T-cell lymphomas. Of these, two of four B-cell samples showed methylation by MSP and one did not amplify. No T-cell sample showed methylation by MSP, but both showed methylation in the 3' CpG island by COBRA. Immunophenotype was not determined for CLL. No normal sample was positive for methylation. The DNA of at least three individual normal dogs was used in the development of the assay.

Dog	N	1	2	3	4	5	6	7	8	9	10	11	12	13
Unmethylated	+	+	-	+	+	+	+		+		+	+		+
Methylated	-	-	+	+	+	-	+		+		+	-		-
No Amplification								+		+			+	
COBRA CpG I 2	-	+	+	+	+	+	+		+		-	+		+
Immunophenotype	M	B	B	N	B	N	N	B	N	N	N	T	N	T

Table 2.3: Summary of the results from MSP and COBRA gel data (Figure 2.3) and the patient immunophenotypes. Dog N was a normal representative sample. Immunophenotype is identified as B or T cell, M if mixed, or N if immunohistochemistry was not performed. Cells are blank if no data was available.

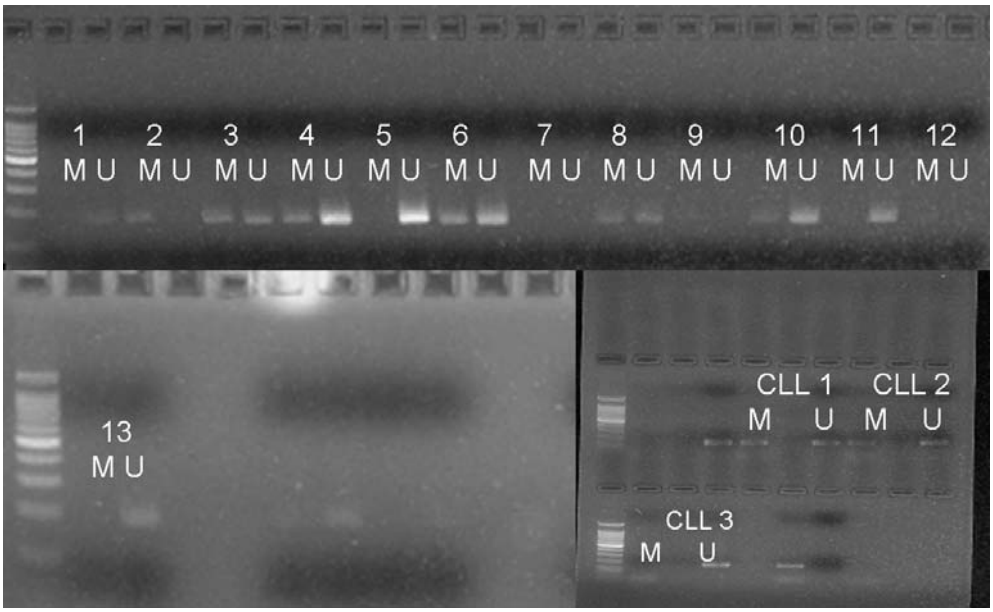

Figure 2.3: Agarose gel of MSP products from thirteen canine NHL samples and three canine CLL samples. Three NHL samples failed to amplify with either methylated or unmethylated primer sets. Six of ten NHL samples that amplified had bands from the methylated primers. Nine of ten NHL samples had bands from the ummethylated primers. Two of three CLL samples had bands from methylated primers. All three had bands from unmethylated primers. Numbers = NHL patient samples. CLL + number = CLL patient samples. M = methylated primer lane. U = unmethylated primer lane.

Sequencing results of the MSP products of five clones from one patient with a methylated primer band revealed mean methylated proportion of 0.52 (SEM 0.0742) (Figure 2.4). Sequencing results of the MSP products of five clones from one patient with an unmethylated primer band revealed mean methylated proportion of 0.080 (SEM 0.0249) (Figure 2.4).

Unmethylated Primer Set Methylated Primer Set

Figure 2.4: Diagram of methylation of specific CpG dinucleotides in the amplicons of unmethylated (left) and methylated (right) MSP primer sets. White circles represent unmethylated CpG dinucleotides and black circles represent methylated CpG dinucleotides.

Discussion

Epigenetic mechanisms have been shown to play an important role in many human cancers, including NHL. Whether these changes are causative or the result of neoplastic transformation has not been clearly established.[3] Environmental influences have been identified which modify the methylation pattern of DNA in laboratory animals.[112] Such changes may cause or promote human cancers, however the epidemiology remains controversial.[113] Companion animals tend to share the lives and environmental exposures of their human counterparts.[55] This represents an untapped resource of information on the interplay of environment and disease. Developing evidence that demonstrates similar epigenetic alterations in human and canine disease is critical to the development of this naturally occurring model of cancer. Evidence for methylation of the tumor suppressor gene *DLC1* in canine lymphoma, as it is in human NHL, is strong evidence that the molecular underpinnings of the two diseases can be highly similar.

The sequence for the canine RhoGAP gene identified using the NCBI site is clearly orthologous to the human *DLC1* gene. With a score of 1328 and an

Expect Value of 0.0, it is a statistical impossibility that this gene is anything but the *DLC1* ortholog. This gene lies on the long arm of canine chromosome 16, a 64Mbp chromosome. Through eons of recombination and fragmentation, this chromosome in the dog contains portions of the genes of human chromosome 8, along with genes located on human chromosomes 4 and 7. The sequence of the predicted promoter region lies within a CpG island 1187bp long, similar to the arrangement of the human gene, with a second, smaller CpG island, 557bp long, lying 223bp 3' to the first. Human *DLC1* has a single CpG island 1559 bases long encompassing its promoter region, using strict criteria. The canine CpG islands are large, as would be expected for a CpG island with significant gene control properties.[15] The promoter score of 260.20 is extremely high for a dog sequence using the web-based tool. With a minimum promoter cutoff of 53.00, this is the highest score that has been seen in our lab for a canine gene. It is much higher than the score for the human promoter region of *DLC1*, 99.09. The UCSC Genome Browser clearly shows good alignment of this predicted region with the promoter, first exon, and first intron of the human *DLC1* gene. The presence of numerous Sp-1 transcription factor binding sites in the promoter region also suggests that methylation plays a role in control of the gene. This transcription factor has been demonstrated in humans to be inhibited from binding by the presence of methylation.[114] The majority of transcription factor binding sites identified in this region of the dog and human sequences are common between the two. The differences, although fewer, could be significant. An example is the presence of a binding motif in the human sequence for JunB,

which may indicate that the gene is the target of *jun* signaling in humans but not dogs. Conversely, KROX24 is present in dogs but not humans. This transcription factor is expressed upstream of many immediate early genes induced by growth factors, possibly linking *DLC1* further with oncogenic apparatus.[115] Further, this transcription factor upregulates the SRE associated with actin rearrangement, suggesting that the canine gene participates in the same pathways identified for the human gene.[116] The similarity between the predicted canine promoter region and the human tumor suppressor gene makes the identified area the most likely 5' region of this canine ortholog. A full-length gene depicted in the NCBI canine database does not match a known splice variant in the human, and probably represents too coarse a sequence examination using early tools. In fact, more recent gene-prediction software predicts transcription to start in the area identified in the present *in silico* experiments.[117]

Further supporting the location of the predicted promoter region is the fact that the full length of the banked gene is not necessary to yield a functional protein. The sequence downstream from the promoter site, and of the N-Scan mRNA prediction, contains the active Rho-GAP protein as well as SAM2, which has been shown to function as a receptor for tyrosine kinases, likely mediating protein-protein interactions.[118] Also, the lipid binding START domain is similar between the rat, human, and predicted dog protein. This domain appears to play a role in intracellular cholesterol transfer and steroidogenesis.[119] The START and Rho-GAP active sites have been shown to be necessary for the tumor

suppressor function of this gene.[51] Dysregulation of these functions by epigenetic silencing could contribute, as previously described, to a neoplastic phenotype.[39]

Methylation of the *DLC1* CpG islands was evident in the majority of the canine NHL and CLL when assayed by MSP and COBRA. The proportion was higher in the COBRA assay, which examined the CpG island located further downstream. The proportion of six of 10 amplifying samples positive for methylation is not dissimilar from the 87% methylated in human B-cell NHL, particularly since two of the 10 were of T-cell origin, and were not methylated.[53] The methylation identified by these two assays occurs in the CpG islands in the region of the predicted first intron. Primer sets in this location were selected because the CpG density of the island was sufficiently high to make the design of primers further interior difficult. Primer sets designed for a more 5' location failed to amplify the bisulfite-treated DNA. Methylation in the first intron has been shown to regulate expression of the *ZAP70* gene in human chronic lymphocytic leukemia.[120] In fact, one CpG dinucleotide appears to be a dominant controlling factor. [120] Thus, methylation in this area of canine genes, including *DLC1*, could prove to contribute to regulation of gene expression.

Three canine NHL samples did not amplify. All three had lower DNA concentration and appeared at least partially degraded on agarose gel analysis. The lack of amplification could also be a result of deletion. Loss of the region of canine chromosome 16 containing this gene location has been reported in one case of T-cell lymphoma in a female Cocker spaniel.[121] Further study will be

necessary to elucidate the frequency of such an event. Two of three canine CLL samples had positive methylated bands as well.

The bisulfite sequencing results confirm a clear difference between the amplicons of the methylated and unmethylated primer set. As depicted in Figure 2.4, the methylation was sparse when amplified with the unmethylated primers. Using the methylated primers, the density of methylated CpG dinucleotides was greater than 50%. This is an important distinction, as the primers depend on only four CpG dinucleotides to discriminate between a methylated and an unmethylated condition. This confirms that the presence of a methylated band in MSP correlates with a significantly greater density of methylated CpG dinucleotides. It is interesting to note that CpG dinucleotides 9 through 12 showed almost no methylation in the methylated sample, while CpG dinucleotides 7 and 8 were completely methylated. CpG dinucleotides 1, 2, 14, and 15 were completely methylated, as would be expected, with the primers selecting for DNA methylated at these locations.

Five of the six NHL and both methylated CLL samples also had a positive unmethylated band. The significance of this ummethylated band is not entirely clear at this time. It is certain that the cell population from which DNA was extracted was heterogeneous in composition, with neoplastic and normal cells mixed. The samples were lymph node aspirates, so would have contained more than one cell type. It is also possible that the neoplastic populations were heterogeneous in nature. Finally, the neoplastic cells could be individually heterozygous for methylation. Simultaneous demonstration of methylated and

unmethylated markers is seen in human tumors as well.[53;67;122] Whatever the source of the unmethylated DNA, the presence of hypermethylation of an important tumor suppressor gene in naturally occurring canine cancer represents the first report of its kind and a significant find.

It is significant that the methylation observed was present only in neoplastic tissue samples. As for the human *DLC1* gene, methylation of the canine gene at this location may serve as a useful marker of the neoplastic phenotype.[54] This may be useful for identifying early or even pre-neoplastic lesions, for monitoring nodes for minimal residual disease, or for detecting early relapse. To have a cancer-specific test that is robust and could be performed on lymph node aspiration samples rapidly and inexpensively would be an asset to rapid diagnosis for canine NHL patients. Such a diagnostic test could also serve as a pre-clinical evaluation of similar technology in humans. Finally, as the clinical use of demethylating therapy is better defined, such a test may serve as a prognostic marker of likely response to therapy, even if expression of the specific gene identified is not modified.

This series of experiments confirmed the first hypothesis that the canine ortholog of the human gene *DLC1* has a large CpG island in its 5' region that contains many similar transcription factor binding sites, particularly Sp1 and AP-2, which are known to be methylation-sensitive. The results of this initial evaluation of the methylation status of *DLC1* in canine NHL confirm that a hypermethylated condition is present in the CpG island containing the promoter in a significant proportion of these cases, supporting the second hypothesis.

Such a hypermethylated gene promoter may become a clinically valuable therapy target, a biomarker of disease and remission, or a prognostic signpost for clinical patients. The presence of a hypermethylated state of this tumor suppressor gene in both human and dog NHL suggests that the underlying pathogenesis of this disease is as similar as previously described. The further evaluation of this phenomenon in naturally occurring canine NHL in which both methylation and expression is evaluated will strengthen the use of companion dogs as models of human NHL.

Materials and Methods

In Silico methods: The NCBI reference number for the human *DLC1* isoform 1 gene, NM_182643 , was used to search a canine genome database (http://genome.ucsc.edu/cgi-bin/hgGateway) for the canine ortholog. The 5‘ region of the gene was examined using the MethPrimer CpG island analysis tool (http://www.urogene.org/methprimer/ index1/html) to identify candidate CpG islands.[123] This region was also examined using the PromoterScan transcription factor binding analysis tool (http://zeon.well.ox.ac.uk/git-bin/proscan) to identify a promoter region within the sequence.[124] The putative promoter region of the gene was then confirmed to match the human gene promoter region using the UCSC Genome Browser (http://genome.ucsc.edu/cgi-bin/hgGateway?clade=vertebrate&org=Dog&db=0&hgsid=69320643). A predicted mRNA sequence was constructed by concatenating the canine orthologs of the human exons of *DLC1* identified using a basic local alignment

search tool (BLAST). The resulting sequence was examined using the InterProScan web-tool to identify protein functional groups (www.ebi.ac.uk/InterProScan/index.html).[125] The same procedure was performed using the N-Scan predicted mRNA sequence.

In Vivo methods: Sample collection and preparation: Lymph node aspirates were performed on clinical patients with lymphoma using 22ga. needles and preserved in Hank's balanced salt solution at -80ºC until analysis. Peripheral blood mononuclear cells were isolated over a ficoll-hypapaque (Sigma-Aldrich, St. Louis, MO) gradient and preserved at -80ºC until analysis. DNA was extracted using the Qiagen DNeasy Tissue (Qiagen, Inc. USA. Valencia, CA) kit, and then bisulfite treated using the Zymo Research EZ DNA Methylation Gold (Zymo Research Corporation, Orange, CA) kit. Bisulfite treated DNA from normal canine lymph nodes was treated with SssI, a DNA methyltransferase, and SAMe to methylate all CpG dinucleotides in the sequence and serve as a positive control.

Methylation Specific PCR: The MethPrimer website was used to construct primer pairs for methylation-specific PCR (MSP) that amplify a product of 185 bp (Table 1). Using bisulfite treated DNA, the conditions for MSP were optimized. The methylated primer set was used to amplify the region with an annealing temperature of 62°C for 30s, an extension temperature of 72°C for 30s, and a melting temperature of 95°C for 15s, repeating for 32 cycles. The unmethylated primer set was used to amplify the region with an annealing temperature of 62°C for 60s, an extension temperature of 72°C for 60s, and a melting temperature of

95°C for 15s, repeating for 32 cycles. The PCR products were run on a 1.5% agarose gel with ethydium bromide. The negative control was bisulfite converted DNA from normal lymph node, and the positive control was SssI treated bisulfite converted DNA from normal lymph node

Combined bisulfite restriction analysis (COBRA): The MethPrimer website was used to construct primer pairs for COBRA (Table 1). These primers do not contain CpG dinucleotides, and will amplify DNA whether or not methylation is present in the gene. The conditions for PCR were an annealing temperature of 58°C for 60s, an extension temperature of 72°C for 60s, and a melting temperature of 95°C for 15s, repeating for 32 cycles. The product size of these primers is 284 bp and contains two BstuI cut-sites that recognize the sequence CGCG and yield fragments of 27 bp, 38 bp, and 219 bp. . For BstuI, 10μL of PCR product was added to 2.5μL of Buffer 2, 1μL of BstuI, and 11.5μL of HyPure water, and incubated at 60ºC for 4h. Controls were identical to MSP. The PCR products were run on a 1.5% agarose gel with ethydium bromide.

Bisulfite sequencing: The MSP product of a methylated and an unmethylated primer set from different patients was prepared for cloning as described above. Five clones of each purified plasmid DNA were submitted with universal primers where they were sequenced by the DNA Core using a standard dideoxynucleotide sequencing technique. CpG dinucleotides within the sequences were mapped and labeled as methylated if cytosine remained unconverted, and unmethylated if a thymidine was in a cytosine position.

Statistical Analysis: DNA sequences were considered similar in BLAST search if the score was > 900 and the Expect Value was < 0.0001. Promoter score cutoff was set at a minimum of 53 on the Promoterscan software to identify a promoter region.[124] For the CpG island determination, parameters were set to identify a sequence with a minimum length of 100 bases, a GC percentage > 50%, and a CpG observed/expected ratio of 0.6.[123]

Chapter 3

Methylation, Expression, and Characterization of *DLC1* in Canine NHL Samples

Introduction

With the evidence from the pilot study that hypermethylation exists in canine NHL samples relative to normal lymph node samples, a larger study of biopsy specimens was undertaken to examine the relationship of this methylation to expression of the *DLC1* gene. This gene has been demonstrated to be entirely silenced in human NHL cell lines and largely silenced in human NHL patients samples.[53] The primer sets developed for the previous study were limited to the 3' region of the primary CpG island and the second CpG island by primer design constraints on CpG density. For this series of experiments, a new primer set was designed with assistance from software, but with modifications made, as described in the Materials and Methods, to force amplification of the CpG rich region of the 5' end of the promoter. This allowed query of methylation in the promoter as well as the first intron (Figure 3.1). The amplicon designed contains six known Sp1 binding sites and an AP-2 binding site. These primers amplify the bisulfite-converted bases 39,535,910 to 39,536,096 of canine chromosome 16. The amplicon contains one cut-site each for the methylation-sensitive restriction enzymes BstuI, TaqaI, and HypCh4IV (Figure 3.3). Each of these cut-sites is successively more 5' in location.

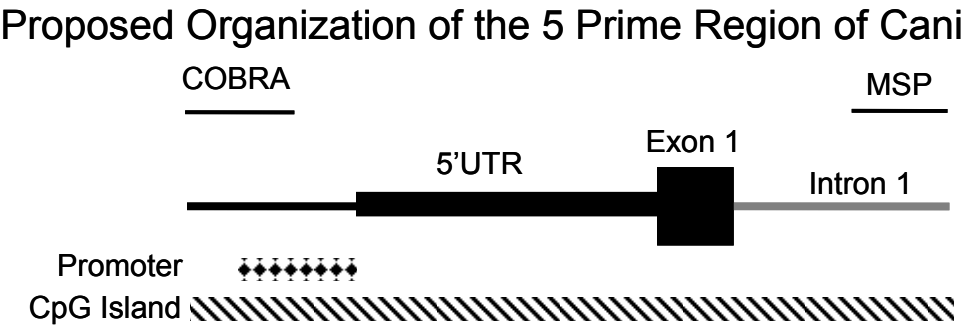

Figure 3.1: Proposed organization of the promoter, 5' untranslated region, first exon, and first intron of the canine *DLC1* gene with the amplicons of the reported analyses noted. The predicted promoter region is in checkerboard, the CpG Island is hashmarked.

The case samples were collected from dogs presenting to the University of Missouri-Columbia Veterinary Medical Teaching Hospital. Samples were obtained by lymphadenectomy or Tru-Cut needle biopsy. Samples were divided in two, placed in RNALater (Ambion, Inc., Austin, TX), and stored immediately at -80ºC for later processing. The majority of the dogs in the study underwent complete staging, including CBC, plasma chemistry profile, bone marrow aspirate, thoracic radiographs, abdominal ultrasound, and biopsy for immunophenotyping, but staging was not required for inclusion. The normal lymphocytes used for this study were from laboratory dogs used for a concurrent protocol[110], blood samples of healthy volunteer dogs, or node samples harvested immediately after euthanasia of donated animals without lymphoma.

The purpose of this series of experiments was to characterize further the canine *DLC1* gene and its relationship to the human gene. No literature or databank information characterizes this gene in dogs. While new, more precise prediction software has identified a putative structure for the canine *DLC1* gene, no biological data confirms its existence or its expression in canine tissue. The

studies presented here attempt to further characterize the similarities and differences of the construction of the dog and human promoter regions of *DLC1*, confirm the sequence of the mRNA, identify expression levels in the normal lymphoid samples and canine NHL samples, and identify DNA methylation patterns and their relationship to the expression of the gene. The hypotheses of this study were:

1) The promoter regions of canine and human *DLC1* share similarities of construction that lend themselves to control by DNA methylation, and differences that may affect the degree of methylation observed.

2) Hypermethylation of the 5' region of the canine *DLC1* gene is present in canine NHL samples, similar to human NHL.

3) The hypermethylation associated with the promoter region results in transcriptional silencing of the canine *DLC1* gene.

4) The mRNA of the canine *DLC1* gene contains the active RhoGAP and START functional domains of the human *DLC1* gene with a transcriptional start site distal to the defined promoter region.

Results

Complete results of conserved motif analysis of the sequence described in Figure 3.1 are listed in Appendix 3. There is a very strong conservation of Sp1 binding motifs between dogs and humans. Of the canine Sp1 sites, 69% are common to human, and 68% of the human sites are common to dogs. Furthermore, within the specific forms of the sites, interaction with pathway

signaling is common between the two, including *jun*, dihydrofolate reductase, and gamma-globulin signaling pathways. Differences observed include cyclooxygenase signaling Sp1 in dogs and heat shock protein 70 signaling Sp1 in humans. The patterns of transcription binding sites are presented in Figure 3.2. The first panel depicts the location of Sp1 binding sites. Note the increased density of CpG dinucleotides in the canine sequence relative to the human sequence. Note also the increased density of the Sp1 sites at the 5' end of the promoter region relative to the human sequence. The second panel depicts the non-Sp1 motifs in these sequences. The conservation is less striking in this grouping. Of the conserved elements, only 41% are common to both the human and canine sequences. Although specific pathway interactions are impossible to predict simply by the presence of conserved elements, the similarities conserved through time and the differences that have arisen are striking between the canine and human promoter elements of *DLC1*. The differences, while not surprising, may hint at convergent functions of this gene in the two species, which might be understood in the future.

Patient demographic data is presented in Table 3.1. The mean and median ages of the dogs with NHL were 7.8 and 7 years, respectively (range: 5-13y). The mean and median weights of the dogs were 24.6kg and 22.7kg, respectively (range: 5.6-48.4kg). Nineteen dogs were diagnosed with B-cell lymphoma and 2 with T-cell lymphoma. Diagnoses included lymphoma, malignant lymphoma, lymphosarcoma, and T-cell-rich B-cell lymphoma.

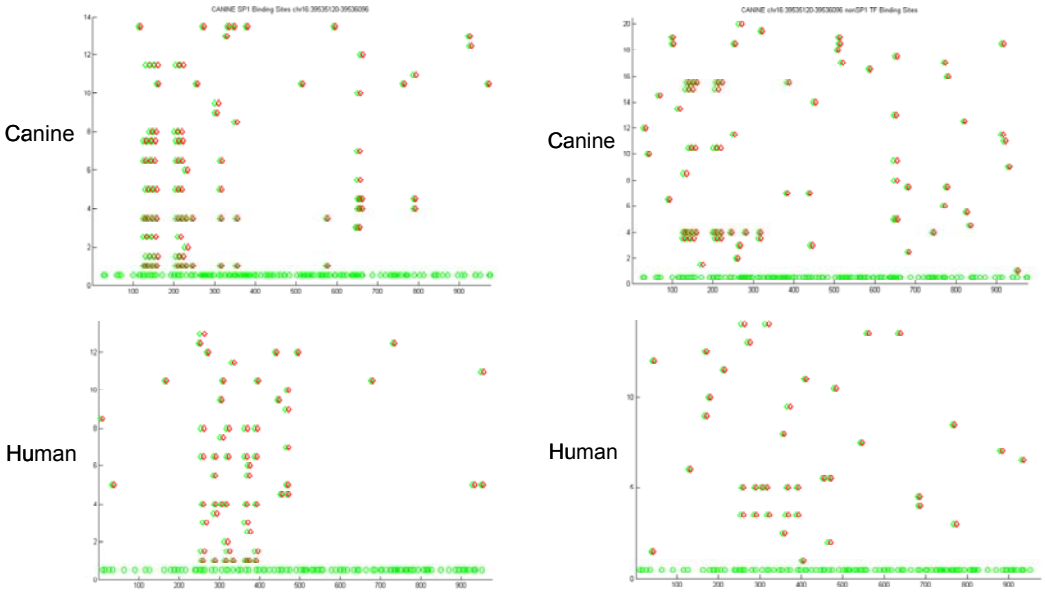

Figure 3.2: Comparison of the conserved element binding regions in the promoter, first exon, and first intron of canine and human *DLC1*. The increased CpG density of the canine sequence is evident in these images. Also, the density of Sp1 sites is greater in the dog at the 5' end of the promoter region. The distribution of the non-Sp1 conserved elements is similar between the two species, although the composition of these elements differs much more than the composition of the Sp1 elements. Elements are listed by number in ascending order beginning at the origin with the first 14 in Appendix 3 for each species listed.

The results of the COBRA analysis are presented in Table 3.2. The BstuI cut-site, located centrally in the amplicon (Figure 3.2) was methylated in seven of 21 cases, with no methylation detected by COBRA in the seven normal samples (Figure 3.4). The TaqaI cut-site demonstrated methylation in 19 of 21 cases, frequently complete in its cutting. This site was also weakly positive in two of seven normal samples (Figure 3.5). The HpyCh4IV cut-site showed visual evidence of methylation in every case and four of seven normal samples (Figure 3.6). By gel software analysis, however, 12 of 21 cases and three of seven normals were deemed positive. At the 3' end of the CpG island, 17 of 21 case

and no normal samples were positive for methylation by MSP. The relative ratios between the methylated and unmethylated bands are presented in Table 3.2.

Patient #	Sex	Breed	Age	BW	B/T	Stage	Diagnosis
6	FS	Am Co Sp	13	14.5	B	IV	Malignant lymphoma
7	FS	Affenpinsch	12	5.6	T	IV	Lymphoma
8	MC	Mix	5	11.7	B	IV	Lymphosarcoma
9	FS	Mix	11	30.4	B	IV	Lymphoma
10	MC	Engl Spring	6	22.7	B	III	Lymphosarcoma
12	MC	Mix	8	22.7	B	IV	Lymphoma
13	FS	Mix	7	22.5	B	IV	Lymphosarcoma
14	MC	Lab	6	43.7	B	III	Lymphoma
15	MC	Staff	10	34.8	B	IV	T cell rich B cell lymphoma
16	MC	Mix	12	28.1	B	IV	Lymphosarcoma
17	FS	Schnauz	11	10	B	N/A	Lymphoma
18	FS	Welsh Corg	7	17.7	B	V	Lymphosarcoma
19	MC	Blue Tick	7	34.1	B	III	N/A *
20	MC	Collie	5	32.2	T	II	Lymphosarcoma
21	FS	Engl Spring	5	25.7	B	V	Lymphosarcoma
24	MC	Rottweiler	5	36	B	V	Lymphoma
25	MC	Am Co Sp	8	15.2	B	IV	Lymphosarcoma
26	MC	Golden	5	48.4	B	III	Lymphoma
27	FS	Beagle	9	11.6	B	V	Lymphosarcoma
28	FS	Mix	5	17.5	B	V	Lymphoma
29	FS	Golden	5	34.2	B	IV	Lymphoma

Table 3.1: Patient demographic data. * This patient was diagnosed with lymphoma, but the original morphologic description was lost.

Bisulfite sequencing data is presented in Figure 3.7. Five clones each from normal 1 and cases 10, 18, and 27 were sequenced. As predicted by the pattern of COBRA results, methylation was present in the 5' region of the sequence at a visibly greater density than at the 3'. Density of methylation was the least in Dog 1, with sporadic methylation more prominent at the 5' end near the edge of the CpG island. Three of five CpG dinucleotides were methylated at the HpyCh4IV, only one of five at TaqaI, and only one of five at the BstuI cut-

sites. Dog 10 displayed slightly less methylation at the TaqaI cut-site than either dog 18 or 27. Dog 18 displayed the least methylation at the BstuI cut-site, with dog 10 intermediate between 18 and 27. All dogs displayed near complete methylation of the HpyCh4IV cut-site as suggested by the visual analysis of the gel, although methylation was slightly less complete in the normal dog. The AP-2 transcription factor binding site is located at the sixth CpG dinucleotide, and the ninth through fifteenth are included in the Sp1 binding sites.

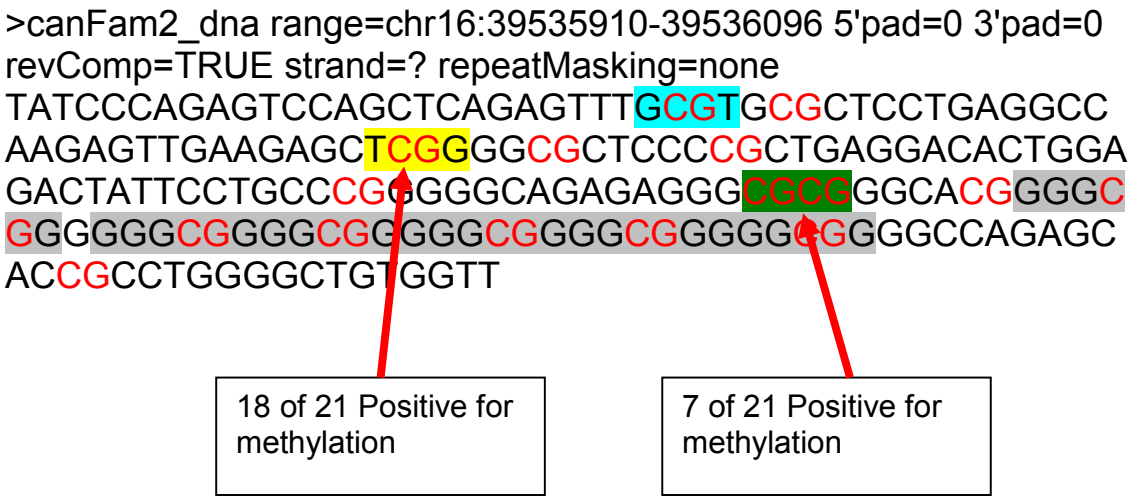

Figure 3.3: Diagram of the 5'COBRA amplicon. The restriction enzyme cut-sites are highlighted as noted. The density of Sp1 binding sites is particularly striking in this sequence. Note that methylation was evident at the HpyCh4IV and TaqaI with high frequency, but was less frequent at the BstuI cut-site.

The relationship between age and relative methylation at each of the assay sites was examined using linear regression analysis. The relationship identified at the TaqaI site was positive (r=0.394), but not significant (P=0.086). The calculated power of the analysis was also low (0.403). This was the highest

correlation identified. Normal samples were not included in this analysis, as they belong to a separate class, and the effect of lymphoma could not be separated from the effect of age.

The real time primers amplified an approximately 100bp fragment of DNA with a template of cDNA derived from normal lymph node. The optimized reaction yielded a single, clean band with no primer-dimer visible on a SybrGreen 1.5% agarose gel. The GAPDH real time primers were similarly optimized. Results of the real time experiment are presented in Table 3.2. Cycle threshold and melting curve results are included in Appendix 4. Expression was variable in both normal and lymphoma samples, ranging from 0 to 3.03 relative to the GAPDH expression within the matching sample. Only for case 29 was the expression undetectable, and this dog demonstrated methylation only in the MSP assay. There was no statistically significant relationship between methylation at any site and the expression of the gene in these NHL samples (P=0.423).

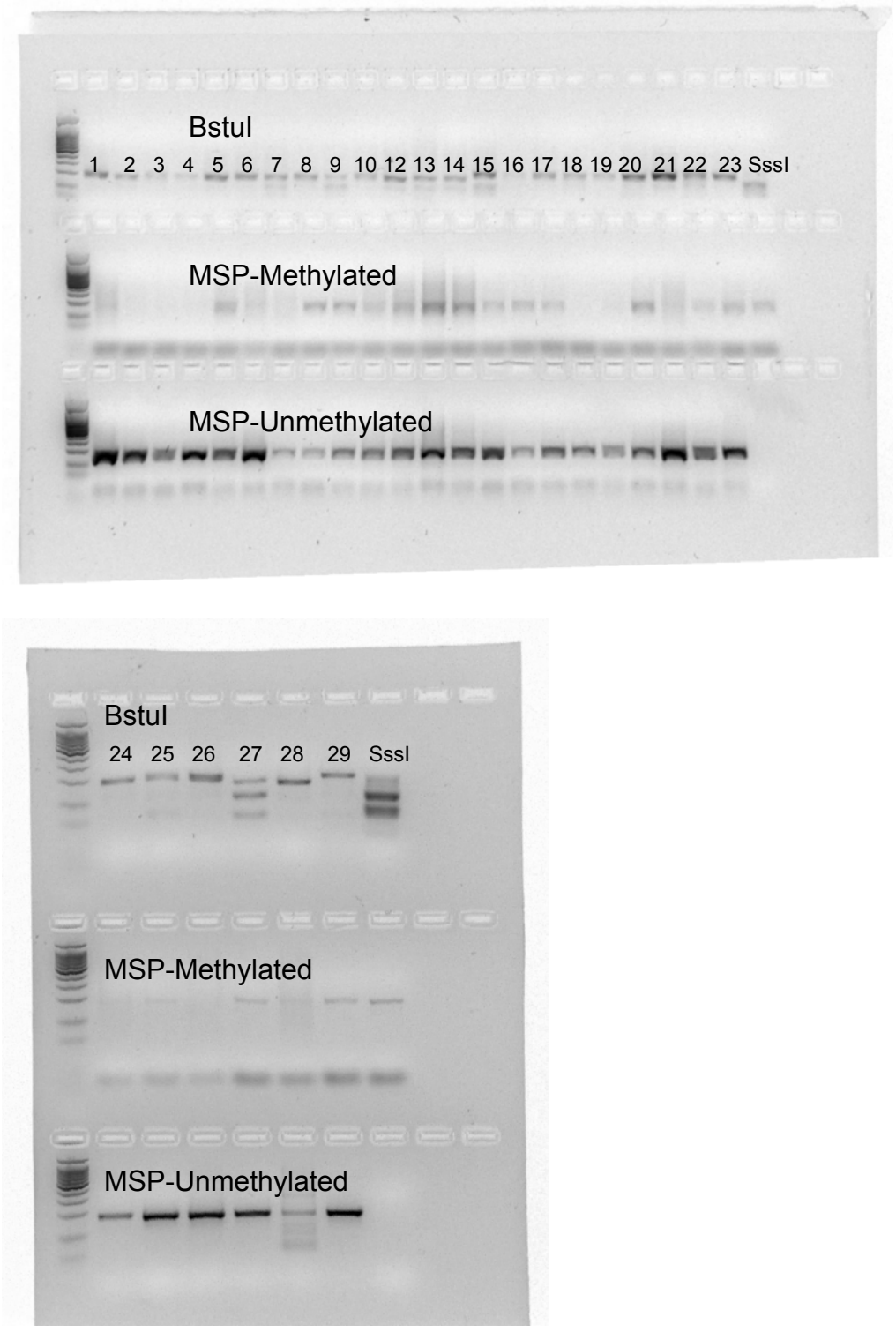

Figure 3.4: Agarose gel results of COBRA with BstuI digestion and MSP. Note positive results for cases 8, 10, 13, 14, 15, 16, and 27 for COBRA. Samples 1 through 5 as well as 22 and 23 are normal.

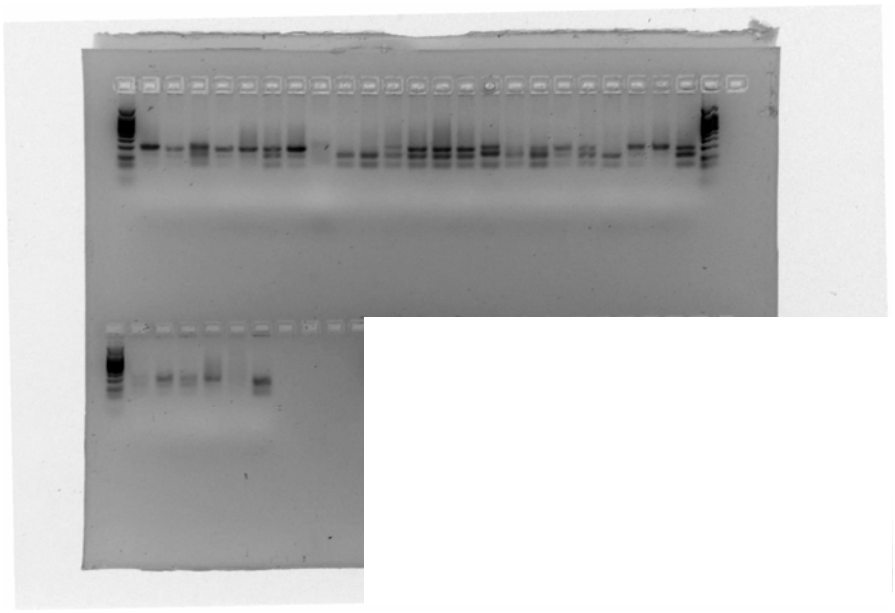

Figure 3.5: Agarose gel results of COBRA with TaqaI digestion. Note the relative increase in positive lanes compared to the BstuI digestion of Figure 3.4.

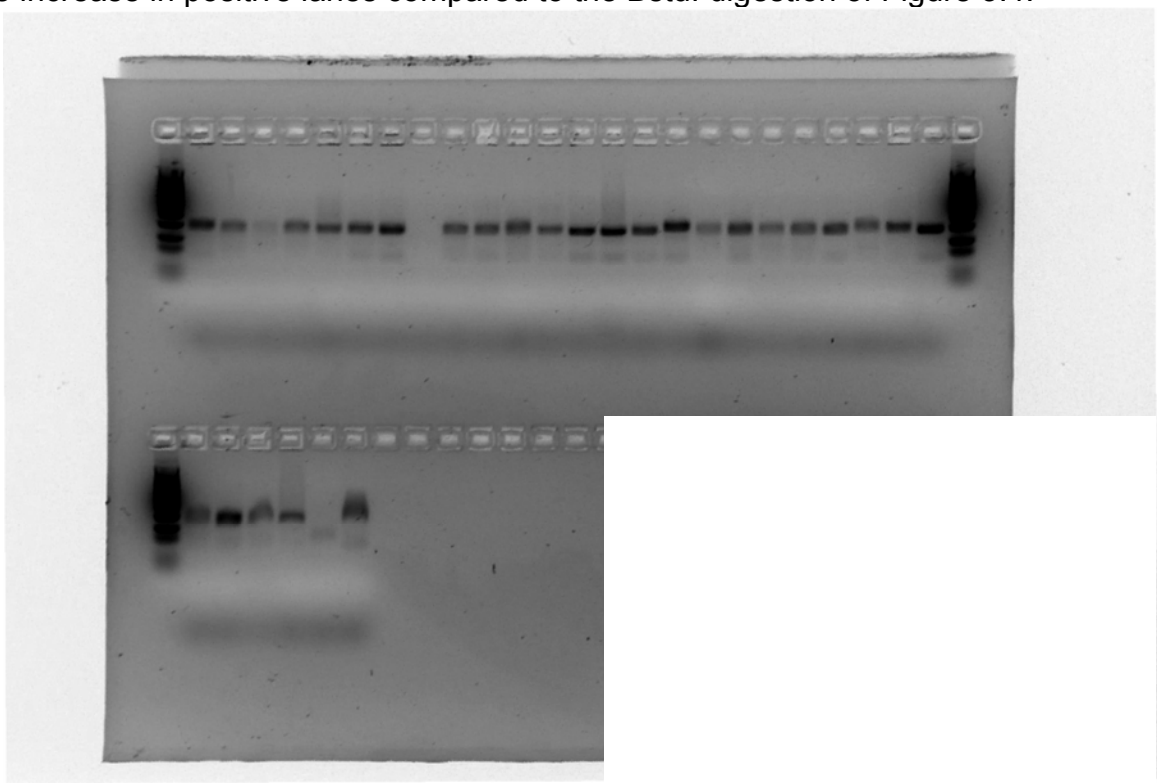

Figure 3.6: Agarose gel results of COBRA with HpyCh4IV digestion. Note the very high frequency of the 27bp band of low intensity. Because of the small size of the fragment, it is difficult to determine whether the site is completely cut, or only partially. Values for relative intensity of the small band by gel analysis are reported in Table 3.2.

5’TTTG**CG**TG**CG**CTCCTGAGGCCAAGAGTTGAAGAGCT**CG**GGG**CG**CT

CCC**CG**CTGAGGACACTGGAGACTATTCCTGCC**CG**GGGGCAGAGAGGG**CG**

CGGGCA**CG**GGG**CG**GGGGG**CG**GGG**CG**GGGG**CG**GGG**CG**GGGG**CG**GGGCC

AGAGCAC**CG**CCTGGG 3’

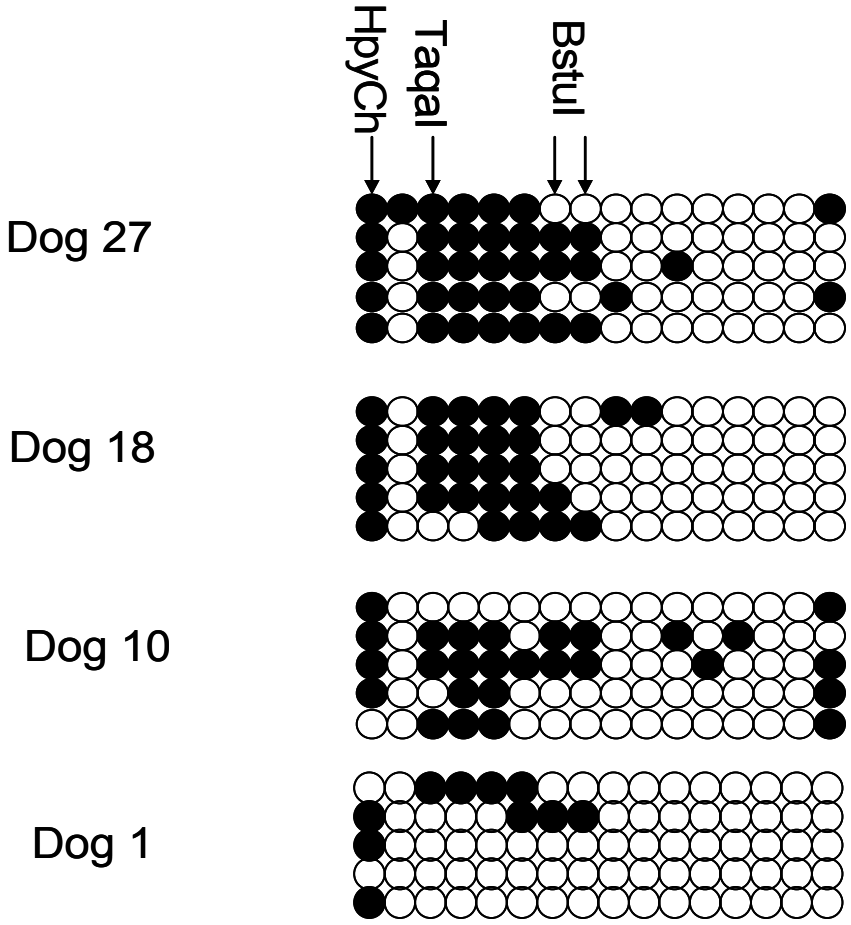

Figure 3.7: Bisulfite sequencing results for normal dog 1, and dogs 10, 18, and 27 with NHL. The corresponding DNA sequence is above with each CpG dinucleotide marked in bold. Open circles denote unmethylated CpG dinucleotides and black are methylated. Five clones for each dog were submitted for sequencing. Note the relatively lower methylation density for the normal dog. The high frequency of methylation at the HpyCh4IV cut-site in all dogs, including the normal dog, suggests that this CpG behaves as a genomic CpG dinucleotide and is routinely methylated. Note the minimal methylation in the right half each set of clones where the Sp1 sites reside.

Dog	B or T Cell	Rel Intesity Meth at HpyCh4IV	Rel Intesity Meth at TaqA	Rel Intesity Meth at BstuI	Meth:Unmeth Ratio for MSP	Relative Expression
1	Normal	0.0461	0	0	0	0.3618
2	Normal	0	0	0	0	N/A
3	Normal	0	0	0	0	0.0103
4	Normal	0	0	0	0	N/A
5	Normal	0	0	0	0	N/A
22	Normal	0.142	0.1148	0	0	0.0175
23	Normal	0.1234	0.0573	0	0	0.0248
6	B	0	1	0	0.2666	0.0686
7	T	0.1961	1	0	0.0661	0.0992
8	B	0	0	0.2625	0	0.0752
9	B	0.1501	0.7505	0	0.9251	0.0164
10	B	0.1616	0.6651	0.4209	0.4932	0.1984
12	B	0.1821	0.7968	0	0.2628	0.0034
13	B	0.1407	0.1093	0.1042	0.3039	0.0260
14	B	0.1345	0.4357	0.2742	0.3431	0.2078
15	B	0	1	0.2481	0.4366	0.1575
16	B	0.1794	1	0.3558	0.1679	0.0655
17	B	0	0.2191	0	0.5008	0.2127
18	B	0	1	0	0.17993	0.0412
19	B	0	1	0	0	0.0884
20	T	0.1428	0.0655	0	0	0.0508
21	B	0	0	0	0.3781	0.0171
24	B	0.0351	0.4653	0	0.0614	0.1063
25	B	0	1	0	0.1700	3.0314
26	B	0.116	1	0	0.1543	0.1895
27	B	0.1654	1	0.4372	0.1366	0.2806
28	B	0	1	0	0	0.1403
29	B	0	0	0	0.1355	0.0000
Totals		11/21	18/21	7/21	17/21	
P value for lymphoma		0.37	0.001	0.14	0.003	

Table 3.2: Results of COBRA and MSP methylation analysis and real time expression analysis of seven normal and 21 lymphoma samples. COBRA results are described as relative intensity of the methylated band out of all bands in the lane. The MSP results are described as a ratio between the methylated and unmethylated primer sets. Because these primer sets use different conditions for amplification, the ratio cannot be directly interpreted as a proportion of methylated DNA, but as a number relative to the other samples.

The cDNA of *DLC1* was cloned in fragments using the product of 5'RACE amplification. The active RhoGAP site of canine *DLC1* was sequenced in the predicted large fourth exon of the gene. It is located on chromosome 16, bases 39,503,331-39,504,328. Sequencing of genomic DNA amplified by the real time primer set confirmed the footprints of that assay in the predicted exons 12 and 13, and confirmed the sequence of the intervening intron. Primers were developed using the sequenced exonic regions to perform further sequencing of the cDNA. The 5' extent of exon 4 was identified to be identical in length to the orthologous exon of the human sequence, and slightly different from the length predicted by N-Scan.

Discussion

The promoter analysis presented in the previous chapter was augmented with a conserved motif analysis in this study of lymphoma biopsy samples. The CpG islands of both species are large, as would be expected in an island with the potential to contribute to epigenetic control. Relative to the human, the primary dog island is slightly smaller, but has greater CpG density. The conservation of Sp1 binding sites between dog and human is striking. The canine Sp1 sites are collected slightly more 5' and more densely relative to the human, with a less dense distribution of sites throughout the first exon and first intron region. The human sequence has a more condensed distribution with only a few sites in the region of the first intron and an overall lower number and density. The non-Sp1 binding sites are more evenly distributed throughout the sequence in both

species. Conserved elements common to both species include ras and jun pathway binding sites, not identified in the Promoterscan analysis. Similar sequences between human and dog include AP-2 sites, although the human site appears to be for AP-2 that interacts with CyclinD2, whereas the canine sites interact with epidermal growth factor receptor and Sp1. These findings suggest significant commonality of transcription control between dogs and humans, with subtle alterations introduced during the years of divergent development.

The COBRA results demonstrate a pattern of greater density of methylation in the 5' and 3' flanking regions of the promoter of the canine gene with less density of methylation near the core of the promoter region where, presumably, transcription is controlled. The likely explanation of this phenomenon may lie in the construction of the proposed canine gene promoter. The greater number and density of Sp1 binding sites, relative to the human gene, may provide a boundary region, preventing the spread of methylation into the core of the promoter, even in neoplastic lymphocytes.[13] In fact, the HpyCh4IV cut site, the first CpG in the bisulfite sequencing analysis, is also the first CpG included in the island in the Methprimer analysis. This CpG dinucleotide may function as a genomic CpG, rather than as part of the island, and be methylated in almost every case. The high rate of methylation in the bisulfite sequencing analysis supports this, as does the visual analysis of the gel image. The TaqaI site is slightly less frequently methylated, and the BstuI site is methylated in only one third of the cases examined. In spite of the apparent association between the BstuI site methylation occurring only in lymphoma cells, the low proportion of

methylation prevents this relationship from being statistically significant. Only the TaqaI site and the MSP data was significantly correlated with the neoplastic phenotype. Of these two, MSP is likely the better discriminator because methylation was present only in the NHL samples. Methylation at the BstuI site should continue to be evaluated in larger trials, as no normal sample was methylated there by COBRA analysis.

The bisulfite sequencing results provide a visual representation of the likely control apparatus of this canine gene. AP-2 does not appear to contribute significantly to the expression of canine *DLC1*, as the binding site was uniformly methylated in two of the three lymphoma samples and partially in the normal sample. It is likely that the high density of Sp1 overwhelms any contribution of AP-2, and protects other transcription factors within the core of the promoter region. There is methylation in only a small minority of the Sp1 binding sites. This is in contrast to the methylation pattern identified in *DLC1* in human prostate cancer. In this disease, it appears that the transcription factor binding region is more heavily methylated, contributing to silencing.[126] An Sp1 boundary phenomenon has been reported in the *BRCA1* promoter of breast cancer cells.[127] Investigators demonstrated that the Sp1 binding sites served as normal boundaries between the methylated and hypomethylated regions at the border of the gene control region. Furthermore, methylation of these binding sites resulted in inhibition of binding of Sp1. This boundary effect has been shown to be abrogated by specific mutation in a mouse model examining the *Aprt* gene.[13] In fact, no relationship appears to exist in the samples studied between the

methylation status of the examined CpG island regions and the expression of this gene. Expression was present in all but one sample, and was highest in one of the lymphoma samples. This is not surprising, given the apparent protection of the majority of the core promoter binding sites identified. Such a phenomenon has been identified in the human gene *hTERT*, which codes for the reverse transcriptase subunit of telomerase. The gene has been found to have discordant methylation and expression by several investigators.[128-130] In each case, transcription status was independent of assayed methylation or present in spite of methylation of the 5' region of the gene. Recently, investigators identified a critical, hypomethylated region around the transcription start site (TSS) of the h*TERT* gene that allows transcription in spite of heavy methylation upstream.[131] Using a ChIP assay, active chromatin marks were demonstrated; associated with the hypomethylated DNA at the TSS, and inactive chromatin marks were identified associated with the methylated region upstream.[131] It is likely that the canine *DLC1* gene is similar, in that methylation not present in normal tissue can be readily demonstrated in the CpG island of canine NHL samples, but the core of the promoter appears unmethylated, which allows transcription to occur.

Of the 21 cases of lymphoma in this study, two were of T-cell immunophenotype. Unlike in the first study, methylation was identified in both cases. Dog 7 demonstrated at least some methylation at every assayed point except the BstuI site. Dog 20 demonstrated methylation at both the HpyCh4IV and TaqaI site. Neither of these were assayed in the previous study, and dog 20 was negative by MSP. It is not surprising that CpG dinucleotides near the edge

of the CpG island would be methylated in T-cells. Nor is it novel that methylation plays a role in T-cell lymphoid neoplasia. Three of six human patients with T-cell ALL demonstrated methylation of *DLC1*, among several genes with significant methylation present.[67] Methylation of the gene *DDX51* was the only gene in a ten gene panel that could reliably distinguish between B-cell and T-cell forms of the disease by its absence in T-cell cases.[67]

Genomic hypomethylation and accumulation of CpG island hypermethylation has been demonstrated to be a common phenomenon associated with aging in humans.[132] This may be contributory to the development of cancer as individuals age. A similar phenomenon of accumulated CpG island hypermethylation has not been demonstrated in dogs. In this series of lymphoma samples, there was no statistically significant association between age and the degree of identified methylation. The relationship between relative methylation at the TaqaI site and age showed the strongest association. This phenomenon should be studied further in normal and diseased populations of dogs with sufficient sample size to answer this question.

The results of the real-time expression study demonstrated no pattern of expression associated with methylation. The foregoing discussion likely explains this result, as the majority of the Sp1 transcription factor binding sites appear not to be methylated. It is possible that this canine gene is constructed such that silencing by methylation will not be identified in cancer samples. It also may be that other forms of cancer will have silenced *DLC1*. Dog 29, the only dog without measurable expression, had no apparent differences in methylation pattern to

explain this change. It may be the case that histone changes are more important for expression of this gene in dogs, although these were not assessed in this study.

Cloning of the cDNA was difficult. Amplification of genomic DNA with the real time primer set resulted in an 800bp amplicon. Sequencing of this amplicon confirmed placement of the primer pairs in two separate exons with a large intron between. It also allowed design of primers near the 3' end of the cDNA for further sequencing attempts. The boundaries of the predicted exon 4 were cloned and sequenced. Contained within this fragment is the code for the RhoGAP active site of the DLC1 protein. This confirms the function of this gene in the dog.

It is worth noting that none of the diagnoses provided by the board-certified pathologists in this study conformed to the Working Formulation classification system. This is an extremely common practice in veterinary medicine. If comparative studies are to bear fruit on a mechanistic level, disciplined classification must become the norm and clear prognostic significance must be attached to the diagnosed forms of NHL. Development of diagnostic technology for flow-cytometry, antigen-receptor gene rearrangement, and, now, epigenetic alterations of cells will define the points of origin of canine NHL in B-cell biology that have already been defined in human NHL.[65;133] Only with this information will the comparative model be complete.

The results of this study further characterize the similarities and differences between the human and canine *DLC1* gene. They confirm the first

hypothesis that the promoters of both human and canine *DLC1* have important similarities in content of methylation sensitive transcription factors. Significantly, the density of Sp1 sites in dogs is more numerous and more concentrated at the 5' end of the promoter, potentially making the CpG island more resistant to hypermethylation. Differences in types of transcription factors also exist, hinting at differences in control pathway mechanisms between the species. As in the 3' region of the canine CpG island, hypermethylation exists at the 5' end of the island, confirming the second hypothesis. It appears to become infrequent and sporadic near the numerous Sp1 sites. This likely explains the lack of support for the third hypothesis that this methylation would be inversely related to expression. In fact, methylation identified by these assays appears to have no effect on gene transcription in the dog. Unlike the human condition, *DLC1* is not silenced in canine NHL. The mRNA of canine *DLC1* contains the RhoGAP active site, confirming the function of this gene in dogs.

This series of studies demonstrates that the molecular machinery is present in dogs that could lead to epigenetic control of gene expression by promoter CpG island hypermethylation. Although silencing of *DLC1* does not appear to be a hallmark of canine NHL, the presence of hypermethylation at the BstuI site and with the MSP assay, compared to normal lymphocytes, suggests that it may be used as a biomarker for neoplasia in abnormal lymphoid populations. A larger study of both normal and NHL samples will be necessary to validate *DLC1* as a biomarker. Expansion of the analysis to more genes, to begin to establish the patterns associated with lymphoma, and ultimately specific

forms of lymphoma, in dogs will further define the comparative framework of NHL etiology, pathobiology, and therapy between dogs and humans.

Materials and Methods:

In Silico methods:

A list of 7660 putative transcription factor motifs was obtained from the SigScan database of the Bioinformatics and Molecular Analysis Section of the Center for Information Technology, National Institutes of Health. (http://www-bimas.cit.nih.gov/). Using the regular expressions pattern matching function in MATLAB® version R2007a (http://www.mathworks.com/), these motifs were compared with the canine and human DLC1 DNA sequences and the start and stop sites were recorded for all perfect matches. This resulted in 83 and 87 matched transcription factor motifs for the dog and human sequences respectively. Of these, 10 canine and 14 human motifs represent consensus motifs that could potentially represent different specific transcription factor binding sites. There were 60 canine and 63 human motifs that were unique. The locations of CpG dinucleotides were determined in a similar fashion. Graphic figures of the results were produced using the plot function of MATLAB®.

Primer design and functional domain analysis: Primers for COBRA were designed in part using MethPrimer CpG island analysis tool (http://www.urogene.org/methprimer/ index1/html.[123] The cloned cDNA sequence was examined using InterProScan web-tool to identify protein functional groups (www.ebi.ac.uk/InterProScan/index.html).[125]

In Vivo methods:

Sample collection and preparation: Samples of five normal lymph nodes and three peripheral blood lymphocyte collections were divided into two aliquots immediately after thawing in an ice bath. DNA and RNA will be harvested using Qiagen DNeasy Tissue and RNeasy according to the provided protocols (Qiagen, Inc. USA. Valencia, CA). Briefly, for RNA the tissue will be stabilized in RNAlater reagent to arrest RNase activity. Samples will be homogenized and lysed, DNA sheared, and ethanol added. The solution will be centrifuged in a proprietary spin column to bind the total RNA. The RNA will be washed three times and, finally, eluted in RNase-free water. Peripheral blood mononuclear cells were isolated over a ficoll-hypapaque (Sigma-Aldrich, St. Louis, MO) gradient and preserved at -80ºC until analysis. DNA was extracted using the Qiagen DNeasy Tissue kit (Qiagen, Inc. USA. Valencia, CA), and then bisulfite treated using the Zymo Research EZ DNA Methylation Gold^{c} kit (Zymo Research Corporation, Orange, CA). DNA from normal canine lymph nodes was treated with SssI, a DNA methyltransferase, and SAMe to methylate all CpG dinucleotides prior to bisulfite treatment in the sequence and serve as a positive control.

Combined bisulfite restriction analysis (COBRA): The MethPrimer website was used to locate a primer region at the 5' end of the CpG island to serve as the left primer. This contained a single CpG dinucleotide, so a second primer was designed to be complementary to a TpG sequence at the same location. The right primer was constructed 187bp 3' to the first primer pairs, and contained a

single CpG dinucleotide as well, so a second primer was constructed at this location as well. The conditions for PCR were an annealing temperature of 60°C for 60s, an extension temperature of 72°C for 60s, and a melting temperature of 95°C for 60s, repeating for 36 cycles. The product size of these primers is 187 bp and contains one BstuI cut-site that recognize the sequence CGCG and yield fragments of 116 bp and 71 bp. It also contains one TaqaI cut site that recognizes the sequence TCGA and yields fragments of 128bp and 59bp. It also contains one HpyCh4IV cut site that recognizes the sequence ACGT and yields fragments of 160 and 27bp. The PCR product was purified with the Zymo Clean and Concentrator kit (Zymo Research Corporation, Orange, CA) and eluted in 20μL of HyPure water. For BstuI, 10μL of PCR product was added to 2.5μL of Buffer 2, 1μL of BstuI, and 11.5μL of HyPure water, and incubated at 60ºC for 4h. For TaqaI, 8μL of PCR product was added to 2.0μL of Buffer 3, 1μL of 10X bovine serum albumin, 1.5μL of TaqaI, and 7.5μL of HyPure water, and incubated at 65ºC for 4h. For HpyCh4IV, 8μL of PCR product was added to 2.0μL of Buffer 3, 1.5μL of HpyCh4IV, and 8.5μL of HyPure water, and incubated at 37ºC for 4h. Controls were bisulfite-treated DNA from normal lymphocytes (negative) and bisulfite-treated SssI-treated DNA from normal lymphocytes (positive). The PCR products were run on a 1.5% agarose gel with ethydium bromide.

Methylation Specific PCR: The MethPrimer website was used to construct primer pairs for methylation-specific PCR (MSP) that amplify a product of 185 base pairs (bp). Using bisulfite treated DNA, the conditions for MSP were

optimized. The methylated primer set was used to amplify the region with an annealing temperature of 62°C for 30s, an extension temperature of 72°C for 30s, and a melting temperature of 95°C for 15 seconds, repeating for 32 cycles. The unmethylated primer set was used to amplify the region with an annealing temperature of 62°C for 60s, an extension temperature of 72°C for 60s, and a melting temperature of 95°C for 15 seconds, repeating for 32 cycles. The PCR products were run on a 1.5% agarose gel with ethydium bromide. Bands present in the methylated primer set lanes indicated the presence of methylated DNA in the template. Bands present in the unmethylated primer set lanes indicated the presence of unmethylated DNA in the template. The negative control was bisulfite converted DNA from normal lymph node, and the positive control was SssI treated bisulfite converted DNA from normal lymph node

Sequencing of cDNA: The Ambion FirstChoice RLM-RACE (rapid amplification of cDNA ends) (Ambion, Inc. Austin Texas) kit was used to isolate the mRNA of canine *DLC1*. This kit creates a copy of the 5' and 3' ends of the mRNA by amplifying only full-length mRNA with a 5'GTP cap in place. This ensures complete amplification of the mRNA strand. Briefly, total RNA was treated with calf intestinal phosphatase to remove free 5' phosphates from rRNA, fragmented mRNA, tRNA, and DNA fragments. The 5' cap of mRNA remains in place. This cap was removed and a 45 base adaptor added to the complete mRNA. A random-primed reverse transcription reaction and nested PCR was used to amplify the remainder of the 5' end. A similar procedure was employed on the 3' end of the complete mRNA by placing a 3' adaptor and repeating the

random-primed reverse transcription and nested PCR. Exonic primers that overlapped by a minimum of 50 bases were designed according to Ambion recommendation to amplify the regions of the mRNA between the 5' and 3' amplified segments. The PCR product was purified with the Zymo Clean and Concentrator kit (Zymo Research Corporation, Orange, CA) and eluted in 10μL of HyPure water. Using the Invitrogen TA Cloning kit (Invitrogen Corporation, Carlsbad, CA), to 1μL of high-salt solution (provided) and 1μL of vector was added 5 μL of PCR product and allowed to incubate at room temperature for 30 minutes. These were ligated directly into the vector without any further processing, and transfected into competent cells provided for transformation on ice for 30 min. After 30s heat-shock at 42ºC, the cells were incubated in SOC medium for 60 minutes, then incubated overnight on ampicillin-containing agar. Colonies were selected and confirmed to contain the desired clone by agarose gel electrophoresis. Five clones per amplification were submitted with plasmid primers to the DNA Core for standard dideoxynucleotide sequencing.

Bisulfite sequencing: The PCR product of 5' COBRA primer set from three cases and a normal dog was amplified, purified with the Qiagen Clean and Concentrator kit (Qiagen, Inc. USA. Valencia, CA) and eluted in 10μL of HyPure water. Using the Invitrogen TA Cloning kit (Invitrogen Corporation, Carlsbad, CA), the product was transfected into competent cells provided for transformation as described above. Single colonies of transformed cells were selected and grown overnight in enrichment broth with ampicillin. Plasmid DNA was extracted using the Qiagen miniprep^{e} kit (Qiagen, Inc. USA. Valencia, CA), and the

presence of an insert, indicating a transformed cell, detected by PCR. Five clones of each purified plasmid DNA were submitted with universal primers where they were sequenced by the DNA Core using a standard dideoxynucleotide sequencing technique. CpG dinucleotides within the sequences were mapped and labeled as methylated if cytosine remained unconverted, and unmethylated if a thymidine was in a cytosine position.

Expression: Primers were designed that reside in two adjacent exons near the 3' end of the mRNA. These primers were based on homologous regions of code using BLAST tools and the human mRNA to identify regions in adjacent exons of the dog gene. It is important that these primers span an intron so that unexpected amplification of DNA will result in a product of markedly different length. Reverse-transcriptase PCR was used to create a cDNA copy of the mRNA. This cDNA copy was amplified in tandem with GAPDH cDNA to yield relative copy numbers in SYBR-Green Real-Time PCR. This was performed in five normal dog samples as a reference point, and all banked NHL samples. Assays were run in triplicate to avoid inter-assay variability.

Statistics: Methylation density of each NHL sample was compared to expression of the mRNA relative to normal lymphoid tissue using an exact Wilcoxon analysis. The relationship between degree of methylation and level of expression and degree of methylation and age were evaluated using a linear correlation model. Significance was set at P=0.05.

Chapter 4

Effect of Zebularine Demethylation Therapy on Radiosensitivity of MEC1 Cells

The foregoing chapters have demonstrated strong evidence that CpG island hypermethylation of the *DLC1* gene occurs in canine NHL but not in normal canine lymphoid tissue, as is the case in human NHL. Although *DLC1* is not silenced in canine NHL, the methylation observed may be a marker of the activity of epigenetic mechanisms in these tissues. Indeed, it has been estimated that hundreds of genes are hypermethylated and epigenetically dysregulated in a single cancer.[134] The aim of this series of experiments was to examine responsiveness of an NHL cell line characterized by hypermethylation of *DLC1* to demethylation therapy preceding external irradiation or radiopharmaceutical therapy.

The demethylating agent zebularine (See Figure 1.4) is a cytidine analog that is incorporated into DNA during replication. As such, it is only effective in dividing cell systems. It appears to exhibit preferential inhibition of DNMT1 through formation of a covalent bond with the enzyme at the 6 position on the pyrimidine ring.[135] The structure of the ring prevents electrophilic substitution for a methyl group at the 5 position, resulting in irreversible binding of the enzyme to the false base.[136] This results in the metabolic destruction of the enzyme, and demethylation of the DNA sequence. Zebularine is an acid-stable ribonucleoside with previously demonstrated oral bioavailability.[137] This makes it an attractive compound for clinical use, as all other cytidine analogues in current use must be injected to have activity.[137]

External beam radiation has been used in conjunction with chemotherapy in treating canine and human NHL.[138;139] Lymphoma cells are known to exhibit greater radiosensitivity than solid tumors.[140] As such, measuring interactive effects of radiation and demethylation therapy requires dose selection that is sublethal. External irradiation with an MDS Nordion Gammacell 40 Exactor ^{137}Cs irradiator delivers a highly homogeneous dose to the contents of the irradiation chamber. It does so at a high dose-rate. In the case of the irradiator used the rate was approximately 100cGy/m. Irradiation of cells *in vitro* in this manner serves as a model for external beam therapy of patients. External irradiation also serves as a well calibrated dose control for comparison to the radiopharmaceutical preparation. For each experiment performed, cells were plated in triplicate aliquots and subjected to repeated daily measures to maximize the statistical power to detect differences among the treatment groups. The combination of the external irradiator and zebularine models the interaction of high dose-rate radiation and epigenetic gene expression modification.

As was discussed earlier, ^{177}Lu-DOTA-TATE has shown promise as a therapy agent in human SSTR expressing tumors.[102-104;141] As human NHL expresses SSTR2 receptors in approximately 80% of cases, this radiopharmaceutical compound offers promise of effective, selectively targeted radiotherapy.[86] The efficacy of radiopharmaceutical therapy has been demonstrated by the currently approved products, Zevalin® and Bexxar®.[79;80] However, their ability to interact with chemotherapy is hampered by bone marrow dose limitations. The favorable plasma kinetics of a radiolabeled peptide may

deliver a similar lethal radioactive payload to the malignant cells with minimal marrow limitation, allowing it to be combined with chemotherapy in close temporal proximity. The question of optimal radionuclide between the currently available RIT drugs is a source of debate.[72] Lutetium-177 offers potential advantages over both current drugs. Compounds labeled with ^{177}Lu have resulted in improved tumor responses in solid tumors over other radionuclides at similar tumor-absorbed doses in a mouse xenograft model.[100] Combination with demethylation therapy may enhance the efficacy of the radiolabeled peptide, resulting in better tumor control and patient outcome. To date, there has been no examination of this question in NHL.

The purpose of this series of experiments was to evaluate the interactive effects of demethylation and two qualities of radiation, high dose-rate external irradiation and low dose-rate radiopharmaceutical therapy. The experiments examined the effect of external irradiation alone, ^{177}Lu-DOTA-TATE therapy alone, and each following treatment with increasing doses of zebularine.[142] Uptake and efflux experiments were performed in the human CLL cell line MEC1, a semi-adherent population of cells which express somatostatin receptors and lack expression of *DLC1* due to promoter hypermethylation. Results were used to determine ^{177}Lu-DOTA-TATE accumulation within the cells for dosimetry.[53] The presence of *DLC1* hypermethylation may serve as a marker signifying that epigenetic modification therapy could enhance targeted therapy of NHL. The hypotheses of this study were:

1) Uptake and efflux of ^{177}Lu-DOTA-TATE will be the same as that determined for ^{111}In-DOTA-TATE in the Lewis laboratory and will not be affected by zebularine treatment.

2) Similar doses of radiation will cause similar effects on MEC1 cell proliferation and viability, regardless of the quality of the radiation.

3) Zebularine dose will have a synergistic effect with radiation dose in causing decreasing proliferation and viability with increasing dose of drug and radiation.

4) Methylation levels of genes associated with cell cycle regulation, progression to apoptosis, and tumor suppression will decrease with increasing doses of zebularine.

Results:

An uptake study of ^{177}Lu-DOTA-TATE was performed with untreated MEC1 cells and MEC1 cells treated with 50μM, 100μM, and 200μM zebularine (Table 4.1). Similar to ^{111}In-DOTA-TATE, uptake peaked at approximately 2% at two hours (Figure 4.1).[94] Overall, the concentration of zebularine resulted in a statistically significant difference in uptake (P=0.02). An efflux study was performed using untreated cells and cells treated with 200μM zebularine (Table 4.1). Efflux was dramatic, with 60% of the activity leaving the cells by 15 min, but the residual remained relatively stable over the four hour window (Figure 4.2) with no statistically significant effect of concentration (P=0.28).

Percent Uptake						
Zebularine	**30min**	**SEM**	**60min**	**SEM**	**120min**	**SEM**
0	1.0863	0.0988	1.3352	0.0718	2.0322	0.2990
50	1.0095	0.0811	1.2257	0.1760	2.0155	0.2720
100	0.8416	0.0570	1.1517	0.1030	1.5871	0.1220
200	0.5544	0.1190	0.7127	0.0840	1.0454	0.1840
Efflux- Percent Cell Retention						
Zebularine	**15min**	**SEM**	**30min**	**SEM**	**60min**	**SEM**
0	39.1889	3.5970	37.3892	2.4620	31.9767	2.0370
200	39.5105	2.7420	42.0717	1.7660	36.1122	1.2310
Zebularine	**120min**	**SEM**	**240min**	**SEM**		
0	29.3233	1.5050	24.7351	1.2510		
200	33.1307	1.2960	27.3712	0.8270		

Table 4.1: Uptake and efflux study data. Each time-point is expressed as a percentage of cell-associated radioactivity with the standard error of the mean provided.

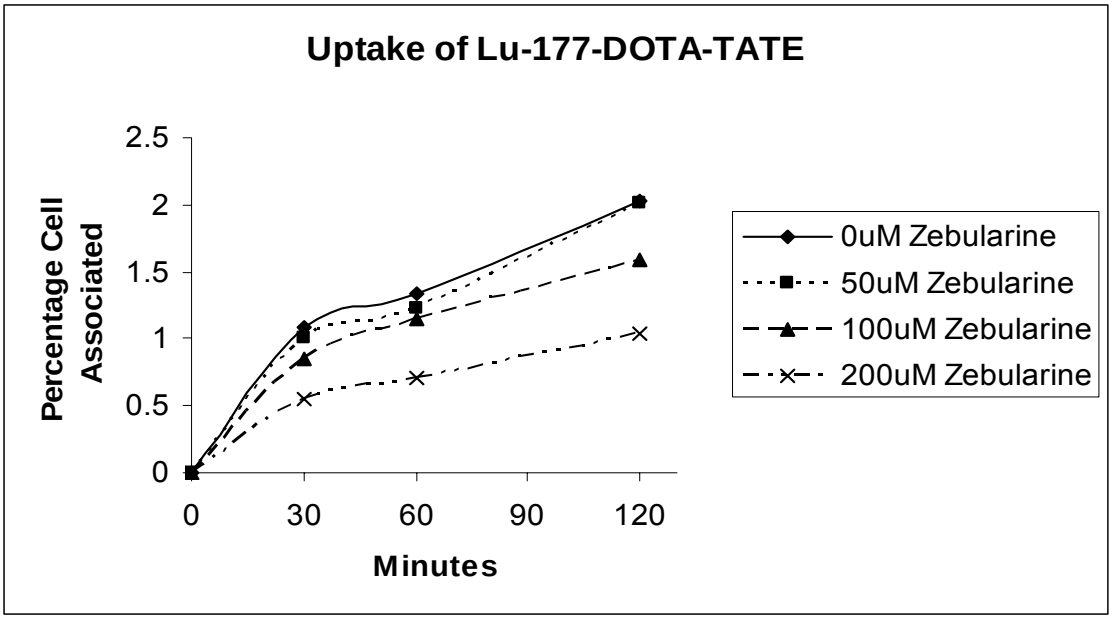

Figure 4.1: Uptake of ^{177}Lu-DOTA-TATE by MEC1 cells over a period of 2h. The differences in uptake as a function of concentration of zebularine were statistically significant over the time-period (P=0.02).

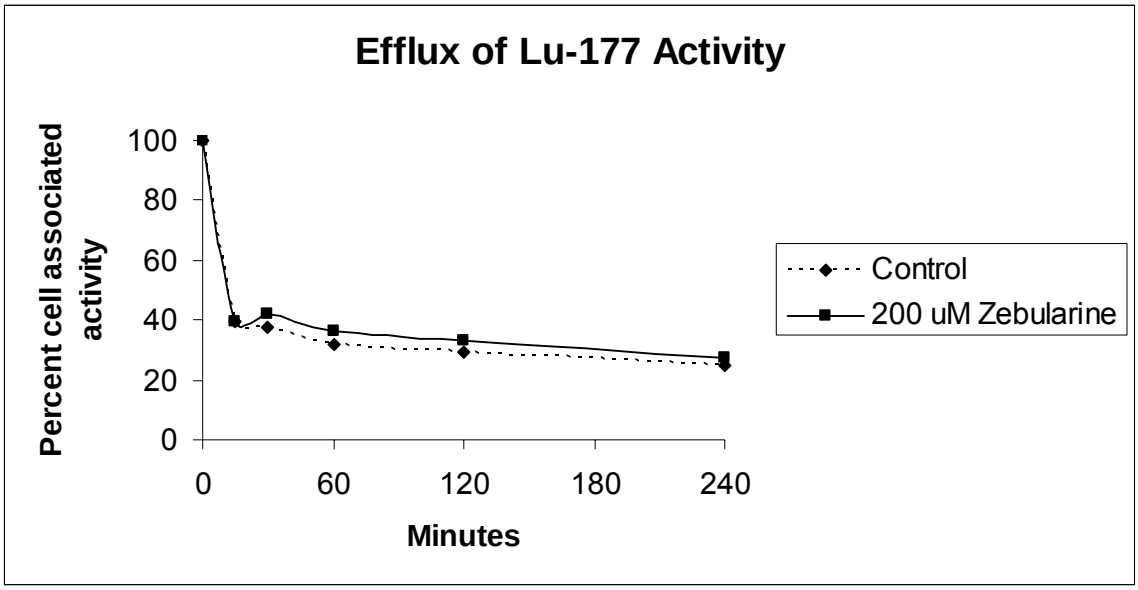

Figure 4.2: Cellular efflux of ^{177}Lu activity over 4h. No difference was observed in efflux between untreated cells and cells treated with 200μM zebularine.

For these experiments, dose to the cells delivered by the MDS Nordion Gammacell 40 Exactor ^{137}Cs irradiator was calculated by a dose rate of 0.984 Gy/min (98.4 rad/min). This irradiator delivers an extremely homogeneous dose to the contents of the chamber. Exposure times were calculated to be 31s, 1:01min, and 2:02min. Doses delivered by the radiopharmaceutical preparation of ^{177}Lu-DOTA-TATE were calculated using an MCNP model (MCNP5). The calculated dose to the nucleus or cytoplasm due to a decay event is listed in Table 4.2. Doses used were 2.78μCi/well for 0.5Gy, 5.55μCi/well for 1 Gy, and 11.1μCi/well for 2 Gy. Complete formatted data is presented in Appendix 4.

Location of Lu-177	Dose to Nucleus (Gy/decay)	Dose to cytoplasm (Gy/decay)
Nucleus	0.0091	0.0041
Cytoplasm	0.0041	0.0053
Water matrix outside of the cell	0.0009	0.001

Table 4.2: Dose to nucleus or cytoplasm based on location of origin of emission.

MEC1 cells plated at 4 X 10^5/mL per well in 24 well plates received 0Gy, 0.5Gy, 1Gy, and 2Gy of radiation as a single dose from the external irradiator. The cell proliferation curves are shown in Figure 4.3. The radiation reduced the proliferative potential of the cells in a dose-dependent manner to a maximum decrease of 37% at a dose of 2Gy on day 2 (P=0.0026). Cell doubling time increased from 24h with no radiation to 39h with 2Gy. Cell viability was also reduced, although only in a trend toward dose-dependence (P=0.0961). The control cells grew to a concentration by day 3 that resulted in a lag phase and decreased proliferation rate and viability.

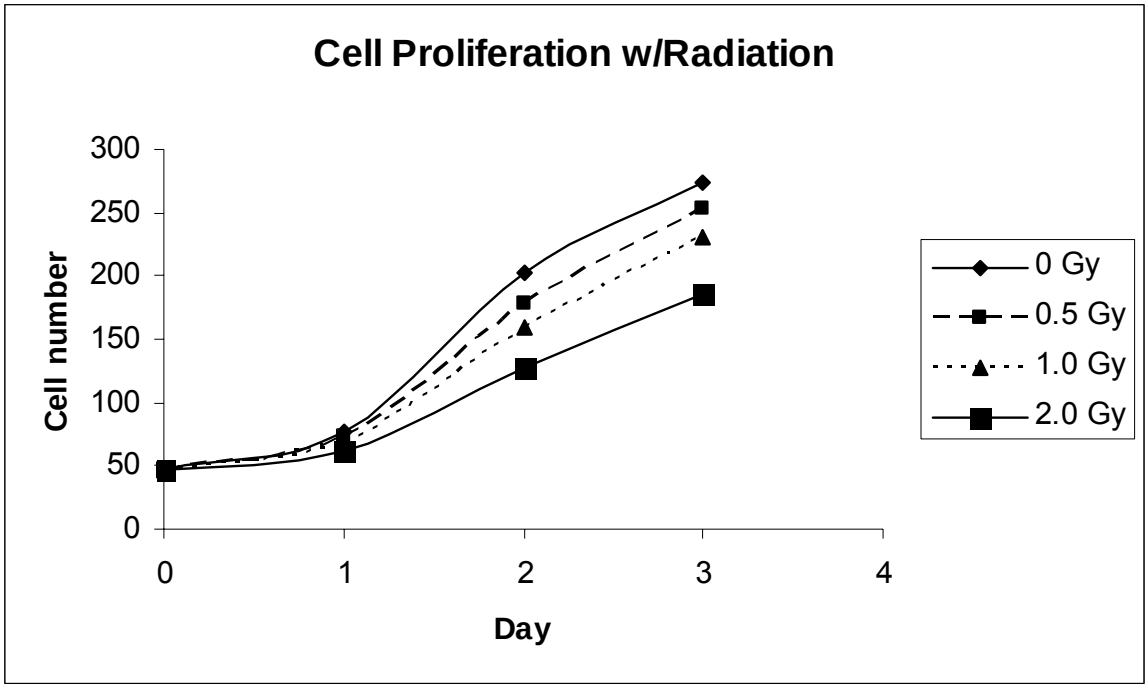

Figure 4.3: Cell proliferation after external irradiation. Proliferation over a three day period was decreased significantly by increasing dose of radiation (P=0.0026).

MEC1 cells plated at 4 X 10^5/mL per well in 24 well plates were treated for 48 h with 0μM (control), 50μM, 100μM, and 200μM zebularine. The zebularine decreased cell proliferation in a dose-dependent manner over this time-period ($P<0.001$, $r^2=0.819$) (Figure 4.4). The IC_{20} and IC_{50} values of zebularine for MEC1 cells were calculated to be 75μM and 195μM. No statistically significant alteration in cell viability was observed. Although zebularine decreased MEC1 proliferation in a dose-dependent manner during the period of exposure, no residual effect remained. Cells grew at the same rate, regardless of prior treatment after removal from zebularine, washing with complete medium, and plating at 4 X 10^5/mL per well in 24 well plates (Figure 4.5).

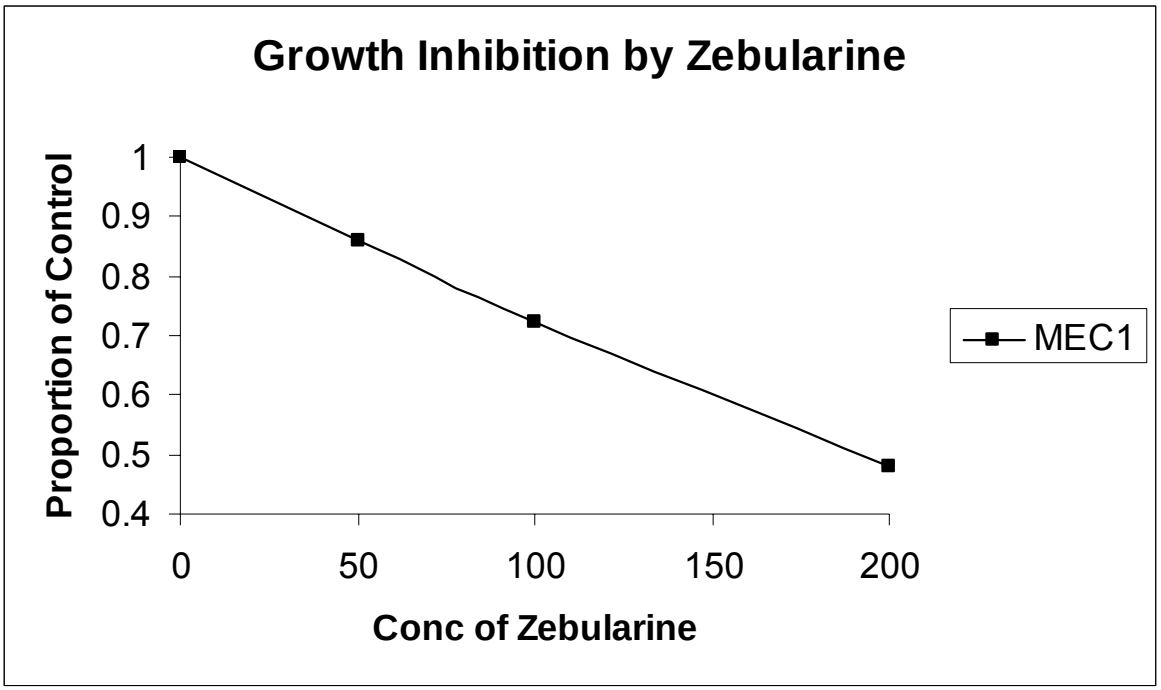

Figure 4.4: MEC1 growth inhibition by zebularine is dose-dependent and linear ($P<0.001$, $r=0.904$, $r^2=0.819$). No similar change in cell viability was observed. IC_{20}=75μM. IC_{50}=195μM.

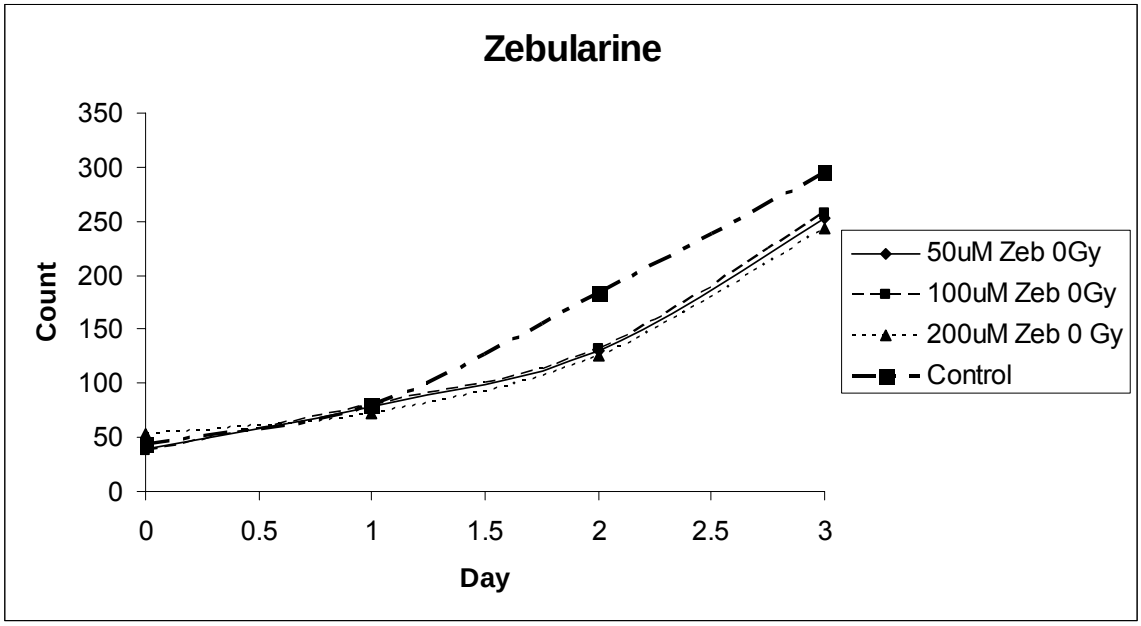

Figure 4.5: Cell growth curves after 48h treatment with 0μM (control), 50μM, 100μM, and 200μM zebularine. No significant difference was observed between the growth rates of these groups.

After treatment with 0μM, 50μM, 100μM, and 200μM zebularine, MEC1 cells plated at 4 X 10^5/mL per well in 24 well plates received 0Gy, 0.5Gy, 1Gy, and 2Gy of radiation as a single dose from the external irradiator. At each dose of radiation, a zebularine dose-dependent decrease in cell proliferation was observed, with the most dramatic effect in the cells treated with 2Gy radiation (Figure 4.6). The interaction between zebularine dose and radiation dose was highly statistically significant ($P<0.0001$). Given the lack of dose-dependent decrease in cell proliferation resulting from zebularine alone, this interaction is synergistic. A decrease in cell viability over time was also observed, with a significant effect of zebularine ($P=0.002$) and radiation ($P=0.0006$), but no

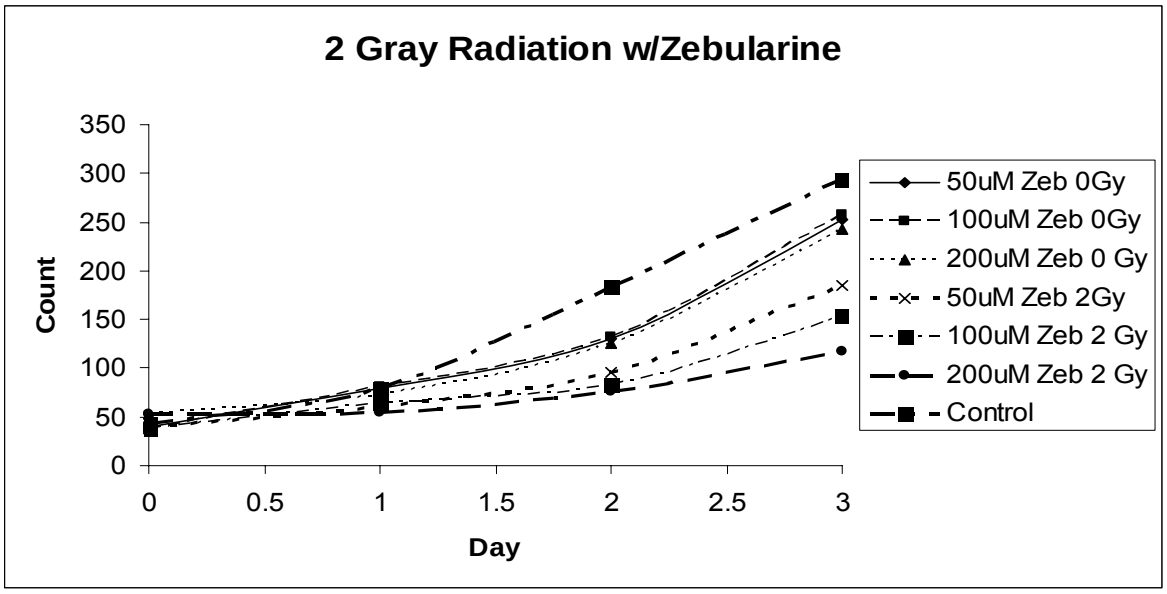

Figure 4.6: Cell proliferation after 2Gy radiation by zebularine dose with all zebularine controls included. Note the progressive, dose-dependent decrease in proliferation observed at increasing concentrations of zebularine treatment up to approximately 50% for the cells treated with 200μM zebularine.

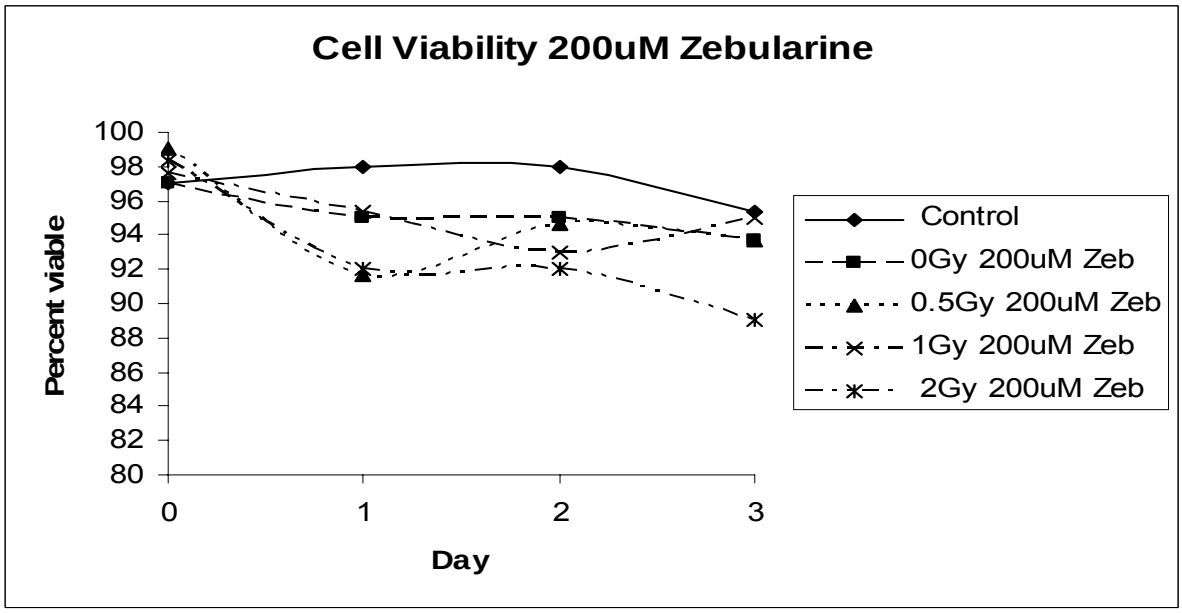

Figure 4.7: Cell viability by radiation dose over time for MEC1 cells treated with 200μM zebularine. The maximal decrease was only 5% relative to controls, compared to a 50% decrease in proliferative potential.

interaction (0.4976). This demonstrates an additive, not a synergistic effect in this instance (Figure 4.7).

After treatment with 0μM, 50μM, 100μM, and 200μM zebularine, MEC1 cells plated at 4 X 10^5/mL per well in 24 well plates received ^{177}Lu-DOTA-TATE calculated to give 0Gy, 0.5Gy, 1Gy, and 2Gy of radiation. The ^{177}Lu-DOTA-TATE ws peak-purified using reverse-phase high-performance liquid chromatography (RP_HPLC) prior to treatment to insure 100% radiochemical purity (See Figure 4.8). Cells were washed of the compound after 2h. There was a dose-dependent decrease in proliferation with increasing radiation dose observed without pretreatment with zebularine, however the differences were not statistically significant (P=0.609) (Figure 4.9).

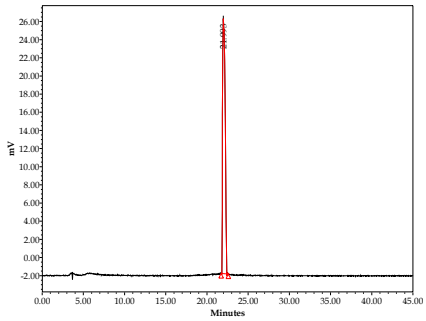

Figure 4.8: HPLC trace of analytical run of ^{177}Lu-DOTA-TATE after peak purification.

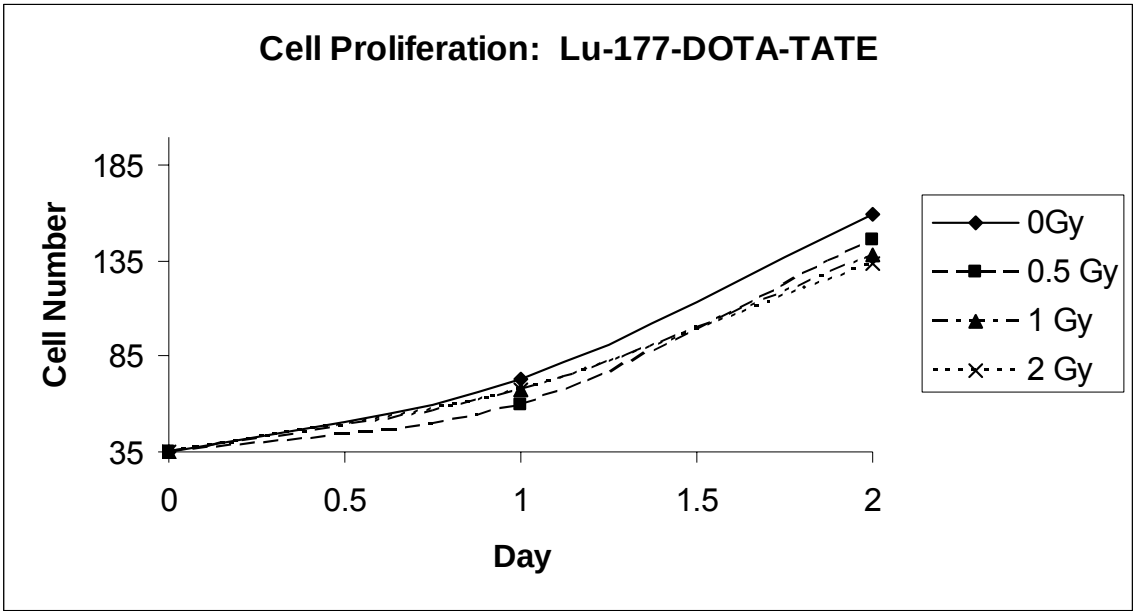

Figure 4.9: Cell proliferation by ^{177}Lu-DOTA-TATE radiation dose over time for MEC1 cells treated with 200μM zebularine. The maximal decrease for 2Gy radiation was only 13% relative to control cells.

For MEC1 cells treated with zebularine followed by ^{177}Lu-DOTA-TATE, there was a significant, interactive dose-response of decreased cell proliferation (P=0.0135). The maximal decrease in proliferation, 34%, was seen in cells treated with the highest doses of each compound (Figure 4.10). This decrease in proliferative potential is significantly lower than that seen with single-dose, external beam irradiation and zebularine (P=0.0135).

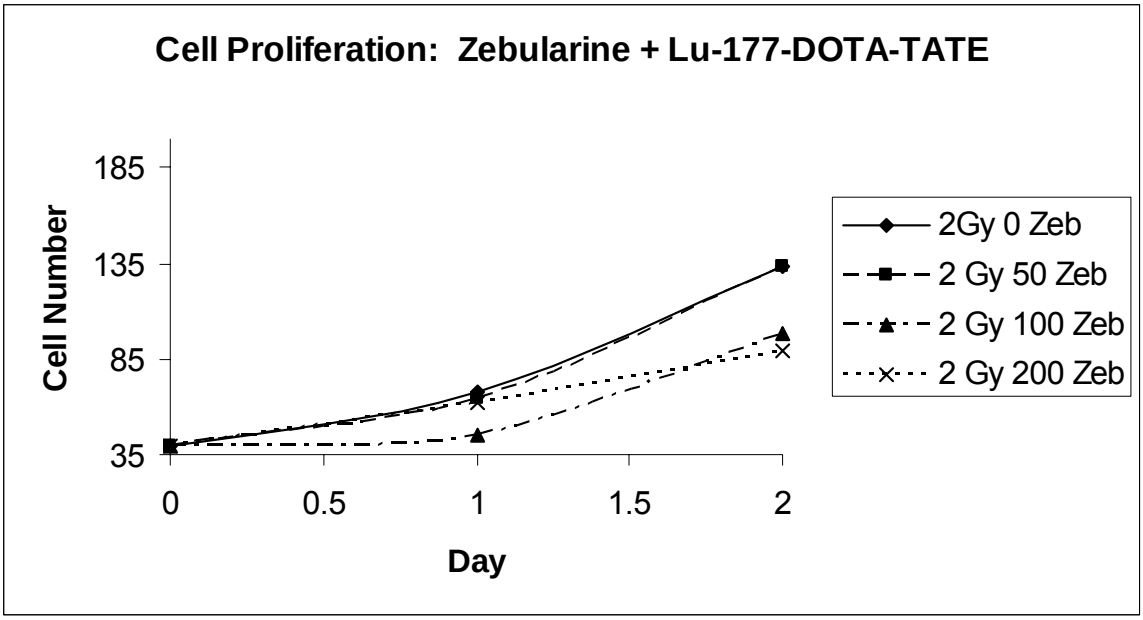

Figure 4.10: Cell proliferation of MEC1 cells at increasing doses of zebularine treated with 2Gy radiation by ^{177}Lu-DOTA-TATE. The effect of day interacted with dose, and the differences among treatment groups were not as clear as with the ^{137}Cs irradiator.

In contrast, cell viability was significantly decreased by zebularine and ^{177}Lu-DOTA-TATE in a dose-dependent manner, with a highly significant interaction between zebularine and targeted radiation (P=<0.001). No difference was observed between the 50μM zebularine and controls, but treatment with 100μM and 200μM zebularine caused a substantial and statistically significant decrease in cell viability (Figure 4.11). Non-viable cells exhibited classic apoptotic morphology ranging from cytoplasmic swelling and blebbing of the membrane to pyknotic cells of various sizes. No necrotic debris was evident. This decrease was larger than that seen with the combination of 200μM zebularine and external beam irradiation (Figure 4.12).

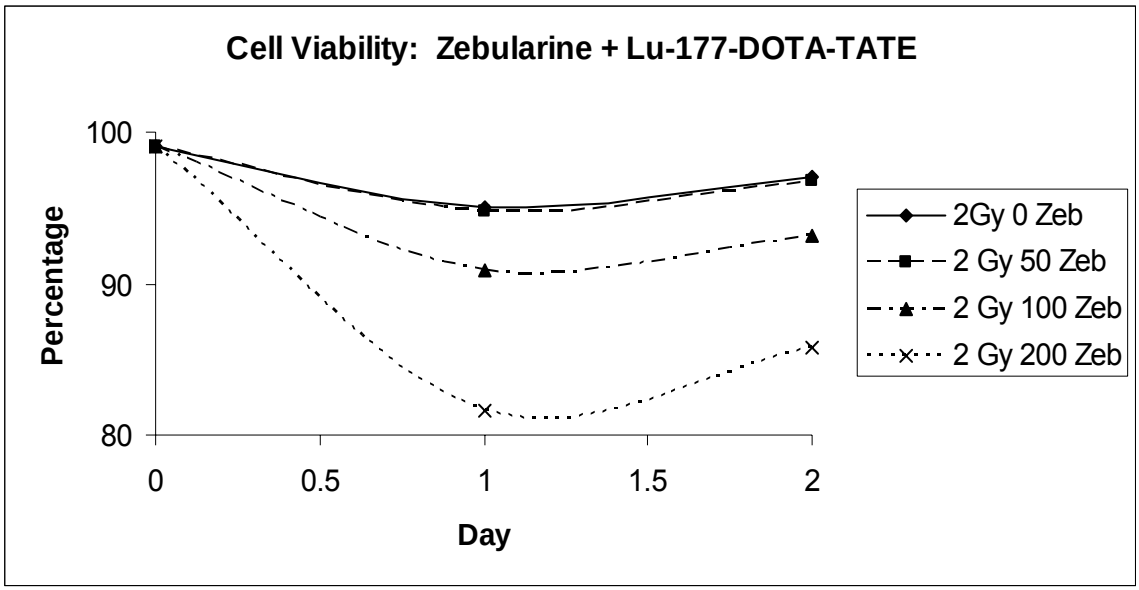

Figure 4.11: Cell viability by radiation dose over time for MEC1 cells treated with 2Gy radiation from ^{177}Lu-DOTA-TATE at increasing doses of zebularine.

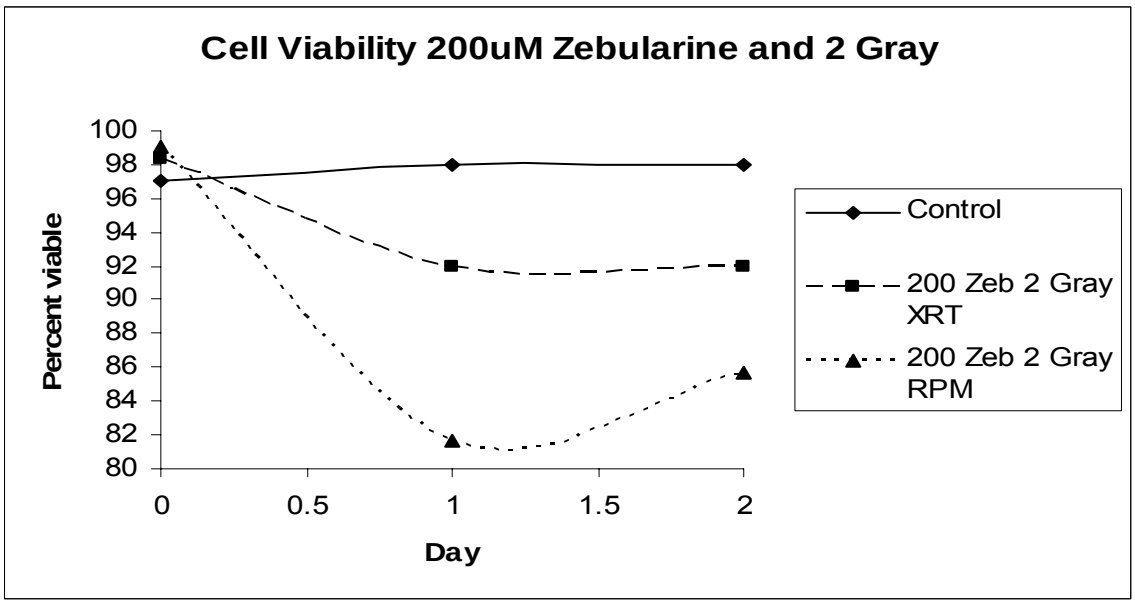

Figure 4.12: Cell viability over time for MEC1 cells treated with 2Gy radiation from ^{177}Lu-DOTA-TATE or external beam radiation at a 200μM dose of zebularine. The maximal decrease using ^{177}Lu-DOTA-TATE was over 16% relative to controls, compared to only 6% decrease in cells receiving external beam irradiation, a >2-fold difference.

Bisulfite-treated DNA harvested from MEC1 cells treated with 0μM, 50μM, 100μM, and 200μM zebularine was evaluated for DNA methylation of the genes *DLC1*, *CDKN2Ab*(*p16*), *MGMT*, and Death-associated protein kinase (*DAPK*) using COBRA for the first three and MSP for *DAPK*, all previously validated in our laboratory. The relative intensity of band associated with methylated status of *DLC1* remained stable across all doses of zebularine at approximately 28%. The relative intensity of band associated with methylated status of *MGMT* fluctuated across doses with no dose-response relationship and did not decrease at the highest dose of zebularine. The ratio of methylated to unmethylated product of *DAPK* decreased linearly across the dose range of zebularine by 5%. There was no evidence of methylation of the *CDKN2A* gene in MEC1 cells.

Discussion

It was necessary to establish the uptake and efflux characteristics of ^{177}Lu-DOTA-TATE in MEC1 cells to define the assumptions of the dosimetry calculation. Indeed, the characteristics of this labeled compound differ from those of ^{111}In-DOTA-TATE somewhat. Uptake of the ^{111}In-labeled compound by MEC1 cells has been shown to be 1.92% at 2h, very similar to the uptake of ^{177}Lu-labeled compound in control cells and those treated with 50μM zebularine.[94] The higher doses of zebularine resulted in a statistically significant, although dosimetrically minor, decrease in the uptake of the compound into the cells. The mechanism of this is unclear. It is possible that alterations in gene methylation reduce the number of receptors available for binding. It is also

possible that the drug results in metabolic stress and alterations of cellular physiology that slow internalization and cycling of the receptors. No previous work has examined such a question. Furthermore, the magnitude of difference in uptake was too small to identify a change in receptor number by competitive assay. Future evaluation of the effects of zebularine on neoplastic cells will seek to address the alterations of normal function that may contribute to this observed phenomenon. The efflux of ^{177}Lu-DOTA-TATE, 24.7% remaining at 4h, was more than twice that of ^{111}In-DOTA-TATE with 69.1% remaining cell-associated at 4h.[94] There was no difference, however, between the control cells and those treated with 200μM zebularine. It is important, in considering future animal studies, to avoid the assumption that this low uptake will necessarily carry into an animal model. Physiologic stimuli and recirculation of the compound may dramatically alter uptake of the radioactivity into the tumor cells and stroma *in vivo*. In fact, MEC1 xenografts in SCID mice had tumor uptake of ^{111}In-DOTA-TATE over 3% of the injected dose per gram, higher than the calculated *in vitro* uptake.[94]

The dosimetry data was calculated based upon assumptions of a closed system with the defined characteristics of cell uptake and efflux. The higher than expected efflux required adjusting the dosimetry calculation to presume only about 0.33% of the total activity remaining within the cell over time. The 2h exposure to ^{177}Lu-DOTA-TATE in solution with the MEC1 cells roughly mimics the exposure of cells *in vivo*. In dogs, over 67% of ^{111}In-labeled octreotide is excreted by 2h, with 92% of the total dose leaving the body by 12h.[96] Thus, full

exposure for 2h appears to be a reasonable *in vitro* approximation of exposure to tumor cells. However, it is difficult to assure the exact dose received by the MEC1 cells treated with ^{177}Lu-DOTA-TATE in these experiments, and this calculation is a best approximation.

External irradiation in the range of 0 to 2Gy resulted in a predictable dose-dependent decrease in cell proliferative capability. The effect on cell viability was less apparent, and not statistically significant. It should be noted that the MEC1 doubling time observed in our laboratory is shorter (24h) than the 40h reported in the initial paper describing the cell line.[142] Proliferative potential and cell viability assays were selected as a result of the growth properties of the MEC1 cells.[143] Attempts at low-concentration plating to perform traditional clonogenic survival assays resulted in inconsistent and irregular growth of the cells. In fact, the noted difference in the effects of external irradiation and radiopharmaceutical treatment highlight the strength of these assays in addressing the question of the interaction of demethylation therapy and treatment with different qualities of radiation. The therapeutic effect of demethylation likely is predicated on the epigenetic profile of the cells being treated. Evaluating cell proliferation and viability gives insight into cell cycle and apoptotic alterations.

Treatment of MEC1 cells with zebularine for 48h resulted in a linear decrease in cell proliferation. For these cells, the calculated IC_{20} and IC_{50} values were 75μM and 195μM, respectively. This contrasts with IC_{50} values of 152μM for A2780/CP cisplatin-resistant ovarian cancer cells, 92μM for A2780 ovarian cancer cells, and 64.7μM for Hey ovarian cancer cells.[143] The IC_{20} values for

human ALL cell lines TK6 and Jurkat were only 20μM and 10μM.[33] This is consistent with the biology of CLL, in which the abnormality is not primarily one of loss of tumor suppressor function resulting in unconstrained growth, but one of loss of appropriate apoptotic function. In fact, after removal of the MEC1 cells from zebularine, the proliferative potential was identical, regardless of dose. This is consistent with the observation that demethylation is transient, and hypermethylation patterns re-establish if therapy is discontinued.[144] The true benefit of this approach may be realized in combination therapy that sensitizes neoplastic cells to the effects of cytotoxic agents.

With respect to proliferation, the addition of external irradiation following exposure proved to be synergistic in its effect on proliferative potential with the prior zebularine treatment. While prior treatment with zebularine at the doses used did not reduce the proliferation rate of the MEC1 cells, there was a clear, dose-dependent and highly statistically significant reduction in proliferative potential by zebularine dose followed by radiation. This alteration in proliferation rate is likely a result of cell cycle arrest induced by radiation. The additive, rather than synergistic, effect of external irradiation and zebularine on cell viability suggests that the primary effect of radiation after 48h exposure to zebularine on MEC1 cells is to restore cell-cycle control, rather than promote apoptosis. This effect could be indirect, mediated through DNA repair pathways, rather than a direct upregulation of cyclin-pathway control constituents. Indeed, in solid tumor cell lines, clonogenic potential was demonstrated to be decreased by radiation after prior treatment with zebularine.[76] These cells did not demonstrate cell cycle

arrest. The primary alteration in these cells appeared to be increased double-strand DNA break lesions as measured by γH2AX foci.[76] The decrease in viability by the combination of the highest dose of zebularine and external irradiation was dramatically less than the decrease in proliferative potential. This may be a function of the low apoptogenic effect of external beam irradiation as well. [140] The primary effect of external irradiation at high dose-rate is typically cell-cycle arrest and mitotic catastrophe. The end-result following the double-strand breaks identified in the aforementioned solid-tumor cell lines likely would not be apoptosis. The lack of an increased apoptotic component of those cells observed by propidium iodide flow cytometry supports this.[76]

In contrast, low dose-rate irradiation with radiopharmaceuticals is thought to cause apoptosis more frequently than mitotic catastrophe.[140] This is supported by the finding in the present study that the viability of the MEC1 cells was synergistically affected by treatment with zebularine followed by ^{177}Lu-DOTA-TATE while the interactive effect on proliferative potential was far less dramatic. This result is similar to the findings of Macklis and others who compared external irradiation to ^{90}Y irradiation added to the cell suspension of NHL cell lines.[140] By measures of DNA fragmentation, apoptosis was significantly more common after ^{90}Y treatment than external irradiation.[140] Futhermore, the addition of caffeine, an apoptosis enhancer, dramatically increased this effect.[140] In contrast, cell cycle arrest was more prominent in the externally irradiated cells, as observed in the present studies.[140] The quality of radiation differs greatly between the single dose over two minutes or less from

external irradiation and the low dose-rate of the ^{177}Lu with a half-life of 6.7d. The difference in outcome between these two experiments suggests that the mechanism of interaction between the types of radiation and zebularine is different. If the effect of zebularine was unimechanistic, the radiation dose from ^{177}Lu should have a similar, likely less dramatic, effect on proliferative potential relative to the external irradiation. Instead, to have a dramatically larger impact on viability suggests that the interaction between the zebularine and ^{177}Lu-DOTA-TATE involves the apoptotic mechanism. It cannot be ignored that this compound has two potential mechanisms of cellular response, the radioactive payload, and the effect of somatostatin agonism. Indeed, somatostatin has been shown to inhibit activated lymphocyte proliferation *in vitro*.[145] Activated lymphocytes are inhibited by octreotide at a concentration in the range of 10^{-11}M to 10^{-9}M. In these experiments, the concentration of TATE was two orders of magnitude lower at 10^{-13}M. This makes a pharmacologic effect of the ligand extremely unlikely. Nevertheless, the interactive effect observed was between the zebularine and ^{177}Lu-DOTA-TATE as a compound. If the TATE has any effect directly on the cancer cells, this would be expected to occur *in vivo* as well. Human patients in imaging studies of related compounds have experienced no beneficial therapeutic effect. The effect of the radiometal is the critical ingredient for therapy.

To examine possible mechanisms of the interaction between zebularine and radiation, the methylation status of several genes was examined. The *DLC1* gene COBRA analysis showed no evidence of alteration of methylation by

zebularine treatment at any dose. This is consistent with the results achieved with decitabine in MEC1 cells.[53] Shi and others found upregulation of *DLC1* to occur only after combined treatment with decitabine and the histone deacetylase inhibitor trichostatin A.[53] It is possible that histone deacetylation plays a critical role in the silencing and maintenance of methylation of *DLC1*. The gene *MGMT* was selected because it plays an important role in DNA repair, and has been shown to be silenced in human B-cell NHL.[27] Methylation of this gene in these MEC1 samples varied, and did not decrease in a dose-dependent manner. The gene CDKN2A was selected because it is a cell-cycle inhibitor that recently has been shown to be silenced by hypermethylation in lymphoid malignancy.[146] It was not methylated in the MEC1 cells. Finally, *DAPK* was selected, as it is a pro-apoptosis gene that also has been shown to be silenced in B-cell NHL.[147] This gene demonstrated methylation in MEC1 cells, which decreased in a dose-dependent fashion with increasing dose of zebularine. The decrease observed was minor, and without multiple replicates to evaluate statistically, is a qualitative observation only. It is, however, tantalizing, given the observed interaction of zebularine and ^{177}Lu-DOTA-TATE leading to decreased MEC1 cell viability with an apparently apoptotic cellular morphology. To understand these interactions fully, expression microarray would be ideal to evaluate a wide range of gene products and the effects of the zebularine therapy on them.

It must be considered that the interaction observed is due to an effect of zebularine independent of its DNMT inhibition effect. Other nucleoside analogues have been used for radiosensitization.[148] Zebularine has a ribose

base, allowing it to be incorporated into RNA, which could contribute to radiosensitization. However, the fact that zebularine treatment preceded radiation and is no longer present in the repair phase makes this explanation unlikely. Indeed, if zebularine radiosensitizes *in vivo* as it appear to do *in vitro*, it may be an ideal radiosensitizer. The compound has been shown to have a preferential effect on cancer cells compared to normal cells *in vitro*.[135] This appears to be mediated by cytidine kinase levels, which are higher in cancer cells than normal cells, and are required to activate zebularine.[135] If this is the case, the compound could serve to radisensitize tumor tissue while having minimal effect on normal tissue, thereby improving the therapeutic ratio.

The results of examining the hypotheses of these studies are very encouraging for pursuing *in vivo* studies combining demethylation therapy and radiation therapy, particularly ^{177}Lu-DOTA-TATE. The first hypothesis was rejected, as zebularine therapy statistically significantly decreased uptake of ^{177}Lu-DOTA-TATE and the efflux of the compound is much greater than that of ^{111}In-DOTA-TATE, the analogous imaging agent. However, the difference was not dosimetrically significant. It remains to be seen whether the difference would be significant *in vivo*. The second hypothesis was also rejected, as the effect of the different qualities of radiation was dramatically different. The important finding of these studies was the effect on cell viability of the ^{177}Lu-DOTA-TATE in combination with zebularine. Synergistic interaction encouraging apoptosis of NHL would be extremely therapeutically beneficial. This confirmed the third hypothesis that a synergistic effect exists on cell proliferation between external

irradiation and zebularine and a synergistic effect exists on viability between ^{177}Lu-DOTA-TATE and zebularine. The fourth hypothesis could not be supported by the results of the methylation analysis performed. The decrease in methylation observed in the promoter of *DAPK* would appear to lend support, but without expression data is difficult to interpret. The mechanisms of the interactions observed deserve further elucidation for potential exploitation in pre-clinical studies.

Materials and Methods

Radiolabeling: Radiolabeling was be performed by adding 1mCi $^{177}LuCl_3$ to 0.2 M NH_4-acetate, pH 5.0, and 1µg DOTA-TATE.[149;150] The ^{177}Lu-labeled peptide was incubated at 95ºC for 25m. Radiometal incorporation and radiochemical purity (typically >98%) were determined by radio-thin layer chromatography (TLC). The radiolabeled peptide was diluted with normal saline for injection with no further processing. Reversed-phase HPLC (RP_HPLC) was performed on a Waters 626 chromatograph equipped with a manual Rheodyne injector, 2487 dual wavelength UV detector, busSAT/IN analog-digital interface and Empower Pro software (Build No. 1154). A Phenomenex (Torrance, CA) Jupiter C18 column (5 µm, 4.6 × 250 mm) was used for purification and analysis of radiolabeled compounds. A gradient of 0-50% solvent B (solvent A, 0.1% TFA/H2O; solvent B, 0.1% TFA/acetonetrile) over 30 min at a flow rate of 1.0 mL/min was used. UV detection was accomplished at 280 nm, and radioactivity

detection was accomplished using a NaI(Tl) radioactivity monitor (Canberra Meriden, CT).

Cell uptake studies: The methods for cell uptake were based on previously described techniques.[151] Three aliquots of 1.5×10^6 MEC1 cells/mL, suspended in 2 mL of serum-free RPMI Medium containing 5% CO2 (Invitrogen Corporation, Carlsbad, CA), were incubated in an orbital shaking water bath at 37 °C. To each was added 1 μCi/mL of ^{177}Lu-DOTA-TATE. After 15 min, 30m, 1h, and 2h of incubation, 200μL aliquots were removed, 800μL of media was added, and the samples were centrifuged at 10,000 rpm for 1 min, after which 900μL of supernatant was removed. To the pellet was added 900μL of media and the centrifugation was repeated. The 900μL wash was removed. Radioactivity in each sample (supernatant, wash, and cell pellet) was counted on the gamma counter. Uptake was calculated by dividing the pellet-associated radioactivity by the total radioactivity less the 1% supernatant activity remaining with the pellet. Cell viability, as determined by trypan blue exclusion and hemacytometry, was >90% after 4h of incubation.

Cell efflux studies: Three aliquots of 1.5×10^6 MEC1 cells/mL, suspended in 2 mL of serum-free RPMI Medium containing 5% CO2 (Invitrogen Corporation, Carlsbad, CA), were incubated in an orbital shaking water bath at 37 °C. To each was added 1 μCi/mL of ^{177}Lu-DOTA-TATE. After a 2h incubation, , 200μL aliquots were removed at 15m, 30m, 1h, 2h and 4h, 800μL of media was added, and the samples were centrifuged at 10,000 rpm for 1 min, after which 900μL of supernatant was removed. To the pellet was added 900μL of media and the

centrifugation was repeated. The 900μL wash was removed. Radioactivity in each sample (supernatant, wash, and cell pellet) was counted on the gamma counter. Efflux was calculated by dividing the pellet-associated radioactivity by the total radioactivity less the 1% supernatant activity remaining with the pellet. Cell viability, as determined by trypan blue exclusion and hemacytometry, was >90% after 4 h of incubation.

Dosimetry: Dose delivered by the radiopharmaceutical preparation of ^{177}Lu-DOTA-TATE was calculated using an MCNP model (MCNP5). This is a Fortran-based program that uses multiple iterations of random modeled decay events to estimate the dose to nucleus or cytoplasm based on the location of the decay and the geometry of the total, closed system.[152] The assumptions for this model were that the MEC1 cells have an average radius of 4μm, a nuclear volume of approximately 40%, and a cell volume fraction of 0.15% of the total water matrix. Dosimetry curves for ^{177}Lu-DOTA-TATE were established using MEC1 cell uptake and efflux data determined in MEC1 cells. This was a two-phase calculation with an initial 2 h phase of homogeneous dosimetry during incubation, then an infinite decay dosimetry model after 2h. An MCNP model[152] will be calculated using the β- of ^{177}Lu. Due to the planar arrangement of the cells, the γ of ^{177}Lu was ignored. The total dose to the cells was calculated according to the formulae in Table 4.2. Doses were delivered to the cell nuclei by activity both within and without the cell, in the water matrix, for the first 2h, then primarily by internalized activity for the remainder of the 48 hour study period. Briefly, the total number of decays was calculated integrating the activity

in Bq over the time-period of interest. Doses were derived from the sum of decays occurring within the entire system for the first 2h, then decays only within the cell over the succeeding 46h were calculated using the uptake and efflux data. Internalized radioactivity was estimated using the uptake and efflux curves generated in MEC1 cells for ^{177}Lu-DOTA-TATE, and an estimated nucleus:cytoplasm distribution of 1:2.

Calculation of the total number of decays	$Decays = \frac{Act_o(Bq)}{\lambda(\sec)}(1-e^{-\lambda t})$
Decay events over 2 hours	=(2.78*37*10^3/0.00433)*(1-(e$^{(-0.00433*2)}$))
Decay events over 72 hours	=(2.78*37*10^3/0.00433)*(1-(e$^{(-0.00433*72)}$))
Percent uptake	Estimated over 72 hours by multiplying uptake by percent efflux
Decays per cell	Total number of decay events divided by the total number of cells in the system
Total dose	Dose is calculated by multiplying each location factor (Table 4.1) by the number of decays expected to occur in that location over the 72 hour study period

Table 4.3: Calculation of cell dose from 2.78μCi ^{177}Lu-DOTA-TATE

Proliferation and viability assays: MEC1 cells were grown in RPMI medium altered to contain 1mM sodium pyruvate, 10mM HEPES, 2mM L-glutamine, 0.4 mg/mL gentamicin supplemented with 10% fetal bovine serum at 37ºC in a 5% CO_2 atmosphere. Cells were diluted to a concentration of 400,000 cells/mL and incubated in 1mL complete RPMI medium as described above in Corning 24 well plates (Corning Inc., Corning, NY). Drug treatment was with 50μM, 100μM, and 200μM zebularine for 48 hours prior to irradiation.[75;76;137;153] Cells were counted daily on a Bright Line hemacytometer (Hausser Scientific, Horsham, PA). Cells were diluted with Trypan Blue vital stain and the viable fraction recorded at each counting. Dilution was appropriate to yield a minimum 100 cell count per the

manufacturers instructions. Three replicates allow detection of a 25% difference with a power of 0.80 and α of 0.05. Irradiated wells will receive a dose of 4Gy, a dose expected to be sublethal.[80]

Irradiation: MEC1 cells were irradiated with a Nordion Gammacell 40 Exactor ^{137}Cs irradiator at a dose-rate of 98.4cGy/min for 31s, 1:01m, or 2:02m.

Radiopharmaceutical study: MEC1 cells were incubated with ^{177}Lu-DOTA-TATE for 2h. After this, the medium was transferred to a microcentrifuge tube, cells were pelleted and washed in complete RPPMI culture medium to remove non-bound agent. Cells were resuspended at 400,000 cells/mL plated in triplicate in 24 well Corning culture plates.

Zebularine treatment: Ten mL of MEC1 cells were incubated at 400,000 cells/mL in four T25 Corning flasks (Corning Inc., Corning, NY). To these were added sufficient zebularine (Sigma-Aldrich, St. Louis, MO) diluted in PBS to yield a final concentration of 0μM, 50μM, 100μM, and 200μM. Cells were incubated for 48h, then removed by centrifugation, washed, and resuspended in complete RPMI medium as described. Zebularine was stored at -20ºC after reconstitution.

Methylation analysis: COBRA assays were performed on *DLC1*, *MGMT*, and *CDK2A* using primers located in the promoter and first exon region of each gene. Conditions for amplification were a 60ºC annealing temperature for DLC1, touchdown 56ºC for *MGMT* and touchdown 58ºC for *CDNK2A*. *DAPK* was analyzed with MSP primers in the 5' region of the gene reported previously.[147] Digestion was accomplished with BstuI for *DLC1* and *CDKN2A* at 60ºC for 4h,

and HpyCh4IV was used for *MGMT* at 37ºC for 4h. The annealing temperature was 60ºC.

Statistics: All treatment groups were compared by a repeated measure ANOVA using SAS 9.0 software (SAS, Cary, NC). A mixed model was used with Fisher's least significant difference used to separate means. Growth inhibition by zebularine was evaluated by linear regression analysis. Significance was set at P=0.05.

Chapter 5

Somatostatin Receptor Imaging of Canine B-cell Lymphoma

Introduction

As previously discussed, somatostatin analogues specific for SSTR2 and, to a lesser degree, SSTR5 have been used to effectively image human NHL tumor burden.[89;91-93;154] No attempt to image canine NHL with similar imaging agents has been reported previously. Tyr^3-octreotate is a modification of octreotide in which tyrosine has replaced phenylalanine at the 3 position in the compound for greater hydrophilicity, which increases the receptor binding affinity, and the final amino acid retains its carboxyl group, allowing faster internalization.[101] Renal excretion is the dominant route of elimination, as it is for octreotide.[96] This pilot study evaluated three dogs with naturally occurring lymphoma with ^{111}In-DOTA-TATE planar scintigraphy. Specific uptake would be expected to yield a target to background ratio greater than 1.0 on planar scintigraphy. Thus, if lymph nodes and organs affected by lymphoma have an uptake greater than the blood-pool background, receptor binding is the most likely explanation for specific tumor uptake. Images of the dogs in this study were evaluated subjectively for tumor burden localization, and confirmed with objective, semi-quantitative region of interest (ROI) analysis to confirm receptor-specific uptake in the tissues.

The purpose of this study was to provide evidence that ^{111}In-DOTA-TATE-SSTR2 binding occurs *in vivo* in dogs with spontaneous NHL. This is necessary for further development of therapeutic radiopharmaceuticals based on this somatostatin analogue platform, as well as to develop somatostatin-targeted molecular imaging and therapy compounds. There is no literature precedent for

the presence of appropriate somatostatin receptors on the surface of canine NHL cells. This could be assayed with immunohistochemistry or Western blot techniques, but the specificity of ^{111}In-DOTA-TATE-SSTR2 interaction is at least as high, and the biological data resulting from these scans is superior to an *in vitro* study. The hypothesis of this study was:

1) Dogs with naturally-occurring NHL will demonstrate tumor-specific uptake of ^{111}In-DOTA-TATE on planar scintigraphy with target to background ratios greater than 1.0 on ROI analysis.

Results

Three dogs with naturally occurring B-cell lymphoma were enrolled in this pilot study. All dogs were spayed females, 8 years old, and of mixed breeding. Dog 1 was 44.3kg, Dog 2 was 11.1kg, and Dog 3 was 6.5kg. Dog 1 was stage IV, based on physical examination, with palpable splenomegaly. No other routine imaging was performed on Dog 1. Dog 2 was stage V, based on palpable splenomegaly and 31,540 circulating large lymphocytes. Dog 2 had a mildly elevated serum alkaline phosphatase of 205 U/L (ref: 5-129 U/L). Dog 3 was stage IV, with palpable hepatosplenomegaly and ultrasound evidence of spleen and liver lymphoma infiltration. Each received a single intravenous injection of between 3 and 5 mCi of ^{111}In-DOTA-TATE. Images were acquired at 1, 4, and 24h after injection in each dog. No dog had an adverse reaction of any kind to the injection. All dogs have subsequently been treated for their lymphoma and are currently in remission. In addition to the standard views

planned, images were acquired of the pelvis and hind limbs of dog 1 and the ventral and dorsal abdomen of dog 3. Regions of interest containing the lymph nodes, liver, spleen, and gastrointestinal tract were compared with regions of interest over muscular regions not containing lymph tissue in the field of view (Table 5.1). Uptake ratios ranged from 0.97 to 2.54 for lymph nodes, 1 to 2.45 for liver, 1.72 to 2.64 for spleen, and 1.22 to 2.32 for gastrointestinal tract. There was no single time-point at which node values were consistently highest for any of the selected nodes. Liver, spleen, and gastrointestinal values peaked at 4h for two of the three dogs.

Case	Hour	Mandibular	Sup Cerv	Popliteal	Liver	Spleen	GI Tract
1	1	1.05	1.08	0.97	1.66	1.72	1.22
	4	1.14	1.18	1.29	1	2.06	1.94
	24	1.39	1.06	1.34	1.77	2.45	2.32
2	1	1	1.03	1.55	1.22	1.64	1.8
	4	1.67	1.61	1.6	2.28	2.4	2.32
	24	1.43	1.11	2.54	2.25	2.17	2.14
3	1	1.83	1.43	1.93	1.86	2.07	1.9
	4	1.08	1.07	1.43	2.45	2.64	2.5
	24	1.8	1.11	N/A	1.95	1.83	1.82
Mean	1	1.29	1.18	1.48	1.58	1.81	1.64
	4	1.30	1.29	1.44	1.91	2.37	2.25
	24	1.54	1.09	1.94	1.99	2.15	2.09

Table 5.1: Lesion to muscle uptake ratios for target tissues of ^{111}In-DOTA-TATE.

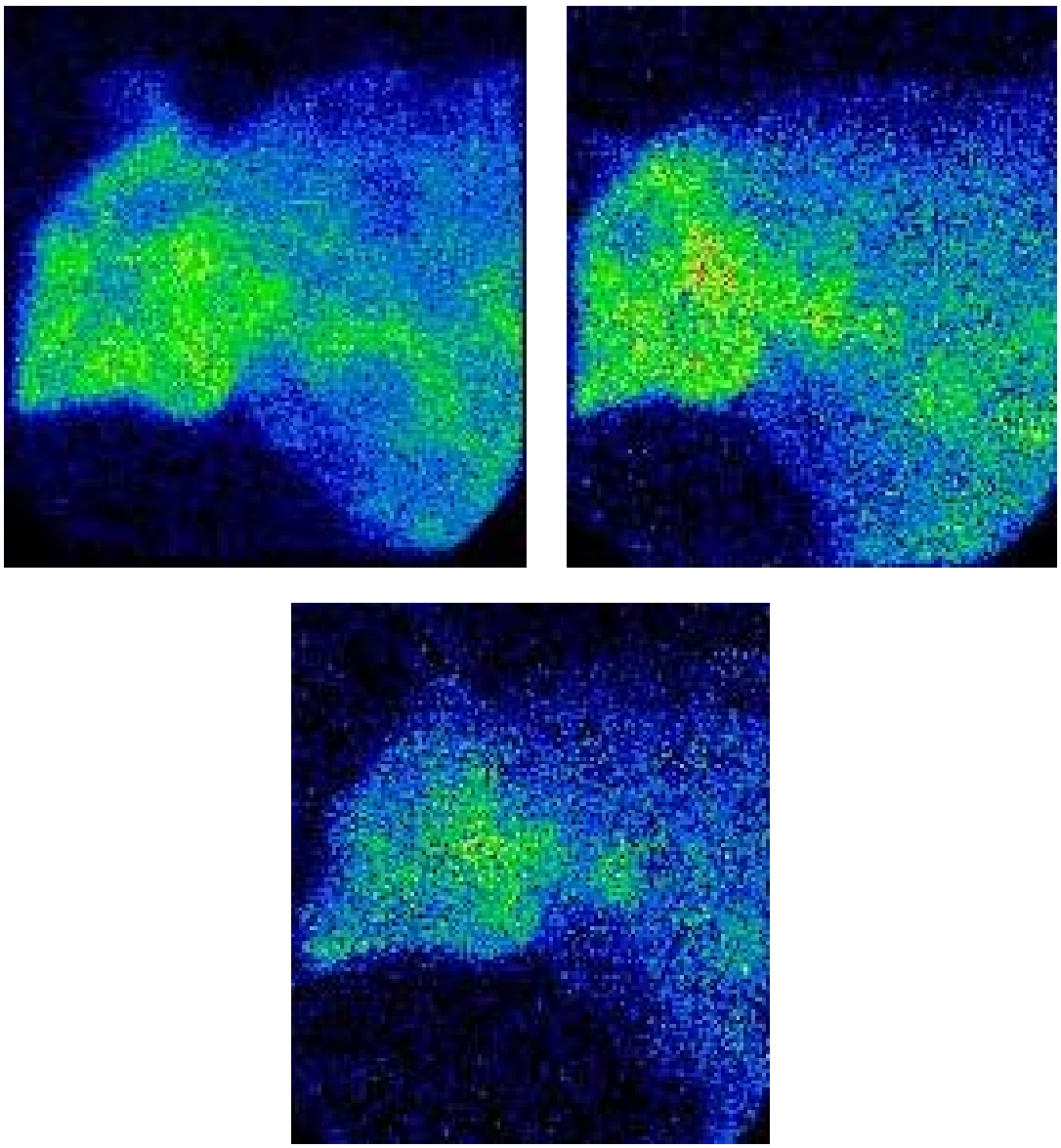

Figure 5.1: Case 1: Right lateral head and neck at 1h, 4h, and 24h. Note the visible mandibular, zygomatic, cervical, and superficial cervical lymph nodes, most visible on the 24 hour scan. The patchy appearance of the 1 hour scan is due to improper calibration of the gamma camera.

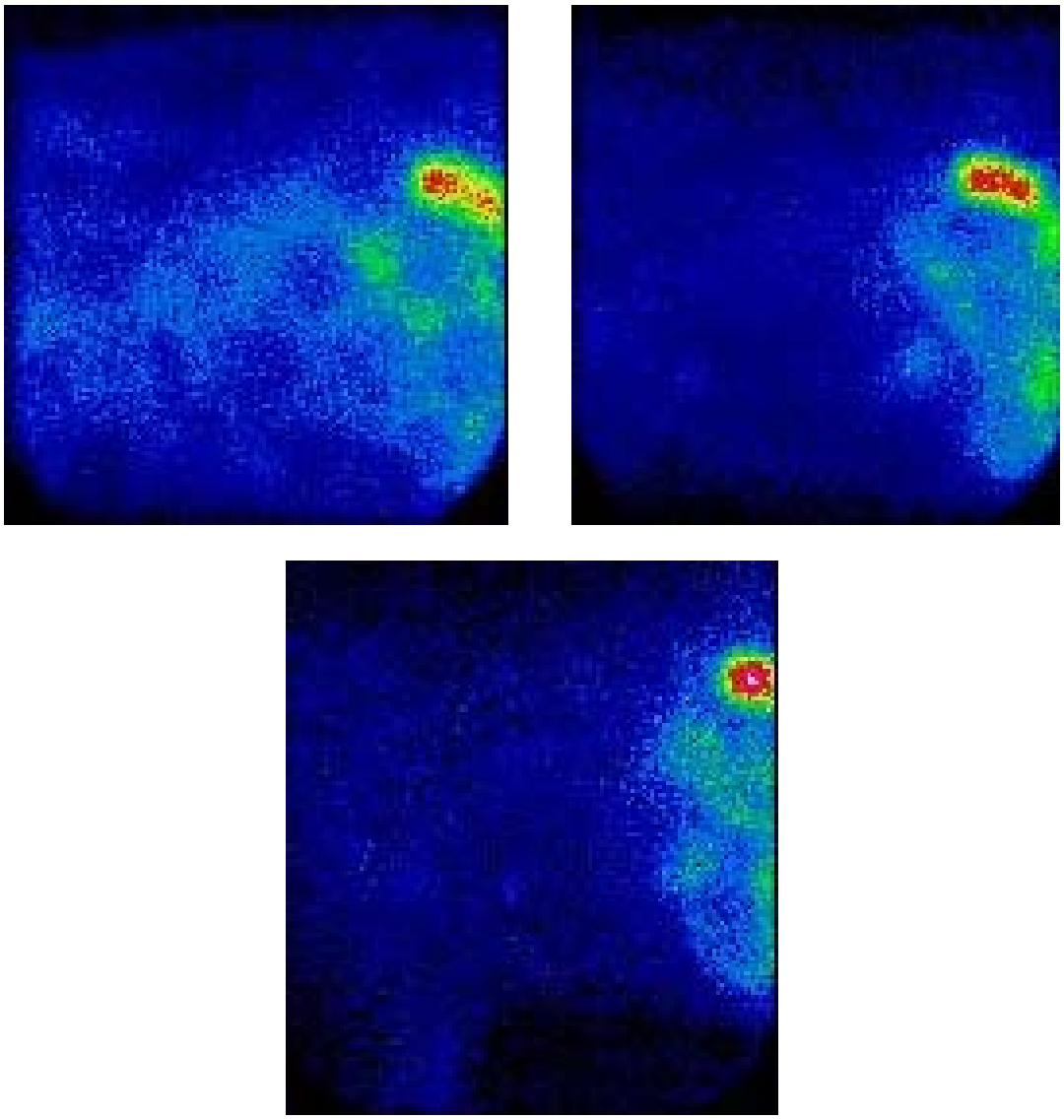

Figure 5.2: Case 1: Right thorax at 1h, 4h, and 24h. Note the relative lack of blood-pool activity visible over the cardiac region. Kidney, spleen, and gastrointestinal activity is clearly visible on these scans.

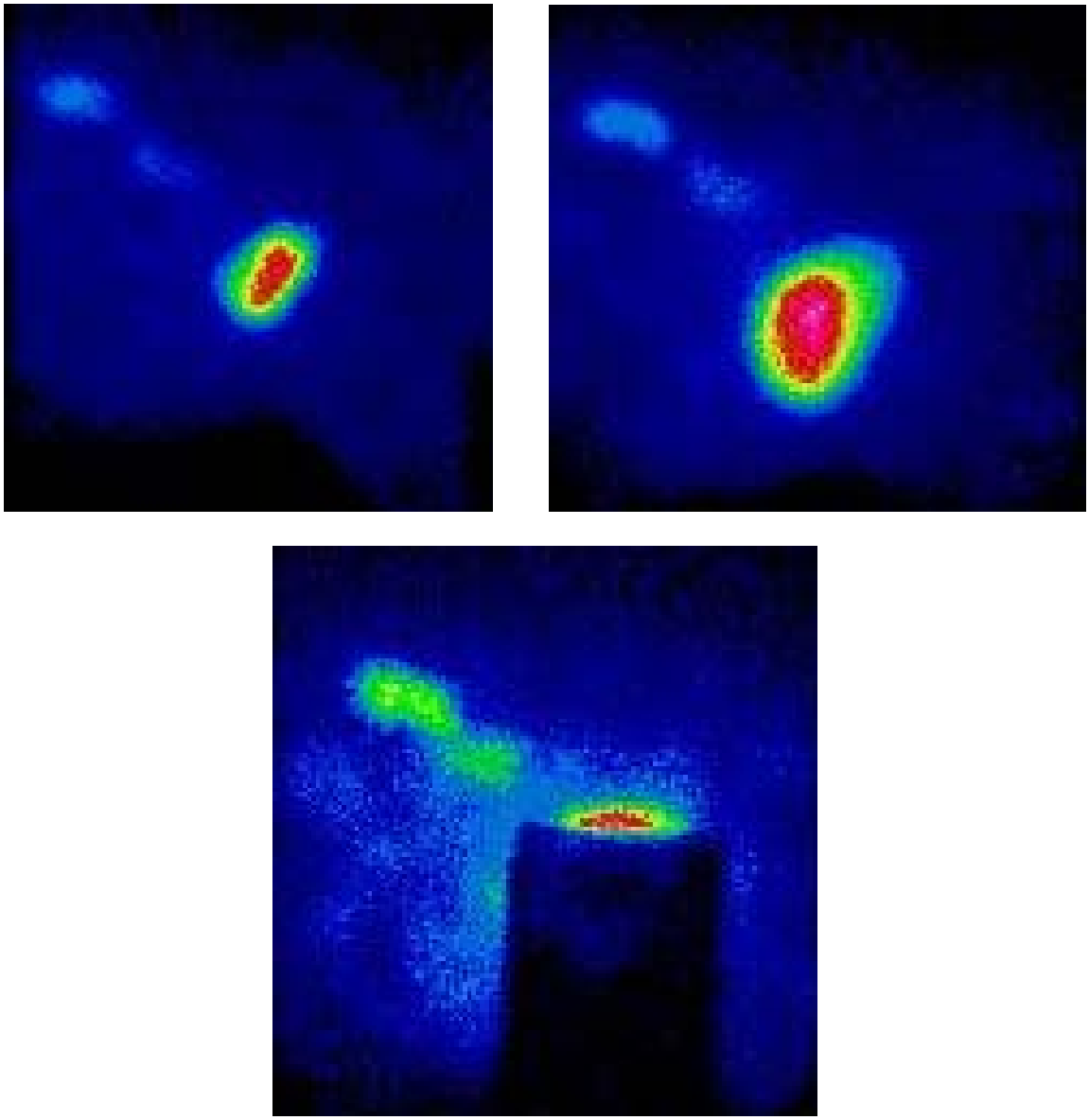

Figure 5.3: Case 1: Right abdomen at 1h, 4h, and 24h. Kidney, urinary bladder, and gastrointestinal activity are most prominent in these scans. The amount of activity in the bladder somewhat overwhelms the subtler features of the first two scans.

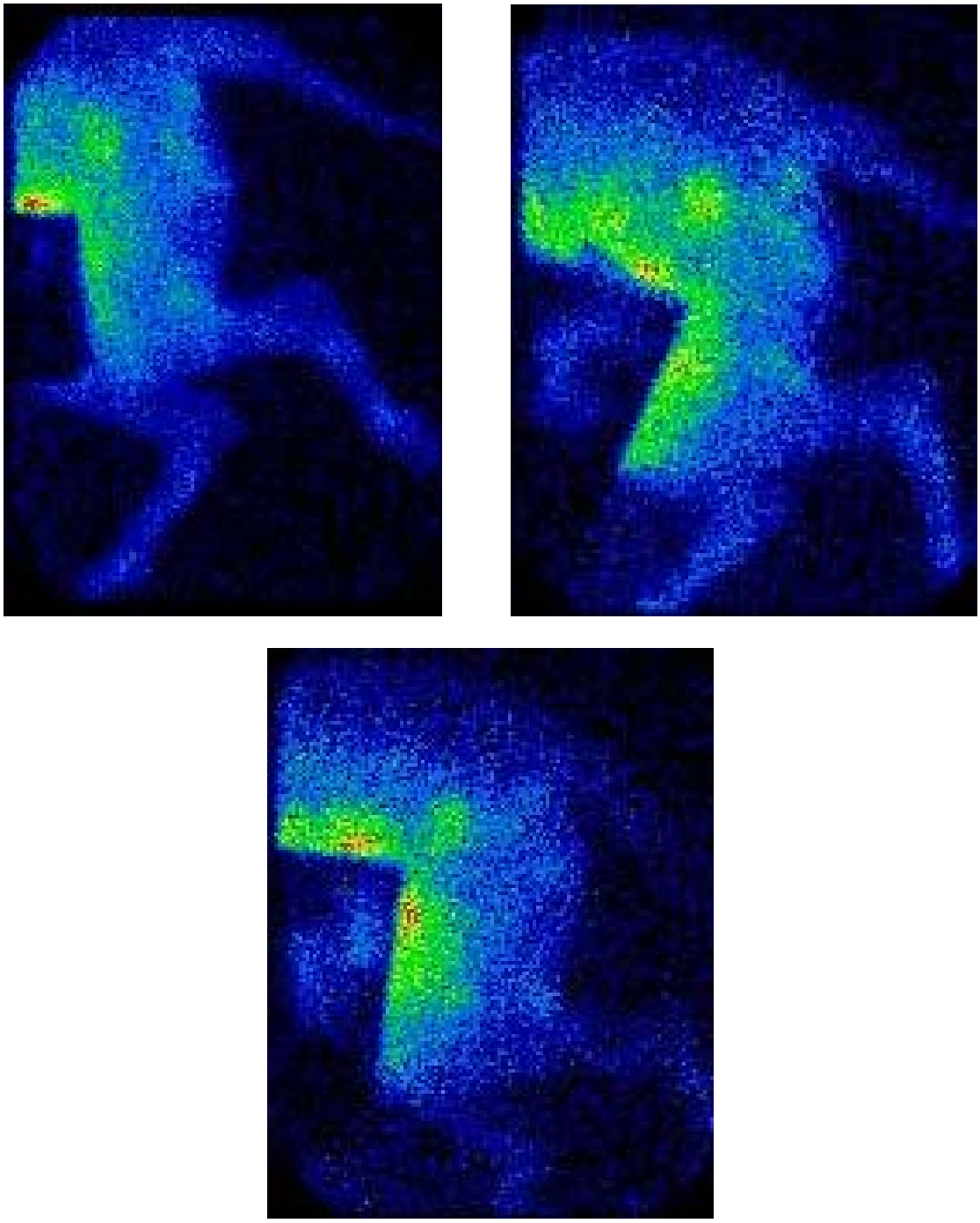

Figure 5.4: Case 1: Right pelvis at 1h, 4h, and 24h. Note the visible popliteal and submlumbar lymph nodes in all three images.

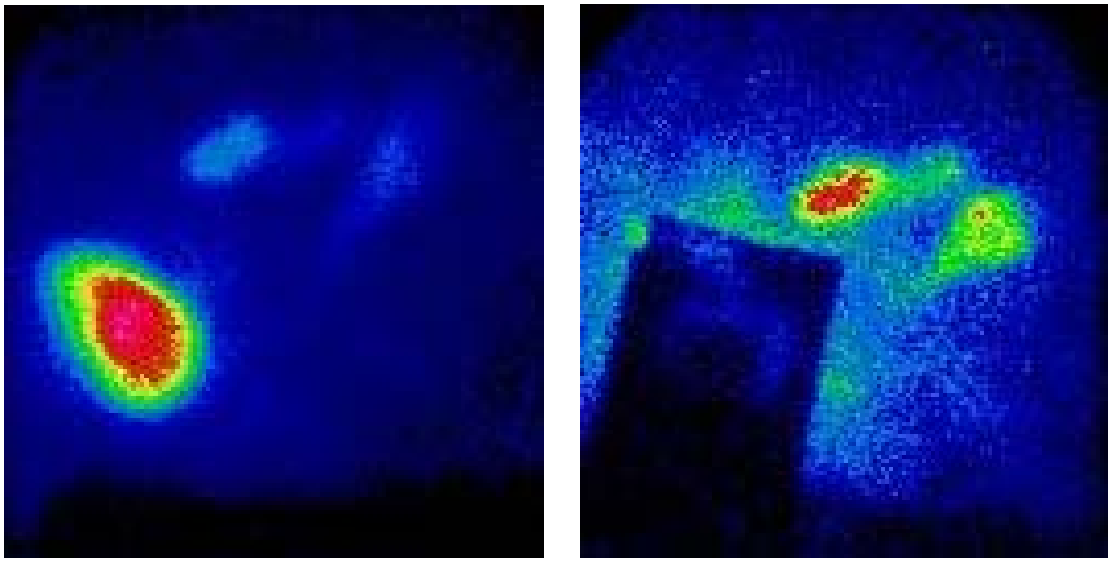

Figure 5.5: Case 1: Left abdomen at 4h and 24h. Relative to the right abdominal view, the spleen is more prominent in these views, particularly at 24h.

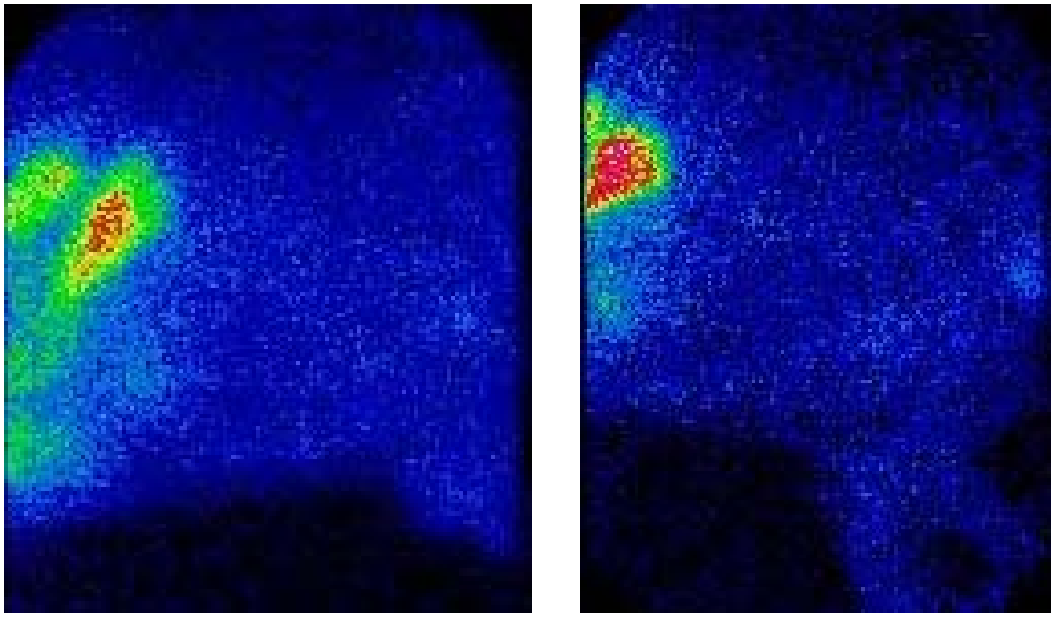

Figure 5.6: Case 1: Left thorax at 4h and 24h. Spleen, kidney, and gastrointestinal activity are visible on these scans.

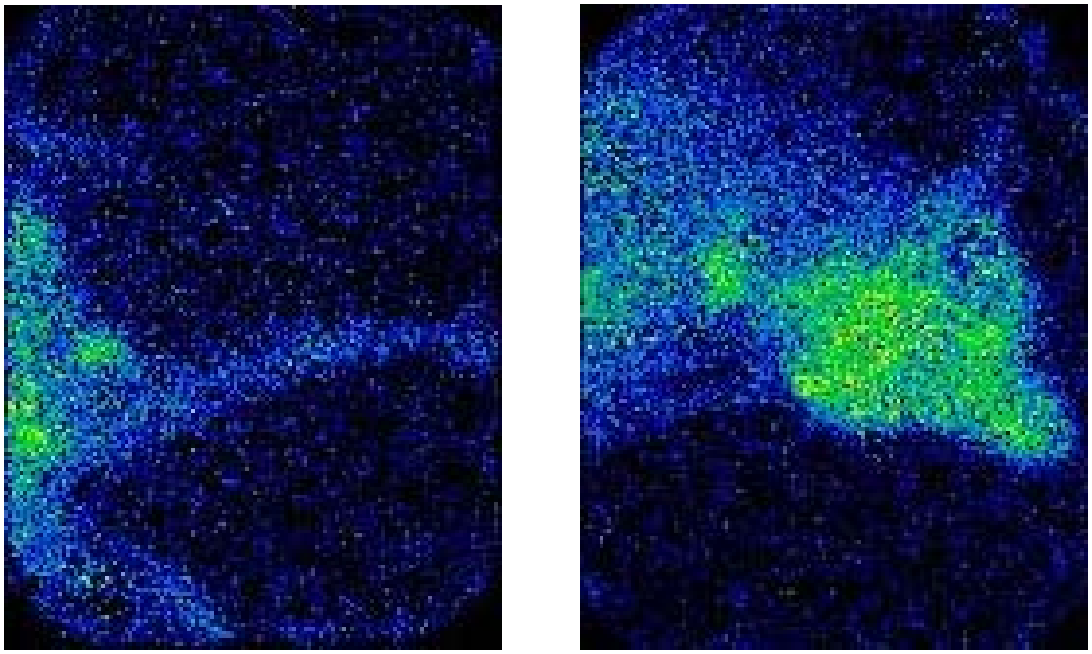

Figure 5.7: Case 1: Hind legs and left head and neck at 24h. Popliteal nodes in the hind limb, and cervical and mandibular nodes in the head and neck are apparent at 24h in these images.

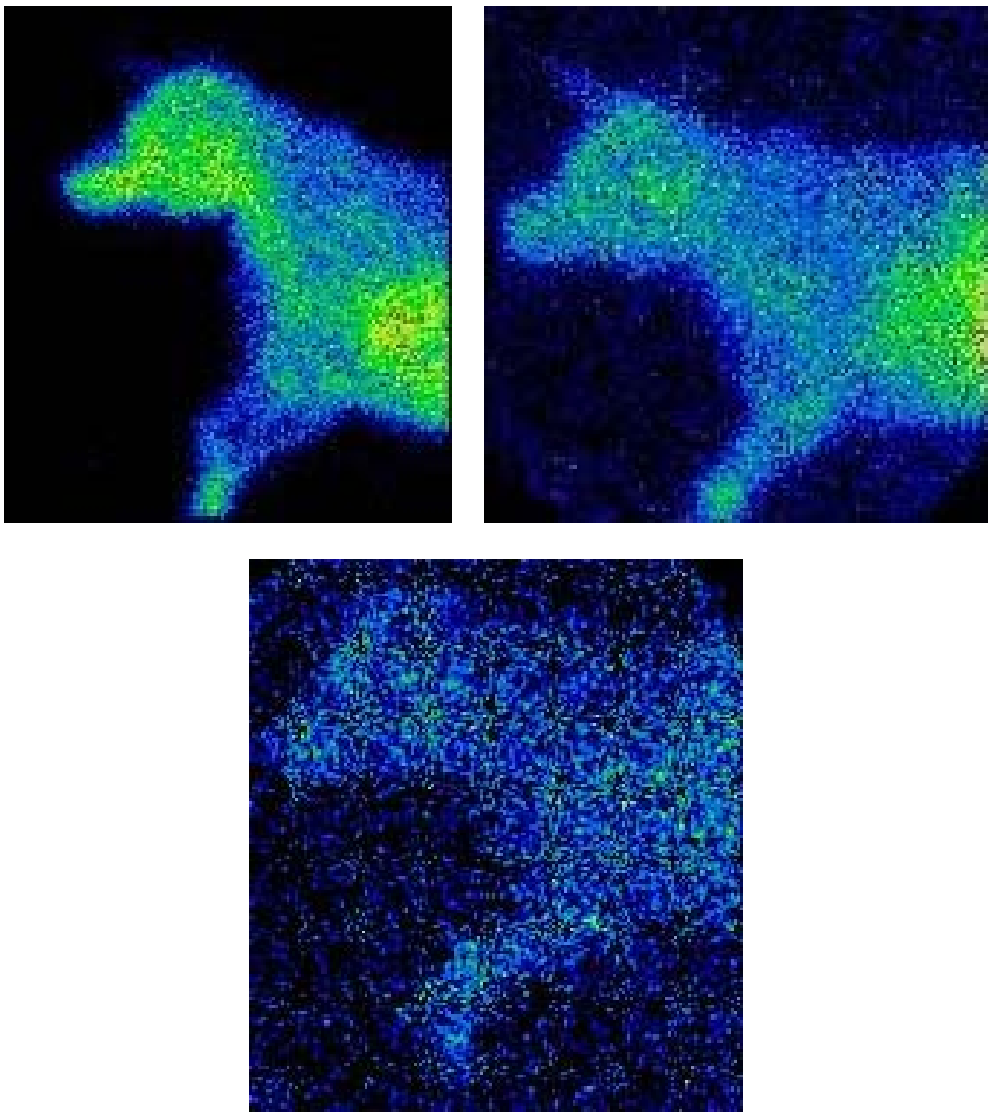

Figure 5.8: Case 2: Right head and neck at 1h, 4h, and 24h. Due to the small size of this patient, much of the thorax is included. In the 1h scan, the cardiac blood pool is more apparent than the previous dog. Subjectively, the mandibular nodes are visible on the 1h and 4h images, but the ratios were actually highest on the 24h scan.

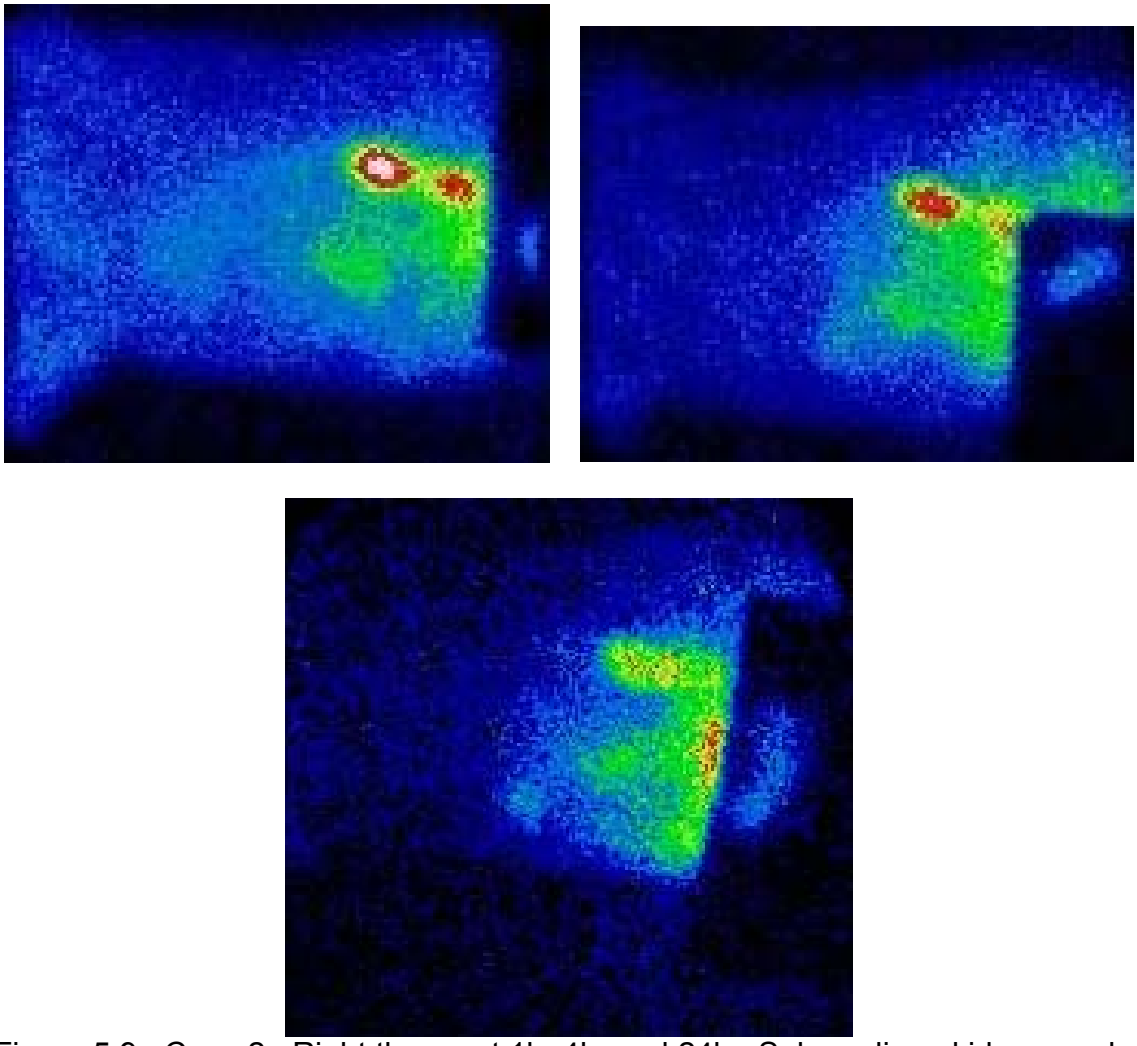

Figure 5.9: Case 2: Right thorax at 1h, 4h, and 24h. Spleen, liver, kidney, and gastrointestinal uptake are apparent on these images. The gall bladder is particularly apparent on the 24 hour image. No other image showed such clear gallbladder activity.

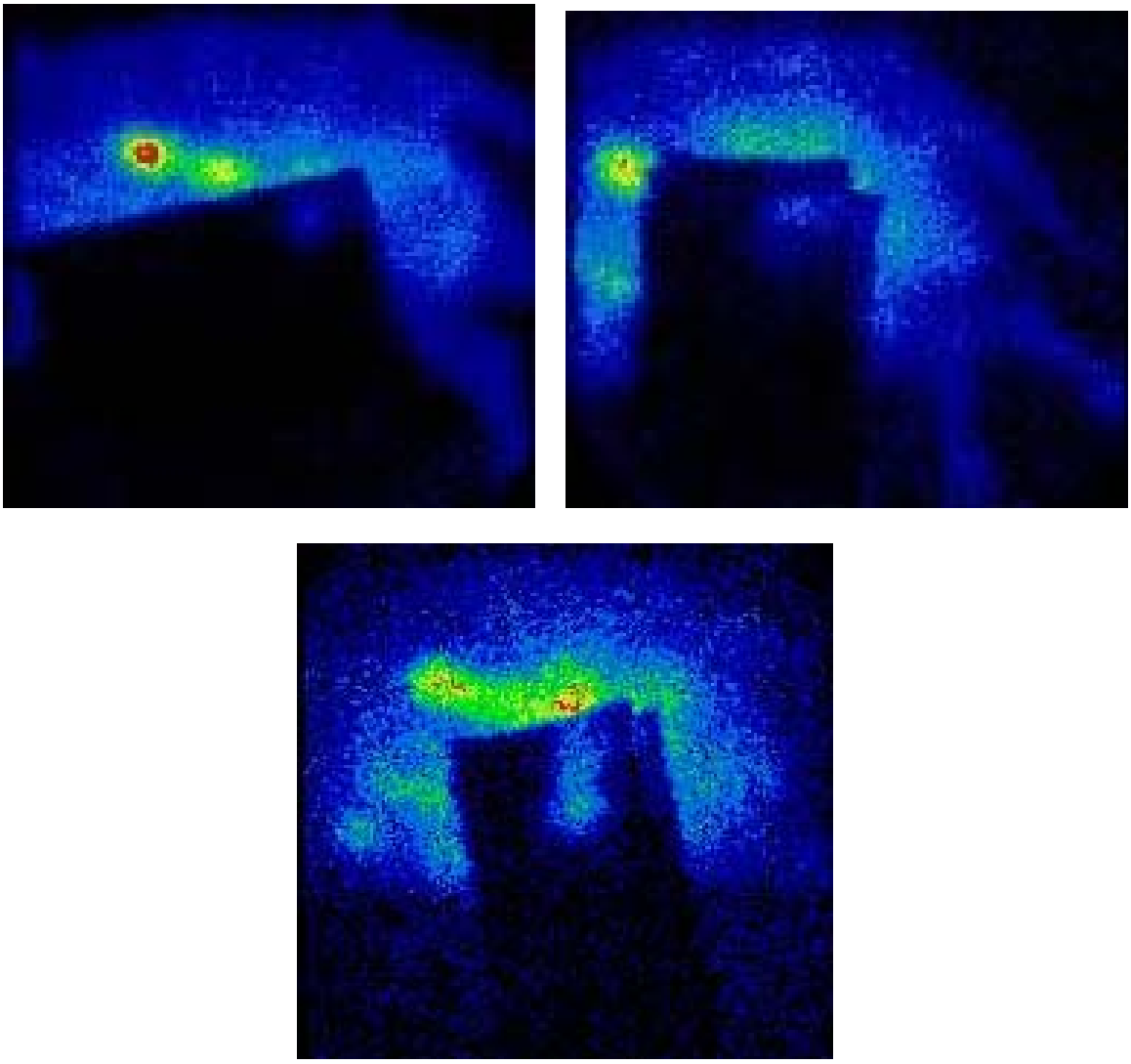

Figure 5.10: Case 2: Right abdomen at 1h, 4h, and 24h. Kidney and gastrointestinal activity is apparent. Popliteal activity was increased, although the node is not easily delineated on the images.

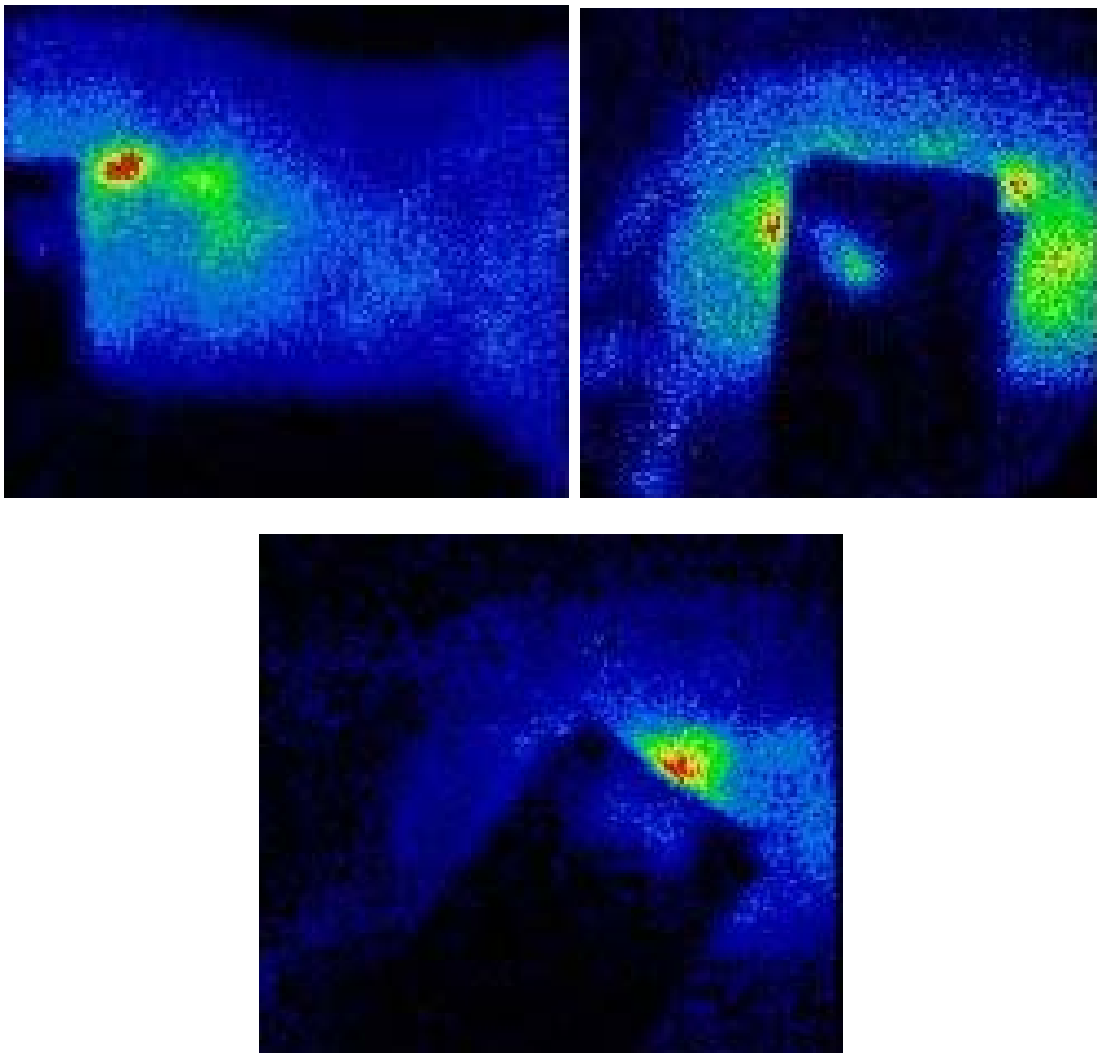

Figure 5.11: Case 2: Left abdomen at 1h, 4h, and 24h. Spleen, liver, kidney, and gastrointestinal activity are evident on these images. Again, the cardiac silhouette is visible on the 1h scan.

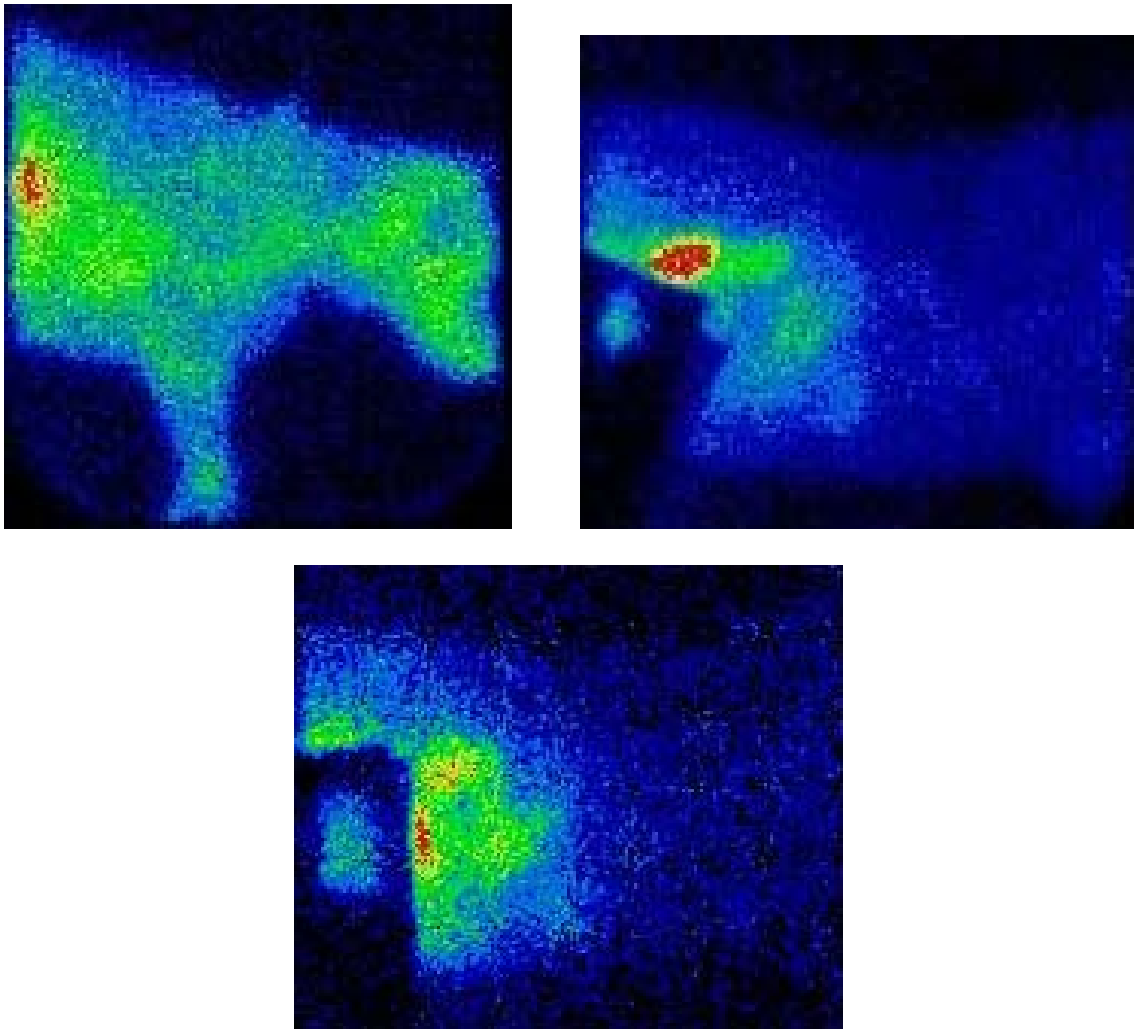

Figure 5.12: Case 2: Left thorax at 1h, 4h, and 24h. While nodes in the region of the head and neck are visible on the 1h scan, the liver and spleen predominate at 4h and 24h.

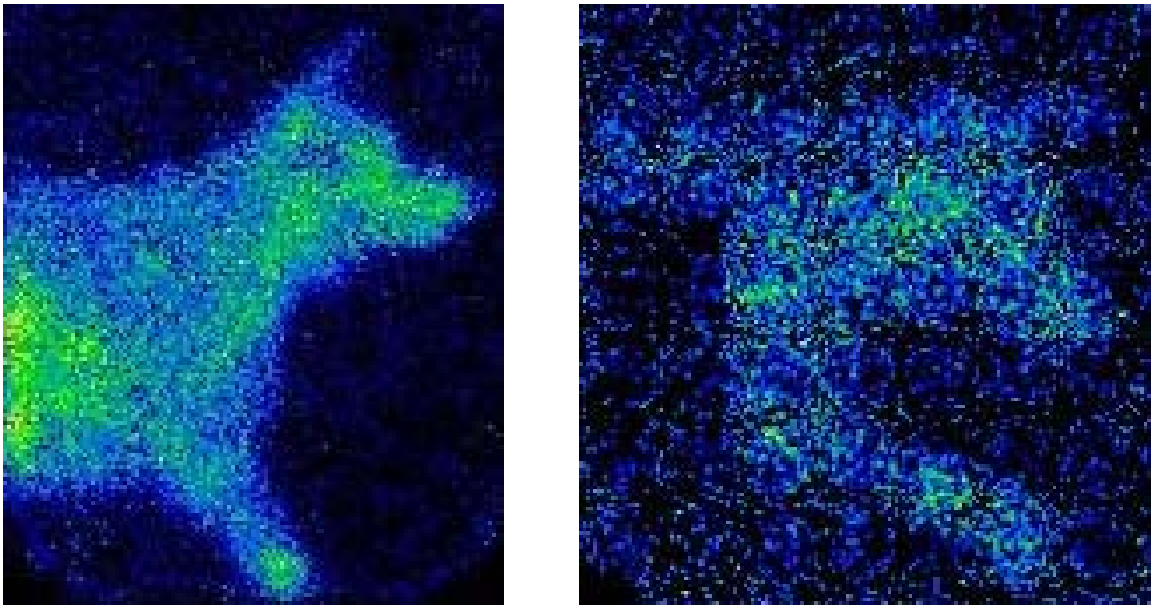

Figure 5.13: Case 2: Left head and neck at 4h and 24h. Node activity is apparent, as is liver and heart activity on the 4h scan.

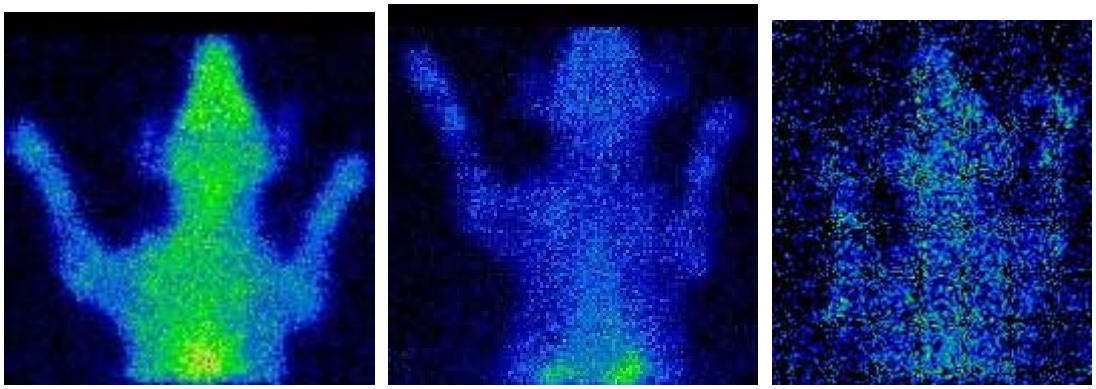

Figure 5.14: Case 2: Ventral head and neck at 1h, 4h, and 24h. Although the nodes are difficult to distinguish subjectively, the measured uptake values were increased for the mandibular nodes in these images.

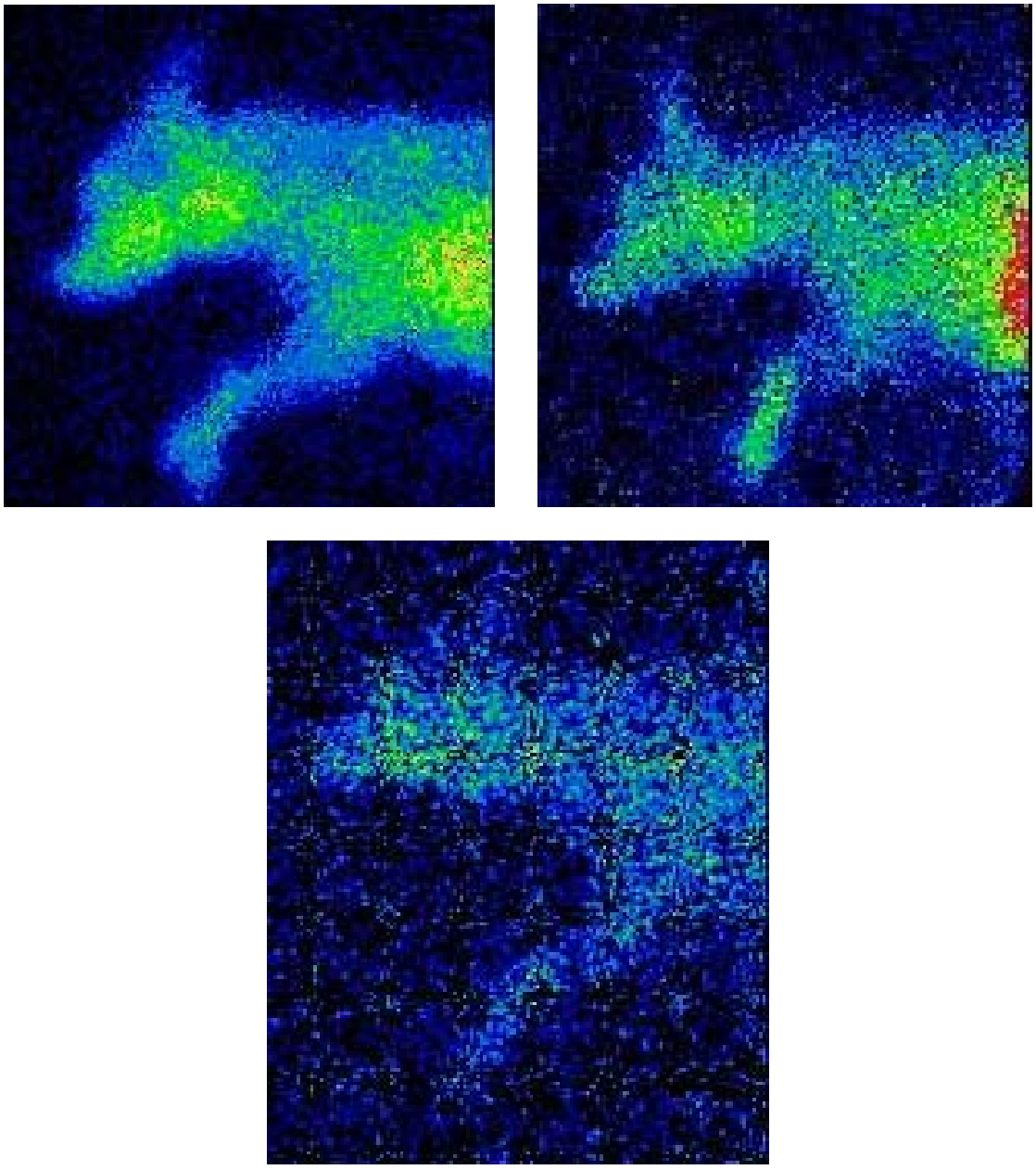

Figure 5.15: Case 3: Right head and neck at 1h, 4h, and 24h. Mandibular node activity is evident in each of these images.

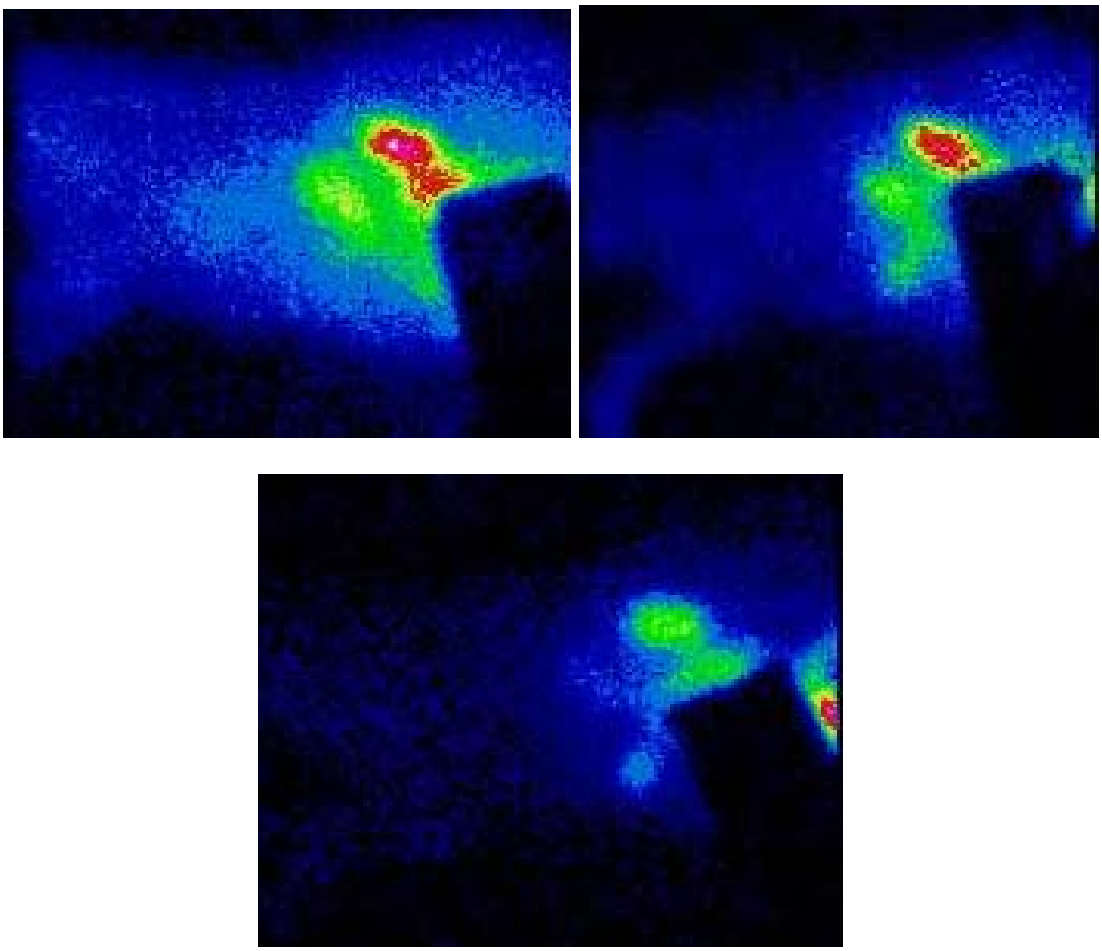

Figure 5.16: Case 3: Right thorax at 1h, 4h, and 24h. Spleen, liver, gastrointestinal, and possibly gallbladder activity is evident on these images.

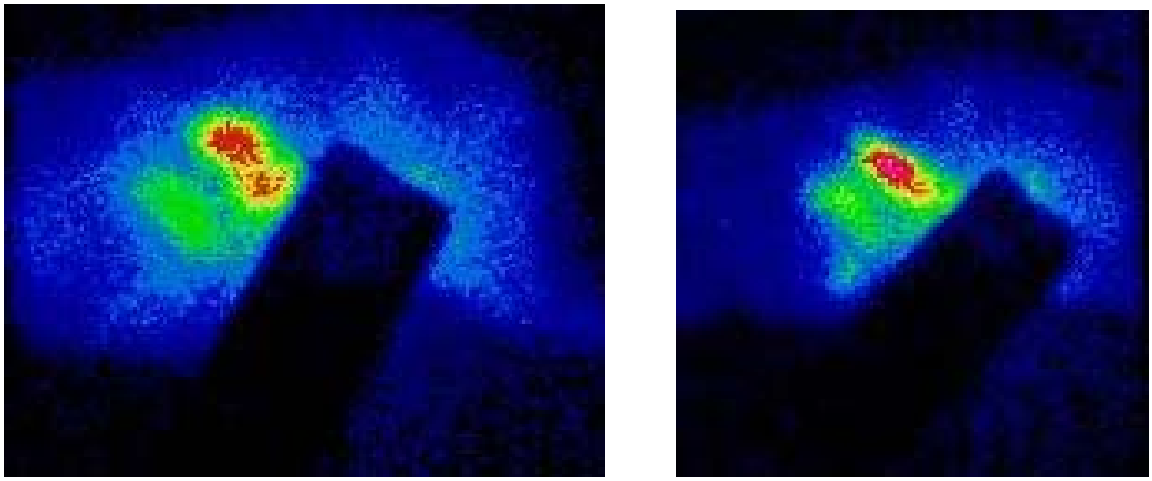

Figure 5.17: Case 3: Right abdomen at 4h andh. Spleen, kidney, gastrointestinal, and liver activity are visible on these images.

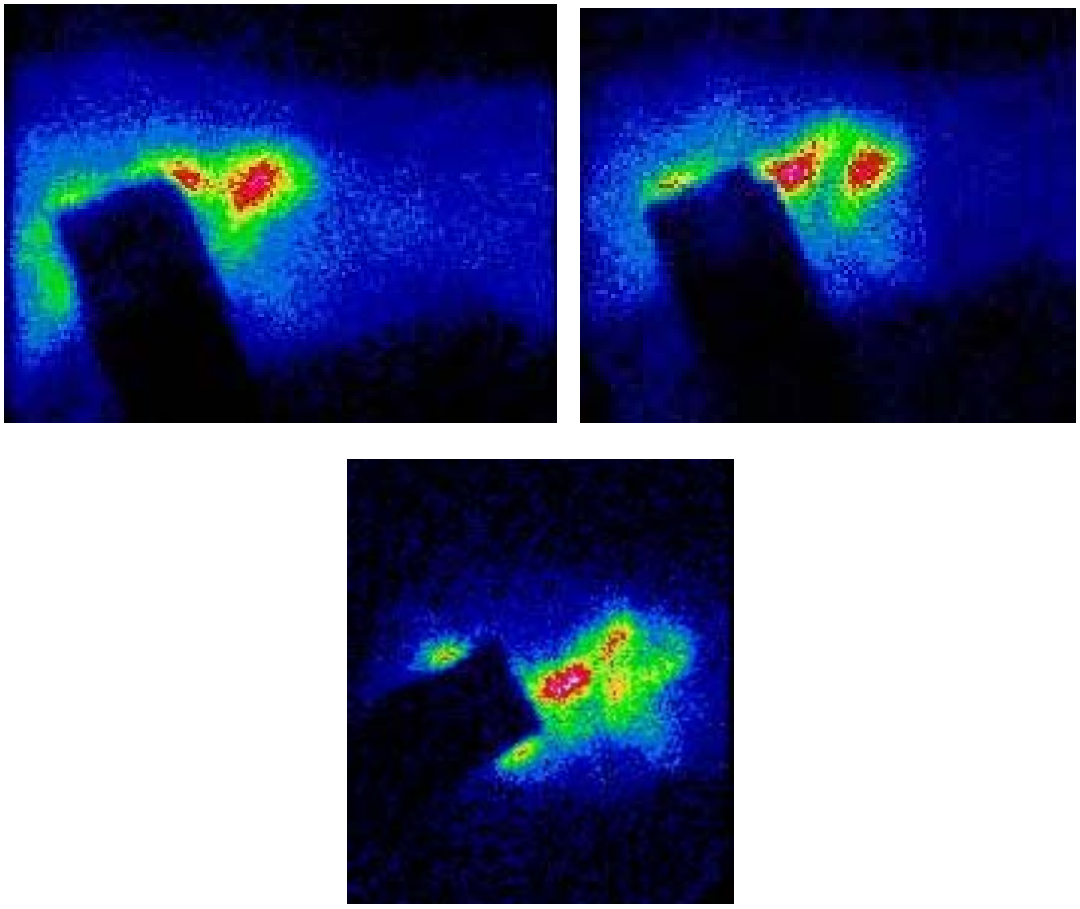

Figure 5.18: Case 3: Left abdomen at 1h, 4h, and 24h. Spleen activity is very prominent on these images. Liver activity is present as well, appearing increasingly prominent over time. Kidney activity is present and constant in appearance.

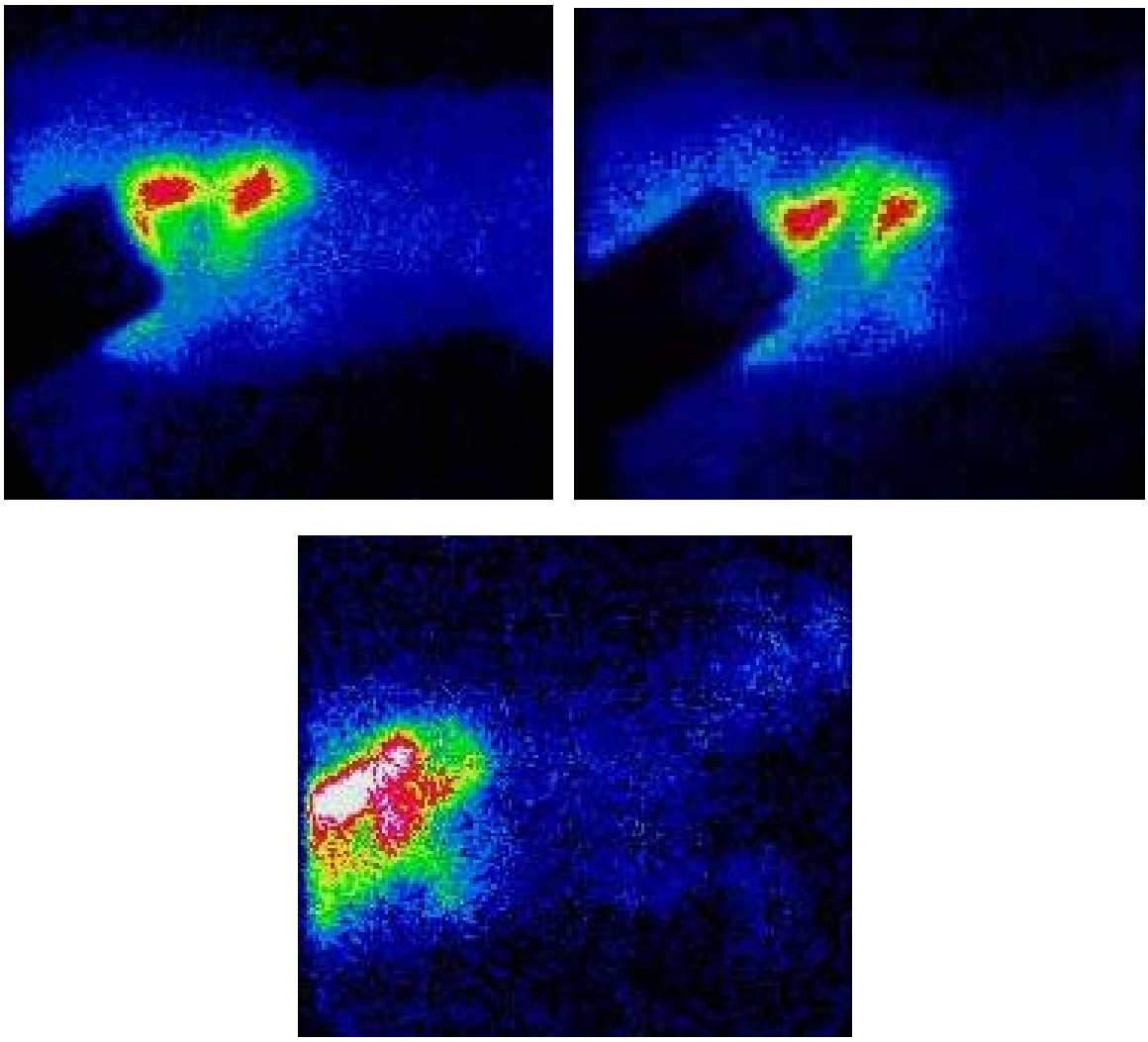

Figure 5.19: Case 3: Left thorax at 1h, 4h, and 24h. Spleen, liver, and gastrointestinal activity are present, but blood pool is minimally visible in the cardiac region. The suggestion of node activity is apparent on the 24h scan.

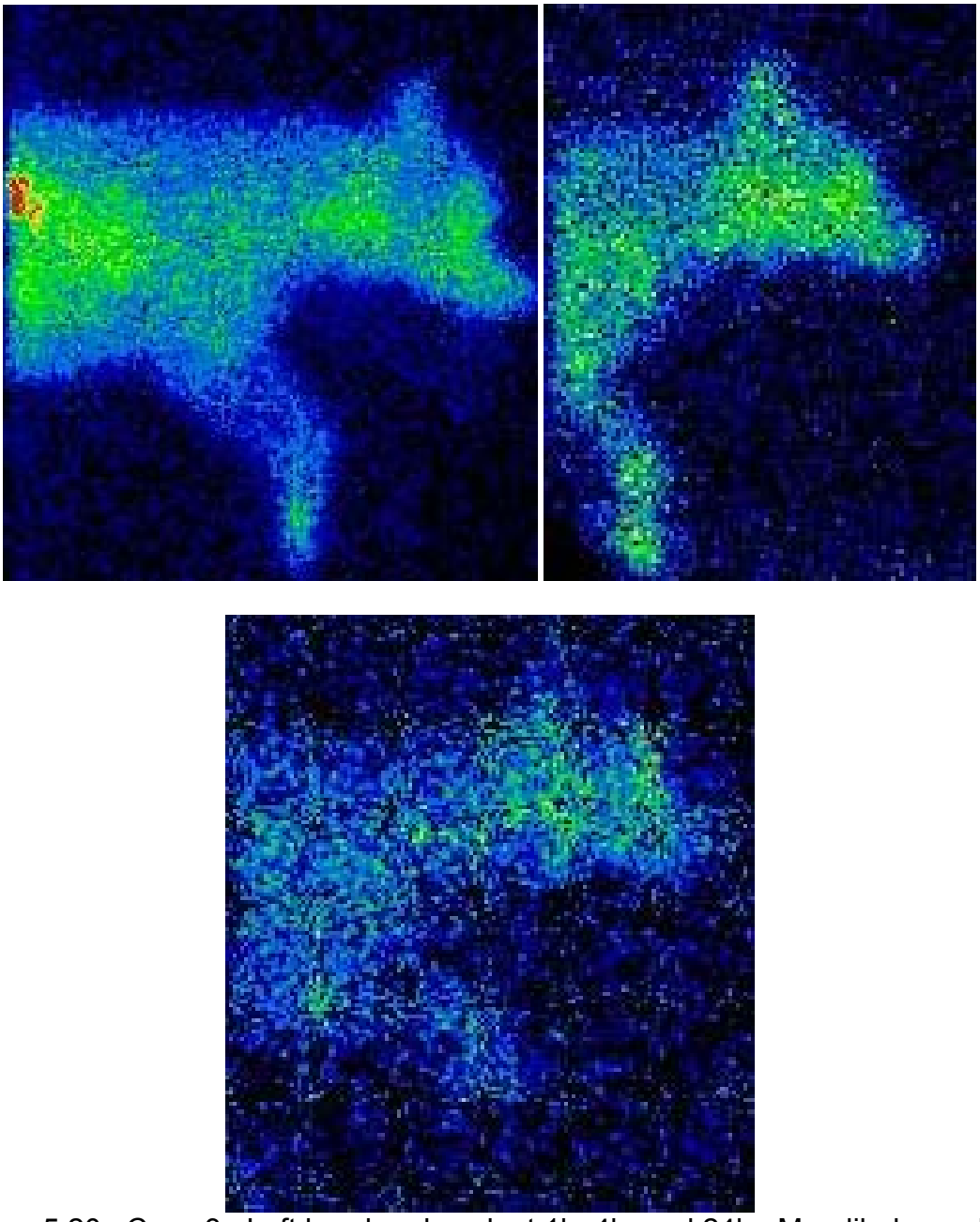

Figure 5.20: Case 3: Left head and neck at 1h, 4h, and 24h. Mandibular and superficial cervical node activity are present in these images.

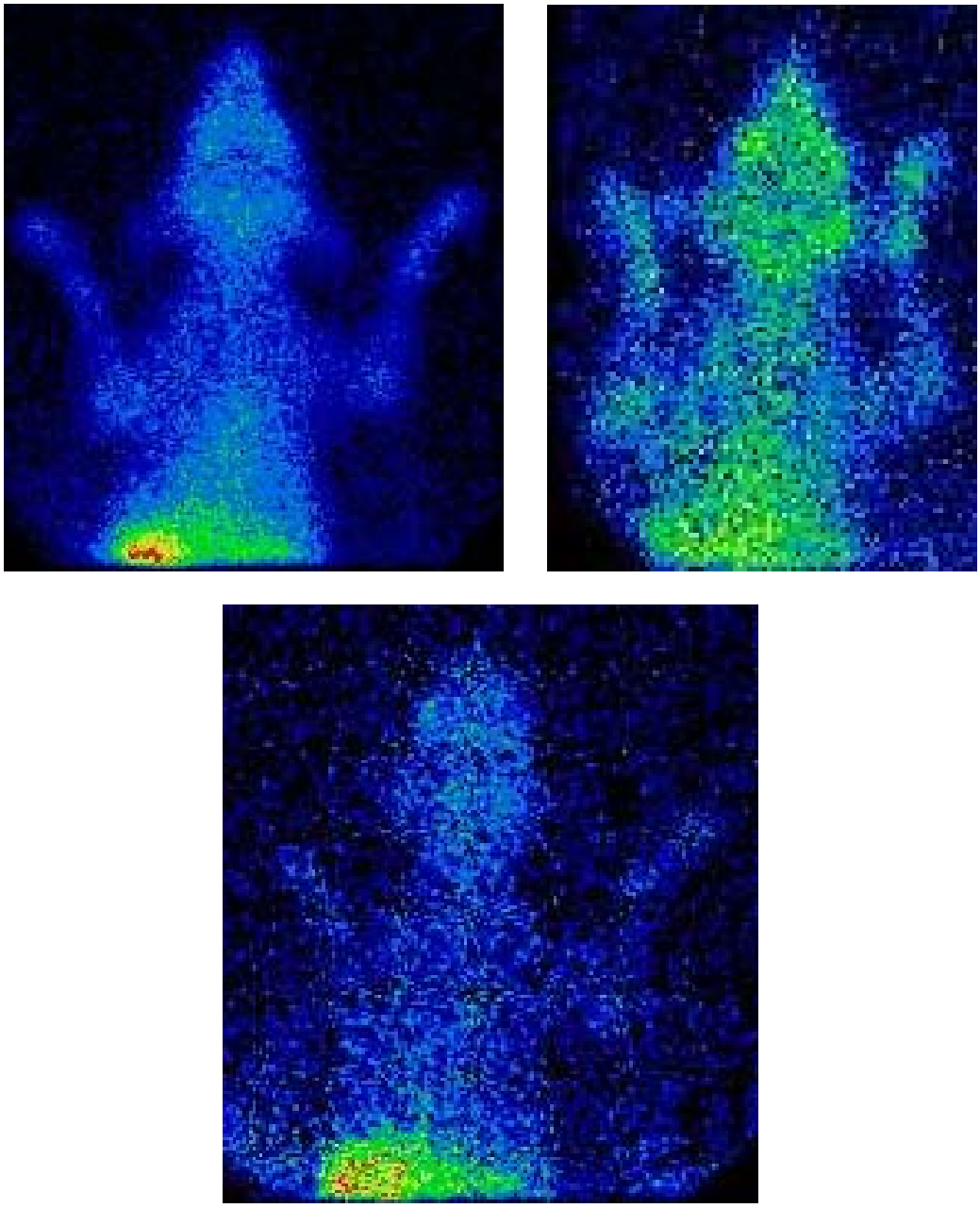

Figure 5.21: Case 3: Ventral head and neck at 1h, 4h, and 24h. Mandibular and superficial cervical node activity is present on these images. Liver activity is present as well.

Discussion

The three dogs in this study shared similarities of being female, eight years old, and having advanced, bulky and organ-based disease. As such, they do not represent a broad cross-section of canine B-cell lymphomas. However,

as proof of principle, the results of these scans demonstrate the potential utility of ^{111}In-DOTA-TATE as an imaging or therapy-targeting agent. The scans demonstrate uptake in tissues affected by lymphoma, by both subjective and objective measures.

In each dog, the area of the mandibular lymph nodes is visually apparent. The objective uptake ratios, however, are only mildly increased relative to muscle. The argument could be made that tumors are associated with increased blood flow, explaining the minor increased ratio at the node regions. However, after the first hour, the ratio of heart activity to muscle activity is 1.0. If blood flow explained the increased activity visible in the lymph nodes, these, too, would be expected to return to background after one hour, when they are at least 39% above background at 24h in every case. In fact, in cases 1 and 2, lack of target to background difference likely explains the low node to muscle ratio at 1h. It is more difficult to explain the low ratio at 4h for dog 3. It should be noted that dog 3 had a large burden of disease in the liver and spleen. It is possible that these highly vascular lymphoma beds served to provide a first-pass effect to remove much of the radiopharmaceutical from the blood. Activity then accumulated slowly in the mandibular lymph nodes over time, after the 1h blush subsided.

The superficial cervical node demonstrated fairly consistent ratios above 1.0, but not as high as the mandibular node. It is likely that the location of this node, with a continuous background of muscle mass and no air boundaries like the mandibular node, would have consistently lower uptake ratios than a more isolated node. The popliteal node demonstrated ratios greater than 1.29 in all

cases except the 1h measurement of Dog 1. This was slightly surprising, as the node was not consistently evident on visual examination of the images. Ratios calculated on other portions of the leg, however, were approximately 1.0, confirming the presence of uptake in the popliteal region.

Organ ratios tended to be higher than node ratios. Splenic involvement was suspected or documented by ultrasound imaging in all three dogs. Liver involvement was only suspected in dogs 2 and 3. It is noteworthy that liver uptake ratios were increased relative to background in all dogs. This would suggest that there was some hepatic clearance in these dogs, unrelated to the localization of the lymphoma. This is consistent with the finding of patchy liver uptake in five Beagle dogs imaged using ^{111}In-DTPA-D-Phe^{1}-octreotide using single photon emission computed tomography (SPECT).[96] Ratios were higher in the dogs with suspected liver involvement, confirming the subjective impression of a liver outline on the images. Spleen uptake was high in all dogs. It is likely that this is a direct result of the lymphoma present in the spleen. Robben and others found no splenic uptake present in normal dogs.[96] Future studies will need to repeat scans in remission from lymphoma to document resolution of splenic uptake. The data presented here cannot rule out spleen uptake by mechanisms other than lymphoma present. Robben and others also found gastrointestinal uptake in the normal dogs that appeared receptor-mediated.[96] Similar to that finding, the dogs in this study had gastrointestinal uptake ratios well above 1.0 at all time points. This should be expected in dogs with no gastrointestinal lymphoma disease burden in future studies. On average, the

uptake ratios for nodes reported here are lower than those reported in a study of ^{111}In-DOTA-DPhe^{1}-Tyr^{3}-octreotide and ^{111}In DOTA-lanreotide in humans.[154] These agents yielded ratios, when positive, ranging from 2.34+/-0.94 to 2.49+/-0.58. Included in the target to background ratios of these measurements were both nodes and organ lesions, with no specifics listed. It is possible that the organ ratios were higher than the node ratios in humans as presently observed in dogs.[154]

The subjective evaluation of the images from dog 1 revealed multiple visible nodes from the 1h time-point. In fact, the zygomatic and sublumbar node involvement had not been noted until they were visualized on the scan images. It is also unlikely that the cervical node involvement would have been detected without the scan. Depreotide scanning in children with either Hodgkin's lymphoma or NHL revealed lesions that changed the stage and therapy plan in three of 11 patients.[90] Lesions were also missed by depreotide scanning in these patients, but none would have altered staging.[90] Staging with ^{111}In-pentetreotide resulted in detection of lesions in 10 patients that altered the clinical course in 5 of them.[92] Similar to the depreotide study, 19 patients had lesions detected by conventional means that were missed on nuclear scintigraphy.[92]

Dog 2 did not have nodes as clearly visible as dog 1. This may be due to this dog's significantly smaller size. The liver and spleen activity was clearly visible in this dog, with a clear gallbladder image on lateral abdominal views at 4h. Gallbladder activity was detected in normal beagles, so is likely a normal

finding in this case.[96] Popliteal node activity was present in this dog, as measured by uptake ratios, but the nodes were not clearly visible subjectively. This is likely a result of the small size of the patient as well. Subjectively, the cardiac silhouette was particularly prominent in this patient. The presence of an active leukemia component of this dog's disease would suggest the possibility that this increased blood-pool activity was receptor mediated. When compared to the other dogs, however, there was not a significant increase in heart activity at any time point. The images of dog 3 were subjectively very similar to those of dog 2. The presence of hepatosplenomegaly in both dogs, and their similar small size, likely contributes to the similarity of the scans.

The results of this study confirm the hypothesis. Uptake of a radiolabeled somatostatin analogue in canine NHL occurred at levels allowing non-invasive detection by with planar scintigraphy. This forms the basis for future development of imaging and therapy agents using SSTR2-specific ligands. The internalizing nature of somatostatin analogues make them suitable for intracellular delivery of imaging and therapeutic nuclides as well as molecules directed at intracellular targets. It also mimics the presence of SSTR2 receptors on the surface of human NHL cells, supporting the use of dogs as a pre-clinical model for human research.

Materials and Methods

Dose Preparation: DOTA-TATE was labeled with ^{111}In as follows: 1mCi of ^{111}InCl3 in 150 µL of 30 mM sodium acetate, 25 mM sodium ascorbate, pH 5.0,

was incubated with 1 μg of DOTA-TATE at 99 °C for 30 min. Radiometal incorporation and radiochemical purity (typically >98%) were determined by radio-thin layer chromatography (TLC). After sterile filtering, the radiolabeled peptide was diluted with normal saline for injection. Reversed-phase HPLC (RP_HPLC) was performed on a Waters 626 chromatograph equipped with a manual Rheodyne injector, 2487 dual wavelength UV detector, busSAT/IN analog-digital interface and Empower Pro software (Build No. 1154). A Phenomenex (Torrance, CA) Jupiter C18 column (5 μm, 4.6 × 250 mm) was used for purification and analysis of radiolabeled compounds. A gradient of 0-50% solvent B (solvent A, 0.1% TFA/H2O; solvent B, 0.1% TFA/acetonetrile) over 30 min at a flow rate of 1.0 mL/min was used. UV detection was accomplished at 280 nm, and radioactivity detection was accomplished using a NaI(Tl) radioactivity monitor (Canberra Meriden, CT).

Dose Administration: A 22ga indwelling catheter was placed in each dog's cephalic vein. The complete dose of 3-5mCi (111-171MBq) of ^{111}In-DOTA-TATE was injected intravenously in a single bolus followed aspiration and flushing to ensure complete dose injection.

Image Acquisition: Dogs were sedated according to standard and IACUC approved protocol, and images were acquired at 1h, 4h, and 24h, following injection. Intended images included the right and left lateral head and neck, right and left lateral thorax, and right and left lateral abdomen using an Equistand II (Diagnostic Imaging, Middlesex, NJ) planar gamma camera with a median energy all purpose collimator (MEAP). Other views were acquired if regions of

interest were discovered on the standard views. Not all views were acquired on the first case at all time points.

Image Analysis: Images were converted to JPG file format and imported into ImageJ analysis software (National Institutes of Health, Bethesda, MD). Regions of interest were drawn around nodes, liver, and spleen. The mean intensity within those regions were compared with a simultaneously acquired ROI overlying muscle in the same image. The result is the reported target to background ratio. No statistical analysis was performed, as the sample size precludes rigorous analysis. Images were also evaluated qualitatively by a board-certified veterinary oncologist trained in nuclear imaging. Dogs were released from radiation isolation 48h after injection per protocol.

Chapter 6

Conclusions and Planned Future Studies of Canine *DLC1* and Epigenetic Modulation of Radiosensitivity

The results of this series of experiments establish solid underpinnings for the use of dogs as a preclinical model for epigenetic study, epigenetic therapy, and targeted imaging and therapy with somatostatin receptor analogues in canine NHL. There is strong evidence that a canine gene, *DLC1*, possesses structure that makes possible epigenetic control through methylation of binding sites of methylation-sensitive transcription factors. The gene also has features that appear to have prevented its methylation in the core promoter region in this series of NHL cases. Likely as a result of this boundary effect, there is no significant alteration in gene expression in these cases. Experiments combining the demethylating drug zebularine show a dramatic difference in the mechanism of radiation sensitization between external irradiation and radiopharmaceutical therapy *in vitro*. This suggests that the methods of cell killing intrinsic to these different qualities of radiation are enhanced by an agent with multiple actions of potentiation. The target of the therapeutic radiopharmaceutical evaluated exists in spontaneous canine lymphoma. These experiments have carried the concept of developing demethylation therapy strategies from the computer to the cageside. They confirm that mechanisms are common between dogs and humans that allow evaluation of epigenetic mechanisms, diagnostic and prognostic assays, therapy strategies, and combination therapy trials. What follows will outline future evaluation of this model.

Further characterization of the *DLC1* gene and mechanisms that regulate hypermethylation in dogs is necessary. To characterize canine *DLC1* fully, complete cloning of the cDNA must continue to be attempted. An alternative

approach would be the creation of a bacterial artificial chromosome library of the dog transcriptome to be screened with the real-time primers for the appropriate sequence. This was not attempted during these projects because of the significant cost associated with this approach. A Northern blot analysis of multiple tissues could be performed to identify the splice variants and tissue type distribution within the dog. Such distribution and relative expression levels could inform selection of other cancers to examine for epigenetic regulation of this interesting tumor suppressor gene. Further sequencing of the promoter region should be performed. Since the density of CpG dinucleotides in the CpG island has hampered efforts to optimize traditional bisulfite-treatment approaches, chromatin immunoprecipitation techniques to identify the methylation status of individual transcription factor binding sites and their occupation status could be used. This would improve the understanding of the function of Sp1, AP-2, and others yet to be discovered in control of this gene. By specifically methylating the DNA, differences in the resulting immunoprecipitate could identify the necessary methylation status of these sequences for binding transcription machinery.[13] These experiments would further characterize the dog *DLC1* gene, identify neoplastic tissues for further study, and serve as a comparative model to human epigenetic mechanisms.

The silencing of genes in canine NHL should be examined by identifying candidate genes through expression microarray experiments showing constitutive downregulation that can be altered by DNMT inhibitor therapy. By growing cells *ex vivo* in the presence or absence of zebularine, or using serial

biopsies prior to and after systemic zebularine therapy, genes whose expression is altered by the zebularine therapy would be likely candidates for epigenetic control.[135] This would narrow the focus of gene selection, rather than identifying and developing assays for genes from a candidate list of human methylated genes. The latter is time-consuming, and the cost of the microarray experiments would result in significant time savings toward developing assays for genes with evidence of epigenetic regulation.

The radiosensitization phenomenon observed in these studies should be further evaluated. First, the simple experiment of reversing the order of radiation and zebularine would demonstrate whether the alterations in proliferative potential and viability are dependent on prior demethylation of genes. As both treatments exert an effect while present, an additive effect would be expected. The demonstration of a synergistic effect would suggest that the mechanism of synergism might be a more basic cellular function than re-expression of genes, such as interference with RNA synthesis or some other anti-metabolite-like effect of zebularine. Alternatively, substituting decitabine, which has a ribose sugar base, would eliminate any possible RNA effect of the demethylating drug.[33] If these experiments confirmed that prior exposure to a demethylating agent is necessary for the observed synergy, examination of cell cycle regulatory and apoptotic pathways using expression microarray analysis could assist in defining the underlying mechanism. This would identify potential pathways for further study that may be altered in the MEC1 cells by demethylation therapy. As this is a human CLL cell line, the available platforms of microarray is vast relative to the

dog. Expression analysis followed by promoter or CpG island array analysis would distinguish those sequences containing significant methylcytosine from the genes that are simply targets for genes upregulated by demethylation. Similar work in solid tumor cell lines identified upregulation of cancer-testis antigens.[135] It is likely that imprinted genes would be upregulated in such studies. Also, gene upregulation is likely to be cancer-specific, as even different forms of NHL have been shown to have different genes silenced by hypermethylation.[53;67;68]

Given the identified *in vitro* synergy between zebularine and radiation, MEC1 tumor studies in mice with dose escalation would demonstrate whether a true therapy benefit exists. Ultimately, the mouse studies are necessary prior to moving into larger animals, because the biological effects on distribution of the radiopharmaceutical must be considered. The *in vitro* conditions are artificial, with known homogeneous delivery to the tumor cells. Blood flow parameters and binding barriers could diminish the effectiveness of the somatostatin receptor delivery of the ^{177}Lu payload in mice. Similarly, the demethylating effect may not be uniform within the tumor *in vivo*. Failure of either compound would likely abrogate the intended effect. Alternatively, either may be more effective *in vivo*. These studies should be dose-escalation studies of both zebularine and ^{177}Lu-DOTA-TATE to determine the optimal interaction to carry forward into preclinical studies in dogs.

There is evidence that zebularine sensitizes ovarian cancer cell lines to cisplatin chemotherapy.[143] Chemosensitivity studies of human and canine lymphoma cells and cell lines could demonstrate sensitization and synergy

similar to the effects from radiation. As chemoresistance is the most common mechanism of failure for NHL patients, this strategy could prove useful. Often, this chemoresistance is attributed to upregulation of the MDR1 gene or expression of bcl2.[155;156] Altering the epigenetic landscape of neoplastic lymphocytes may abrogate these resistance mechanisms. As zebularine is an agent with oral bioavailability, it is attractive for addition to a chemotherapy regimen, as it would minimize a patient's required trips to the chemotherapy center.

Further exploitation of somatostatin analogues as a delivery platform for imaging and therapy nuclides and targeted molecules is warranted. The imaging study presented here was a pilot to a larger study evaluating a peptide-nucleic acid conjugate complementary to the mRNA of the anti-apoptotic gene bcl2. The purpose will be to evaluate expression of this gene *in vivo* using naturally occurring canine NHL as a model for the human disease. Such technology would allow real-time decision making about treatment based on the dominant patterns of gene expression imaged in the patient. The results of the target analysis in this imaging study portend a future of clinically useful molecular imaging in oncology.

Ultimately, dog studies evaluating ^{177}Lu-DOTA-TATE alone and in combination with zebularine would be useful for development of these agents for human use. The studies described here have demonstrated many similarities in the epigenomic apparatus of humans and dogs. These results suggest that further, broader analysis to define the similarities as they apply to stages of B-cell

development are warranted to develop the dog as a truly comparative model of human disease. This would give cancer researchers a clinically relevant, large animal model of NHL for preclinical evaluation of novel diagnostic, imaging, and therapy strategies. Such models will advance the understanding of human disease, and benefit dogs through increased research funding and available clinical trials.

Appendix 1: Candidate Hypermethylated Genes

Homo sapiens:

Gene Name, accession no, chromosome, CpG Island, function

AAK1, NM_014911, 2p13.3, YES, AP2 associated Kinase 1

Canis familiaris:

Accession Number, function, homology, expect, chromosome

NW_139870.1, AP2 associated Kinase 1. 193/210, 6.00E-79, 10

NW_139870.1, Alpha 1 collagen, 223/233, 2.00E-105,10

Homo sapiens:

Gene Name, accession no, chromosome, CpG Island, function

ABCG1, NM_207630, 21q22.3, NO, ATP binding cassette transporter G1

Canis familiaris:

Accession Number, function, homology, expect, chromosome

NW_139908.1, ATP binding cassette transporter G1, 172/188, 2.00E-68, 31

NW_139851.1, NOD9 protein isoform 1, 136-169, 9.00E-27, 5

Homo sapiens:

Gene Name, accession no, chromosome, CpG Island, function

ACTR6, NM_022496, 12q23.1, YES, Activated protein 6

Canis familiaris:

Accession Number, function, homology, expect, chromosome

NW_139876.1, ACTIN-RELATED PROTEIN 6, ARP6, 413/490, 2.00E-129, 15

NW_139876.1, similar to KIAA0701 protein, 106/115, 1.00E-38, 15

Homo sapiens:

Gene Name, accession no, chromosome, CpG Island, function

ALX4, AB058691, 11p11.2 , YES, Aristaless-like homoebox 4

Canis familiaris:

Accession Number, function, homology, expect, chromosome

NW_139885.1, Aristaless-like homoebox 4, 671/798, 0.00E+00, 18

NW_139885.1, SIMILAR TO EXOSTOSIN-2 (3' SIDE), 195/218, 7.00E-73, 18

Homo sapiens:

Gene Name, accession no, chromosome, CpG Island, function

ANX4, NM_001153, 2p13.3, YES, Annexin A4

Canis familiaris:

Accession Number, function, homology, expect, chromosome

NW_139870.1, similar to germ cell-less, 831/1067, 3.00E-150, 10

Homo sapiens:

Gene Name, accession no, chromosome, CpG Island, function

ARF4, BC016325, 3p21.2-p21.1, YES, ADP-ribosylation factor 4

Canis familiaris:

Accession Number, function, homology, expect, chromosome

NW_139889.1, hypothetical protein FLJ34969, 867/966, 0.00E+00, 20

NW_139876.1, RING finger protein 11, 85/94, 6.00E-26, 15

Homo sapiens:

Gene Name, accession no, chromosome, CpG Island, function

ARX, AY038071, Xp22.1-p21.3, YES, Aristaless related homeobox

Canis familiaris:

Accession Number, function, homology, expect, chromosome

NW_139919.1, Aristaless related homeobox, 292/325, 6.00E-114, X

Homo sapiens:

Gene Name, accession no, chromosome, CpG Island, function

ATOX2, NM_004045, 5q33.1, YES, Antioxidant protein 1

Canis familiaris:

Accession Number, function, homology, expect, chromosome

NW_139885.1, 5' syaptotagmin XII 3' pyruvate carboxylase, 353/439, 1.00E-86, 18

NW_139886.1, 5' Jade 1 protein 3' importin alpha-2 subunit, 352/442, 8.00E-81, 19

NW_139850.1, copper chaperone, 147/177, 3.00E-36

Homo sapiens:

Gene Name, accession no, chromosome, CpG Island, function

BLK, NM_001715, 8p23.1, NO, B lymphoid tyrosine kinase

Canis familiaris:

Accession Number, function, homology, expect, chromosome

NW_139898.1, B lymphoid tyrosine kinase, 198/210, 8.00E-89, 25

NW_139841.1, proto-oncogene tyrosine-protein kinase FGR, 73/88, 7.00E-12, 2

Homo sapiens:

Gene Name, accession no, chromosome, CpG Island, function

BZW1, NM_014670, 2q33.1, YES, Basic leucine zipper and W2 domains 1

Canis familiaris:

Accession Number, function, homology, expect, chromosome

NW_139919.1, carbohydrate N-acetylglucosamine 6-o sulfotr, 885/923, 0, X

NW_139916.1, Basic leucine zipper and W2 domains 1, 556/584, 0, 37

Homo sapiens

Gene Name, accession no, chromosome, CpG Island, function

CG1-150, AF177342, 17p13.3, NO, Hypothetical protein

Canis familiaris:

Accession Number, function, homology, expect, chromosome

NW_139866.1 similar to chromosome 17 open reading frame 25

137/143 5.00E-60 9

Homo sapiens

Gene Name, accession no, chromosome, CpG Island, function

CHODL, AF257472, 12q12.1, YES, Chondrolectin

Canis familiaris:

Accession Number, function, homology, expect, chromosome

NW_139908.1, Chondrolectin, 1192/1464, 0, 31

Homo sapiens

Gene Name, accession no, chromosome, CpG Island, function

CHP, NM_007236, 15q15.1, YES, Calcium binding protein

Canis familiaris:

Accession Number, function, homology, expect, chromosome

NW_139907.1, Calcium binding protein, 623/738, 0, 30

NW_139888.1, similar to KIAA0779, 63/69, 5.00E-17, 20

Homo sapiens

Gene Name, accession no, chromosome, CpG Island, function

CROC4, NM_006365, 1q22, YES, Transcriptional activator

Homo sapiens

Gene Name, accession no, chromosome, CpG Island, function

CSDA, BC021926, 12q13.2, YES, Cold Shock Domain Protein A

Canis familiaris:

Accession Number, function, homology, expect, chromosome

NW_139903.1, 5' Y-box protein ZONAB-A 3' protein kinase STYK1, 514/572, 0, 27

NW_139892.1, similar to protocadherin 8 isoform 2, 109/116, 2.00E-37, 22

Homo sapiens

Gene Name, accession no, chromosome, CpG Island, function

CYP27B1, NM_000785, 12q14.1, YES, Cytochrome P450

Canis familiaris:

Accession Number, function, homology, expect, chromosome

NW_139869.1, similar to 25-hydroxyvitamin D1 alpha hydroxylase, mitochondrial precursor, 184/196, 3.00E-80, 10

Homo sapiens

Gene Name, accession no, chromosome, CpG Island, function

DBC1, AF027734, 9q32-q33, NO, Deleted in Bladder Cancer 1

Canis familiaris:

Accession Number, function, homology, expect, chromosome

NW_139871.1, Deleted in Bladder Cancer 1, 1108/1184, 0, 11

NW_139860.1, BMP-retinoic acid-inducible meural-specific protein, 221/298, 1.00E-18, 7

Homo sapiens

Gene Name, accession no, chromosome, CpG Island, function

DEDD, BC046149, 1q23.3, YES, Death factor domain containing

Canis familiaris:

Accession Number, function, homology, expect, chromosome

NW_139918.1, Death factor domain containing, SIMILAR TO NITRILASE 1, 487/548, 0, 38

NW_139888.1, similar to KIAA0779 protein, 58/64, 7.00E-15, 20

Homo sapiens

Gene Name, accession no, chromosome, CpG Island, function

DKFZP586D0919, BC016395, 12q14.1, YES, Hepatocellular carcinoma-associated antigen HCA557a, isoform a

Canis familiaris:

Accession Number, function, homology, expect, chromosome

NW_139869.1, elongation factor Ts, 651/761, 0, 10

Homo sapiens

Gene Name, accession no, chromosome, CpG Island, function

DOX54, BC005848, 12q24.13, NO, Dead box polypeptide 54

Canis familiaris:

Accession Number, function, homology, expect, chromosome

NW_139900.1, Dead box polypeptide 54, 179/192, 7.00E-76, 26

Homo sapiens

Gene Name, accession no, chromosome, CpG Island, function

EIF2AK3, NM_004836, 2p11.2, YES, Eukaryotic translation initiation factor 2-alphakinase 3

Canis familiaris:

Accession Number, function, homology, expect, chromosome

NW_139880.1, 5' hypothetical protein XP_532963 3' hypothetical protein XP_540190, 1045/1218, 0, 17

Homo sapiens

Gene Name, accession no, chromosome, CpG Island, function

EIF3S8, BC001571, 16p11.2, YES, Eukaryotic translation initiation factor 3

Canis familiaris:

Accession Number, function, homology, expect, chromosome

NW_139859.1, Eukaryotic translation initiation factor 3, 340/369, 3.00E-151

Homo sapiens

Gene Name, accession no, chromosome, CpG Island, function

EIF4E, NM_001968, 4q23, YES, Eukaryotic translation initiation factor

Canis familiaris:

Accession Number, function, homology, expect, chromosome

NW_139905.1, similar to chromosome 107 open reading frame 12 and Eukaryotic translation initiation factor, 1153/1240, 0, 28

NW_139909.1, Eukaryotic translation initiation factor, 635/675, 0, 32

Homo sapiens

Gene Name, accession no, chromosome, CpG Island, function

EN2, NM_001427, 7q36.3, YES, engrailed homolog 2

Canis familiaris:

Accession Number, function, homology, expect, chromosome

NW_139877.1, similar to insulin-induced protein 1, 738/810, 0, 16

NW_139886.1, similar to homeobox protein engrailed-1, 243/269, 7.00E-80, 19

Homo sapiens

Gene Name, accession no, chromosome, CpG Island, function

ENSA, NM_207042, 1q21.2, YES, Endosulfine alpha isoform 3

Canis familiaris:

Accession Number, function, homology, expect, chromosome

NW_139881.1, Endosulfine alpha isoform 3 ALSO myeloid cell leukemia sequence 1, 197/208, 4.00E-89, 17

Homo sapiens

Gene Name, accession no, chromosome, CpG Island, function

FOXD2, NM_004474, 1p33, YES, Forkhead box D2

Canis familiaris:

Accession Number, function, homology, expect, chromosome

NW_139876.1, UMP-CMP cytidylate kinase, 429/447, 0, 15

NW_139852.1, 60s ribosomal protein, 282/304, 2.00E-124, 5

NW_139854.1, Forkhead box F1, 193/247, 2.00E-32

Homo sapiens

Gene Name, accession no, chromosome, CpG Island, function

GSH1, AB044157, 13q12.2, YES, GS homeobox 1

Canis familiaris:

Accession Number, function, homology, expect, chromosome

NW_139897.1, GS homeobox 1, 424/460, 0, 25

Homo sapiens

Gene Name, accession no, chromosome, CpG Island, function

GSTA4, NM_001512, 6p12.1, NO, Glutatione S-transferase A4

Canis familiaris:

Accession Number, function, homology, expect, chromosome

NW_139910.1, similar to hypothetical protein XP_535712, 877/1041, 0, 33

NW_139908.1, Glutatione S-transferase A4, 842/994, 0, 31

NW_139872.1, Glutatione S-transferase A4, 323/411, 2.00E-61, 12

Homo sapiens

Gene Name, accession no, chromosome, CpG Island, function

GSTM5, LO2321, 1p13.3, NO, Glutathione s-transferase M5

Canis familiaris:

Accession Number, function, homology, expect, chromosome

NW_139852.1, hypothetical protein XP_546682 3' similar to human PDZ domain, 508/624, 2.00E-139, 5

Homo sapiens

Gene Name, accession no, chromosome, CpG Island, function

GTF3C1, U02619, 16p12, YES, General transcription factor IIIC

Canis familiaris:

Accession Number, function, homology, expect, chromosome

NW_139859.1, General transcription factor IIIC, 227/250, 7.00E-92, 6

Homo sapiens

Gene Name, accession no, chromosome, CpG Island, function

H3F3A, NM_002107, 1q41, YES, H 3 histone family 3A

SEE PRINTOUT

Homo sapiens

Gene Name, accession no, chromosome, CpG Island, function

HAS2, NM_005328, 8q24.13, YES, Hyaluronan synthase 2

Canis familiaris:

Accession Number, function, homology, expect, chromosome

NW_139873.1, Hyaluronan synthase 2, 1245/1342, 0, 13

Homo sapiens

Gene Name, accession no, chromosome, CpG Island, function

HIRIP3, BC000588, 16p11.2, YES, HIRA interacting protein 3

Canis familiaris:

Accession Number, function, homology, expect, chromosome

NW_139859.1, HIRA interacting protein 3, 151/171, 3.00E-51, 6

Homo sapiens

Gene Name, accession no, chromosome, CpG Island, function

HIST1H4F, NM_003540, 6p22.2, NO, Histone 1, H2ad

Canis familiaris:

Accession Number, function, homology, expect, chromosome

NW_139914.1, Histone 1, H2ad, 248/279, 4.00E-96, 35

Homo sapiens

Gene Name, accession no, chromosome, CpG Island, function

HMGCS1, NM_002130, 5p12, YES, 3 hydroxy 3-methylglutaryl-coenzymeA synthase

Canis familiaris:

Accession Number, function, homology, expect, chromosome

NW_139908.1, 5' similar to 60s ribosomal protein l6 (TAX-responsive) 3' similar to ORF2, 1425/1607, 0, 31

NW_139911.1, 5' sorting nexin 4 3' oxysterol-binding protein-like protein 11, 1046/1318, 0, 33

NW_139850.1, 3 hydroxy 3-methylglutaryl-coenzymeA synthase ALSO Cyclin G1, 525/570, 0, 4

Homo sapiens

Gene Name, accession no, chromosome, CpG Island, function

HNRPM, NM_005968, 19p13.2, NO, M4 protein deletion mutant

Canis familiaris:

Accession Number, function, homology, expect, chromosome

NW_139889.1, M4 protein deletion mutant, 764/805, 0, 20

NW_139876.1, 5' mineralocorticoid receptor 3' voltage-dependent anion channel 3, 749/904, 0, 15

Homo sapiens

Gene Name, accession no, chromosome, CpG Island, function

HOXC10, BC001293, 12q13.3, YES, Homeo box C10

Canis familiaris:

Accession Number, function, homology, expect, chromosome

NW_139903.1, Homeo box C10, 738/807, 0, 27

Homo sapiens

Gene Name, accession no, chromosome, CpG Island, function

IDE, M21188, 10q23-q25, YES, Insulin-degrading enzyme

Canis familiaris:

Accession Number, function, homology, expect, chromosome

NW_139909.1, ribosomal protein L7a, 983/1196, 0, 32

NW_139905.1, Insulin-degrading enzyme, 258/279, 2.00E-112, 28

Homo sapiens

Gene Name, accession no, chromosome, CpG Island, function

INFK, NM_020124, 9p21.2, YES, Interferon like protein precursor

Homo sapiens

Gene Name, accession no, chromosome, CpG Island, function

ITM2C, AF271781, 2q37.1, YES, Integral membrane Protein 2C

Canis familiaris:

Accession Number, function, homology, expect, chromosome

NW_139898.1, Integral membrane Protein 2C, 308/355, 3.00E-106, 25

Homo sapiens

Gene Name, accession no, chromosome, CpG Island, function

KCN2, NM_021614, 5q22.3, YES, Potassium intermediate/ small conductance calcium activated channel superfamily N, member 2

Canis familiaris:

Accession Number, function, homology, expect, chromosome

NW_139871.1, Potassium intermediate/ small conductance calcium activated channel superfamily N, member 2, 583/608, 0, 11

Homo sapiens

Gene Name, accession no, chromosome, CpG Island, function

KCNK2, NM_001017424, 1q41, NO, Potassium channel superfamily K membrane 2 isoform

Canis familiaris:

Accession Number, function, homology, expect, chromosome

NW_139860.1, Potassium channel superfamily K membrane 2 isoform, 1084/1241, 0, 7

Homo sapiens

Gene Name, accession no, chromosome, CpG Island, function

KCNK4, NM_016611, 11q13.1, YES, Potassium channel superfamily K member 4 isoform

Canis familiaris:

Accession Number, function, homology, expect, chromosome

NW_139885.1, 5' estrogen-related receptor alpha 3' similar to BCL2-antagonist of cell death protein, 631/812, 1.00E-109, 18

NW_139908.1, ATP-binding cassette transporter 13, 141/167, 7.00E-38

Homo sapiens

Gene Name, accession no, chromosome, CpG Island, function

KIAA0152, D63486, 12q24.31, YES, Hypothetical protein KIAA0152

Canis familiaris:

Accession Number, function, homology, expect, chromosome

NW_139900.1, similar to expressed sequence AA407659, 1713/2033, 0, 26

Homo sapiens

Gene Name, accession no, chromosome, CpG Island, function

KIF23, NM_004856, 15q23, YES, Kinesin family member 23

Canis familiaris:

Accession Number, function, homology, expect, chromosome

NW_139907.1, Kinesin family member 23, 244/250, 3.00E-122, 30

Homo sapiens

Gene Name, accession no, chromosome, CpG Island, function

KLHL2, NM_007246, 4q32.3, YES, Kelch-like 2

Canis familiaris:

Accession Number, function, homology, expect, chromosome

NW_139876.1, Kelch-like 2, 745/803, 0, 15

Homo sapiens

Gene Name, accession no, chromosome, CpG Island, function

LHX2, AF124735, 9q33-q34.1, YES, LIM homeobox 2

Canis familiaris:

Accession Number, function, homology, expect, chromosome

NW_139867.1, LIM homeobox 2, 643/690, 0, 9

Homo sapiens

Gene Name, accession no, chromosome, CpG Island, function

LRP1B, AF176832, 2q21.2, YES, Low Density lipoprotein receptor related protein (deleted in tumors)

Canis familiaris:

Accession Number, function, homology, expect, chromosome

NW_139887.1, hypothetical protein XP_533342, XP_533343, XP_541025, 3' XP-533344, 1430/1628, 0, 19

Homo sapiens

Gene Name, accession no, chromosome, CpG Island, function

MAGEF1, BC010056, 3q13, YES, Melanoma-associated antigen F1

Canis familiaris:

Accession Number, function, homology, expect, chromosome

NW_139913.1, hypothetical protein XP_545233, 381/419, 3.00E-164, 34

Homo sapiens

Gene Name, accession no, chromosome, CpG Island, function

MGC21416, BC012469, Xq13.1, YES, Hypothetical protein LOC286451

Canis familiaris:

Accession Number, function, homology, expect, chromosome

NW_139920.1, hypothetical protein MGC21316, 489/578, 3.00E-159, X

Homo sapiens

Gene Name, accession no, chromosome, CpG Island, function

MLLT2, L13773, 4q21, YES, Myeloid/lymphoid or mixed-lineage leukemia,

Canis familiaris:

Accession Number, function, homology, expect, chromosome

NW_139909.1, AF-4, 811/933, 0, 32

Homo sapiens

Gene Name, accession no, chromosome, CpG Island, function

MT2A, NM_005953, 16q12.2, YES, Metallothionein 2A

Canis familiaris:

Accession Number, function, homology, expect, chromosome

NW_139851.1, 5' protein tau 3' PDGF D polypeptide, 170/189, 3.00E-64, 5

NW_139841.1, metallothionein-1, 187/229, 5.00E-44, 2

Homo sapiens

Gene Name, accession no, chromosome, CpG Island, function

MTND1, NM_173708, chr. M, NO, NADH dehydrogenase 1

Homo sapiens

Gene Name, accession no, chromosome, CpG Island, function

MYBBP1A, NM_014520, 17q13.2, YES, MYB binding protein (P160) 1 A

Canis familiaris:

Accession Number, function, homology, expect, chromosome

NW_139852.1, BC011467 protein, 123/127, 2.00E-54, 5

Homo sapiens

Gene Name, accession no, chromosome, CpG Island, function

MYLk, NM_053030, 3q21.1, NO, Myosin light chain kinase isoform 5

Canis familiaris:

Accession Number, function, homology, expect, chromosome

NW_139911.1, Myosin light chain kinase isoform 6, 1313/1562, 0, 33

Homo sapiens

Gene Name, accession no, chromosome, CpG Island, function

NAV1, NM_020443, 1q32.1, YES, Neuron navigator

Canis familiaris:

Accession Number, function, homology, expect, chromosome

NW_139860.1, 5' importin 9 3' neuron navigotor 1, 1531/1861, 0

Homo sapiens

Gene Name, accession no, chromosome, CpG Island, function

NF-IL 3A, NM_005384, 9q22.31, NO, Nuclear factor interleukin 3 regulated

Canis familiaris:

Accession Number, function, homology, expect, chromosome

NW_139837.1, Nuclear factor interleukin 3 regulated, 1394/1713, 0, 1

Homo sapiens

Gene Name, accession no, chromosome, CpG Island, function

NGEF, BC031573, 2q37, NO, Neuronal guanine nucleotide exchange factor

Canis familiaris:

Accession Number, function, homology, expect, chromosome

NW_139898.1, Neuronal guanine nucleotide exchange factor, 191/196, 8.00E-93, 25

Homo sapiens

Gene Name, accession no, chromosome, CpG Island, function

NKX6-1, NM_006168, 4q21.2-q22, NO, NK6 transcription factor related, locus 1

Canis familiaris:

Accession Number, function, homology, expect, chromosome

NW_139909.1, NK6 transcription factor related, locus 1, 193/203, 1.00E-88, 32

Homo sapiens

Gene Name, accession no, chromosome, CpG Island, function

NLGN1, AB028993, 3q26.31, NO, Neuroligin 1

Canis familiaris:

Accession Number, function, homology, expect, chromosome

NW_139913.1, hypothetical protein XP_545297, 2526/2669, 0, 34

Homo sapiens

Gene Name, accession no, chromosome, CpG Island, function

NNT, AL831822, 5p13.1-5cen, YES, Nicotinamide nucleotide transhydrogenase

Canis familiaris:

Accession Number, function, homology, expect, chromosome

NW_139850.1, Nicotinamide nucleotide transhydrogenase, 1045/1279, 0, 4

Homo sapiens

Gene Name, accession no, chromosome, CpG Island, function

NRP2, BC009222, 2q33.3, YES, NRP2 protein

Canis familiaris:

Accession Number, function, homology, expect, chromosome

NW_139916.1, NRP2 protein, 172/182, 9.00E-76, 37

Homo sapiens

Gene Name, accession no, chromosome, CpG Island, function

OAZZIN, BC013420, 8q22.3, YES, Ornithine decarboxylase antizyme inhibitor

Canis familiaris:

Accession Number, function, homology, expect, chromosome

NW_139873.1, Ornithine decarboxylase antizyme inhibitor, 815/8760, 13

NW_139844.1, 3-hydroxy-3-methylglutaryl-coenzyme A reductase, 173/200, 6.00E-53, 3

Homo sapiens

Gene Name, accession no, chromosome, CpG Island, function

P2RY6, NM_1767981, 11q13.4, NO, Pyrimidinergic receptor P2Y

Canis familiaris:

Accession Number, function, homology, expect, chromosome

NW_139890.1, Pyrimidinergic receptor P2Y, 1031/1201, 0, 21

Homo sapiens

Gene Name, accession no, chromosome, CpG Island, function

PD2, NM_019088, 19q13.2, NO, PD2 protein

Canis familiaris:

Accession Number, function, homology, expect, chromosome

NW_139837.1, similar to RIKEN cDNA 5730511K23, 513/603, 1.00E-171, 1

Homo sapiens

Gene Name, accession no, chromosome, CpG Island, function

PER1, NM_002616, 7p13.1, YES, Period 1

Canis familiaris:

Accession Number, function, homology, expect, chromosome

NW_139852.1, similar to period 1 and arachidonate lipoxygenase 3, 738/911, 0, 5

Homo sapiens

Gene Name, accession no, chromosome, CpG Island, function

PES1, BC032489, 22q12.1, YES, Pescadillo homolog 1

Canis familiaris:

Accession Number, function, homology, expect, chromosome

NW_139920.1, Pescadillo homolog 1, 541/698, 2.00E-96, X

NW_139900.1, Pescadillo homolog 1, 160/175, 2.00E-63, 26

Homo sapiens

Gene Name, accession no, chromosome, CpG Island, function

PLEKHK1, NM_145307, 10q21.2, YES, Rhotekin 2

Canis familiaris:

Accession Number, function, homology, expect, chromosome

NW_139850.1, pleckstrin homology domain, 2368/2753, 0, 4

Homo sapiens

Gene Name, accession no, chromosome, CpG Island, function

PLK, BC002369, 16p12.1, YES, Polo-like kinase 1

Canis familiaris:

Accession Number, function, homology, expect, chromosome

NW_139859.1, Polo-like kinase 1, 392/432, 3.00E-168, 6

NW_139916.1, CD28, 189/361, 3.00E-65, 37

NW_139852.1, Glis1 Kruppel-like zinc finger protein, 295/372, 1.00E-60, 5

Homo sapiens

Gene Name, accession no, chromosome, CpG Island, function

PLXDC1, NM_020405, 17q12, YES, Tumor endothelial marker 3 precursor

Canis familiaris:

Accession Number, function, homology, expect, chromosome

NW_139866.1, plexin domain containing 1 precursor, 152/162, 4.00E-64, 9

Homo sapiens

Gene Name, accession no, chromosome, CpG Island, function

POLA, NM_016937, Xp21.3, YES, Polymerase DNA directed

Canis familiaris:

Accession Number, function, homology, expect, chromosome

NW_139919.1, Polymerase DNA directed, 194/209, 1.00E-74, X

Homo sapiens

Gene Name, accession no, chromosome, CpG Island, function

POU2F1, BC052274, 1q24.2, YES, POU domain class 2 transcriptional factor 1

Canis familiaris:

Accession Number, function, homology, expect, chromosome

NW_139860.1, OCT-1 protein, 403/446, 3.00E-169, 7

Homo sapiens

POU3F3 (*BRN1*), NM_006236, 2q12.1, YES, POU domain, class 3, transcription factor 3

Canis familiaris:

Accession Number, function, homology, expect, chromosome

NW_139870.1, POU domain, class 3, transcription factor 3, 580/599, 0, 10

NW_139876.1, hypothetical protein XP_549433, 434/493, 0, 15

NW_139872.1, POU domain, class 3, transcription factor 3, 424/486, 3.00E-160, 12

Homo sapiens

Gene Name, accession no, chromosome, CpG Island, function

PRKCE, NM_005400, 2p21, YES, Protein kinase C, epsilon

Canis familiaris:

Accession Number, function, homology, expect, chromosome

NW_139870.1, similar to ORF2, protein kinase c epsilon, 1802/2158, 0, 10

Homo sapiens

Gene Name, accession no, chromosome, CpG Island, function

PTX1, BC064522, 12p11.22,YES, Hypothetical protein

Canis familiaris:

Accession Number, function, homology, expect, chromosome

NW_139903.1, similar to RIKEN cDNA 1200009B18, 161/165, 6.00E-77, 27

Homo sapiens

Gene Name, accession no, chromosome, CpG Island, function

RAMP, BC033297, 1, YES, L2DTL protein (RA-regulated nuclear matrix-associated protein)

Canis familiaris:

Accession Number, function, homology, expect, chromosome

NW_139860.1, L2DTL protein (RA-regulated nuclear matrix-associated protein), 755/822, 0, 7

Homo sapiens

Gene Name, accession no, chromosome, CpG Island, function

RHD, NM_016124, 1p36.11, Yes, Blood group D antigen DBA

Canis familiaris:

Accession Number, function, homology, expect, chromosome

NW_139841.1, similar to hypothetical protein FLJ10747, 145/162, 1.00E-50, 2

NW_139865.1, LRR-repeat protein 1, 47/52, 2.00E-09

Homo sapiens

Gene Name, accession no, chromosome, CpG Island, function

RNF121, AK0231391, 1q13.4, NO, Ring finger protein 121

Canis familiaris:

Accession Number, function, homology, expect, chromosome

NW_139890.1, Ring finger protein 121, 648/798, 1.00E-164, 21

NW_139914.1, similar to KIAA0146, 681/862, 4.00E-142

Homo sapiens

Gene Name, accession no, chromosome, CpG Island, function

RNPC2, L10911, 20q11.22, YES, Hypothetical protein DKFZp686A11192

Canis familiaris:

Accession Number, function, homology, expect, chromosome

NW_139896.1, similar to RNA-binding region containing protein 2, 921/994, 0, 24

NW_139894.1, similar to ubiquitin-activating enzyme E1-domain, 375/405, 2.00E-166

Homo sapiens

Gene Name, accession no, chromosome, CpG Island, function

RPL3, BC004323, 12q13.1, YES, Hypothetical protein L3

Canis familiaris:

Accession Number, function, homology, expect, chromosome

NW_139872.1, similar to 60s ribosomal protein L3, 850/928, 0, 12

NW_139920.1, similar to KIAA2022 protein, 764/941, 0, X

NW_139870.1, similar to 60s ribosomal protein L3, 177/190, 6.00E-76, 10

Homo sapiens

Gene Name, accession no, chromosome, CpG Island, function

SEC23B, NM_032986, 20p11.23, YES, Sec23homologB

Canis familiaris:

Accession Number, function, homology, expect, chromosome

NW_139896.1, Sec23homologB, 460/565, 4.00E-117, 24

Homo sapiens

Gene Name, accession no, chromosome, CpG Island, function

SFRS3, NM_003017, 6p21.31, NO, Splicing factor arginine/serine rich 3

Canis familiaris:

Accession Number, function, homology, expect, chromosome

NW_139872.1, Splicing factor arginine/serine rich 3, 908/1070, 0, 12

NW_139921.1, Splicing factor arginine/serine rich 3, 300/349, 5.00E-97, X

Homo sapiens

Gene Name, accession no, chromosome, CpG Island, function

SHC1, NM_003029, 1q22, YES, Src Homology 2 domain containing transforming protein 1

Canis familiaris:

Accession Number, function, homology, expect, chromosome

NW_139860.1, Src Homology 2 domain containing transforming protein 1, 1067/1360, 0, 7

Homo sapiens

Gene Name, accession no, chromosome, CpG Island, function

SLC39A5, BC027884, 12q13.3, NO, Solute Carrier family 39 (metal ion transporter)

Canis familiaris:

Accession Number, function, homology, expect, chromosome

NW_139869.1, Solute Carrier family 39 (metal ion transporter), 317/365, 3.00E-113, 10

Homo sapiens

Gene Name, accession no, chromosome, CpG Island, function

SMAD9, BC067766, 13q12-q14, NO, MADH9 protein

Canis familiaris:

Accession Number, function, homology, expect, chromosome

NW_139897.1, MADH9 protein, 383/421, 4.00E-164, 25

Homo sapiens

Gene Name, accession no, chromosome, CpG Island, function

SNRPC, X12517, 6p21.31, YES, Small nuclear ribonucleoprotein polypeptide C

Homo sapiens

Gene Name, accession no, chromosome, CpG Island, function

TAO1, AF061943, 16p11.2, YES, Prostate derived STE20 like kinase PSK

Canis familiaris:

Accession Number, function, homology, expect, chromosome

NW_139859.1, similar to TAOK2 protein, 1863/2119, 0, 6

NW_139844.1, similar to solute carrier organic anion transporter family, 272/322, 4.00E-74, 3

Homo sapiens

Gene Name, accession no, chromosome, CpG Island, function

TBC107, BC050465, 6p24.1, YES, Hypothetical protein

Canis familiaris:

Accession Number, function, homology, expect, chromosome

NW_139914.1, TBC1 domain family member, 173/192, 2.00E-65, 35

Homo sapiens

Gene Name, accession no, chromosome, CpG Island, function

TFAP2B, NM_003221, 6p12.3, YES, Transcriptional factor AP-2 beta

Canis familiaris:

Accession Number, function, homology, expect, chromosome

NW_139872.1, Transcriptional factor AP-2 beta, 445/462, 0, 0

NW_139914.1, Transcriptional factor AP-2 beta, 195/237, 1.00E-49, 35

Homo sapiens

Gene Name, accession no, chromosome, CpG Island, function

TMEM29, NM_014138, chr. X, YES, Transmembrane protein 29

Homo sapiens

Gene Name, accession no, chromosome, CpG Island, function

TNFRSF6, NM_000043, 10q23.31, NO, Tumor necrosis factor receptor superfamily member 6

Canis familiaris:

Accession Number, function, homology, expect, chromosome

NW_139901.1, Fas, 58/63, 7.00E-16, 26

Homo sapiens

Gene Name, accession no, chromosome, CpG Island, function

TPX2, AF287265, 20q11.2, YES, Hepatocellular carcinoma-associated antigen 90

Canis familiaris:

Accession Number, function, homology, expect, chromosome

NW_139907.1, Targeting protein for Xklp2, 643/729, 0, 30

NW_139896.1, Targeting protein for Xklp2, 346/420, 6.00E-94, 24

Homo sapiens

Gene Name, accession no, chromosome, CpG Island, function

TTF2, BC030058, 1p13.1, YES, Similar to transcription termination factor, RNA polymerase II

Canis familiaris:

Accession Number, function, homology, expect, chromosome

NW_139881.1, Similar to transcription termination factor, RNA polymerase II, 102/118, 1.00E-28, 17

Homo sapiens

Gene Name, accession no, chromosome, CpG Island, function

WT10B, NM-005430,12q13.12, NO, Wingless type MMTU integration site family

Canis familiaris:

Accession Number, function, homology, expect, chromosome

NW_139903.1, Wingless type MMTU integration site family, 1144/1315, 0, 27

Homo sapiens

Gene Name, accession no, chromosome, CpG Island, function

ZBTB4, NM_020899, 17p13.1, YES, Zinc finger and BT3 domain containing protein 4

Canis familiaris:

Accession Number, function, homology, expect, chromosome

NW_139852.1, mKIAA1538 protein, 2583/3041, 0.00E+00, 5

Homo sapiens

Gene Name, accession no, chromosome, CpG Island, function

ZINC1, D76435, 3q24, YES, Zic family member 1

Canis familiaris:

Accession Number, function, homology, expect, chromosome

NW_139894.1, Zic4, 491/512, 0, 23

Homo sapiens

Gene Name, accession no, chromosome, CpG Island, function

ZINC5, NM_0331321, 13q32.3, YES, Zinc family member 5

Canis familiaris:

Accession Number, function, homology, expect, chromosome

NW_139892.1, 5' similar to citrate lyase beta like 3' similar to zinc finger protein ZIC 2, 632/693, 0, 22

NW_139920.1, similar to tropomyosin 3, fibroblast-rat, 545/641, 0, X

Homo sapiens

Gene Name, accession no, chromosome, CpG Island, function

ZMPSTE24, NM_005857, 1p34.2, YES, Zinc metallo proteinase

Canis familiaris:

Accession Number, function, homology, expect, chromosome

NW_139876.1, CAAX prenyl protease 1 homolog, procollagen IX, alpha 2, 757/888, 0, 15

Homo sapiens

Gene Name, accession no, chromosome, CpG Island, function

ZNF160, NM_198893, 19q13.41, YES, Zinc finger protein 160

Canis familiaris:

Accession Number, function, homology, expect, chromosome

MANY MANYMANY INCLUDING ZINC FINGER FAMILIES

Homo sapiens

Gene Name, accession no, chromosome, CpG Island, function

ZNF263, BC008805, 16p13.3, YES, Zinc finger protein 263

Canis familiaris:

Accession Number, function, homology, expect, chromosome

NW_139859.1, Zinc finger protein 263, 1566/1901, 0, 6

Homo sapiens

Gene Name, accession no, chromosome, CpG Island, function

ZNF307, NM_019110, 6p22.1, YES, Zinc finger protein 307

Canis familiaris:

Accession Number, function, homology, expect, chromosome

NW_139914.1, Zinc finger protein 307, 1062/1296, 0, 35

Homo sapiens

Gene Name, accession no, chromosome, CpG Island, function

ZNF432, NM_014650, 19q13.41, YES, Zinc finger protein 432

Canis familiaris:

Accession Number, function, homology, expect, chromosome

NW_139837.1, Zinc finger protein 615, 1578/1796, 0, 1

Homo sapiens

Gene Name, accession no, chromosome, CpG Island, function

ZNF614, NM_025040, 19q.41, YES, Zinc finger protein 432

Canis familiaris:

Accession Number, function, homology, expect, chromosome

NW_139837.1, Zinc finger protein 615, 1645/2008, 0, 1

Homo sapiens

Gene Name, accession no, chromosome, CpG Island, function

ZYX, NM_003461, 7q34, NO, ZYX protein

Canis familiaris:

Accession Number, function, homology, expect, chromosome

NW_139877.1, ZYX protein, 449/537, 2.00E-136, 16

NW_139919.1, Zinc finger protein 41, 500/683, 2.00E-46, X

Appendix 2: Primer sequences and conditions

Gene					
DLC1					
Primer					
MSP	Unmethylated F	TGGTTTTAAGTTTAGTGGTTAGTGG			
	Unmethylated R	CCTTATCAAACCAATACCTATCATT			
	Methylated F	GCGGTTTTAAGTTTAGTGGTTAGC			
	Methylated R	CCTTATCAAACCGATACCTATCGT			
COBRA	COBRA F	GAGAGGTTTTAATATTTTTTAGATG			
	COBRA R	ACCTTTAAAAACCCTACCCC			
		Volume (uL)			
Recipe	Template	1	**Program**	95	10m
	10X Buffer	2.5		94	15s
Meth	25uM MgCl	1		62	30s
	10uM dNTP	0.5		72	30s
	10uM Forward	1		Goto 2	32 X
	10uM Reverse	1		72	5m
	Taq Gold	0.125		4	Forever
	HyPure water	17.875			
Unmeth	Template	1	**Program**	95	10m
	10X Buffer	2.5		94	15s
	25uM MgCl	2.5		62	1m
	10uM dNTP	0.5		72	1m
	10uM Forward	1		Goto 2	32X
	10uM Reverse	1		72	5m
	Taq Gold	0.125		4	Forever
	HyPure water	16.375			
COBRA	Template	1	**Program**	95	10m
	10X Buffer	5		95	15s
	25uM MgCl	5		58	1m
	10uM dNTP	1		72	1m
	10uM Forward	2		Goto 2	35X
	10uM Reverse	2		72	5m
	Taq Gold	0.125		4	Forever
	HyPure water	31.875			
Gene					
POU3F3					
Primer					
MSP	Unmethylated F	AGTTTAGTTGTAGGGTTTCGAAGC			
	Unmethylated R	ACTAAACTTCACGCAAACCGA			
	Methylated F	GTTTAGTTGTAGGGTTTTGAAGTGG			

	Methylated R	ATCAAACTAAACTTCACACAAACCA			
COBRA	COBRA F	GGGATATTTGAGGAAGTGGTTTT			
	COBRA R	AACTTCAAAAACATATACAAACTCAAAC			
		Volume (uL)			
Recipe	Template	1	**Program**	95	10m
	10X Buffer	2.5		94	15s
Meth	25uM MgCl	2.5		62	30s
	10uM dNTP	0.5		72	30s
	10uM Forward	1		Goto 2	32 X
	10uM Reverse	1		72	5m
	Taq Gold	0.125		4	Forever
	HyPure water	16.375			
Unmeth	Template	1	**Program**	95	10m
	10X Buffer	2.5		94	15s
	25uM MgCl	2.5		62	1m
	10uM dNTP	0.5		72	1m
	10uM Forward	1		Goto 2	32X
	10uM Reverse	1		72	5m
	Taq Gold	0.125		4	Forever
	HyPure water	16.375			
COBRA	Template	1	**Program**	95	10m
	10X Buffer	5		95	15s
	25uM MgCl	10		57	1m
	10uM dNTP	1		72	1m
	10uM Forward	2		Goto 2	35X
	10uM Reverse	2		72	5m
	Taq Gold	0.125		4	Forever
	HyPure water	26.875			
Gene					
PRKCE					
Primer					
COBRA	COBRA F	GTTTTTAGGTGTAGGGGGAGAG			
	COBRA R	AAAACCATTAAACACTACCATAATC			
		Volume (uL)			
Recipe	Template	1	**Program**	95	10m
	10X Buffer	5		95	15s
	25uM MgCl	10		57	1m
	10uM dNTP	1		72	1m
	10uM Forward	2		Goto 2	35X
	10uM Reverse	2		72	5m
	Taq Gold	0.125		4	Forever
	HyPure water	26.875			
Gene					
LHX2					

Primer					
COBRA	COBRA F	GTTTTTAGTTATTAATAGTTTTTTG			
	COBRA R	AAATAAAAACTCCTCAAACATCCTC			
		Volume (uL)			
Recipe	Template	1	**Program**	95	10m
	10X Buffer	5		95	15s
	25uM MgCl	10		52	1m
	10uM dNTP	1		72	1m
	10uM Forward	2		Goto 2	35X
	10uM Reverse	2		72	5m
	Taq Gold	0.125		4	Forever
	HyPure water	26.875			
Gene					
DLC1 5 Prime					
Primer					
COBRA	COBRA F	TATAGTTTTAGGCGGTGTTTTGG			
		TATAGTTTTAGGTGGTGTTTTGG			
	COBRA R	CCCAAAATCCAACTCAAAATTTACG			
		CCCAAAATCCAACTCAAAATTTACA			
		Volume (uL)			
Recipe	Template	2	**Program**	95	10m
	10X Buffer	5		95	1m
	25uM MgCl	5		60	1m
	10uM dNTP	4		72	1m
	10uM Forward	4		Goto 2	35X
	10uM Reverse	4		72	7m
	Taq Gold	0.25		4	Forever
	HyPure water	25.75			

Appendix 3: Conserved elements

Canine	Human	Present in both	
SP1	**SP1**		
names	**names**		
'Sp1_CS2'	'Sp1_CS2'	1	1
'c-GC-box'	'c-GC-box'	1	1
'SP1-DHFR.1'	'SP1-IE3/34'	1	0
'SP1-IE3/1'	'SP1-DHFR.1'	1	1
'Sp1-IE-3.1'	'SP1-IE3/1'	1	1
'Sp1-IE-3.2'	'SP1-SV/6'	0	0
'Sp1-IE-3.3'	'Sp1-hsp70'	1	0
'Sp1-IE-4/5'	'Sp1-IE-3.1'	1	1
'(Sp1)-MT-I.1'	'Sp1-IE-3.3'	0	1
'Sp1-ras1.5'	'(Sp1)-MT-I.1'	1	1
'Sp1-SV40.2'	'Sp1-SV40.2'	1	1
'Sp1-SV40.1'	'Sp1-SV40.1'	1	1
'(Sp1)-TK.1'	'(Sp1)-TK.1'	1	1
'IR-site_A'	'DSE_(1)'	1	0
'Zif_(1)'	'IR-site_A'	0	1
'Zif_(3)'	'Sp1-NPY'	0	1
'Sp1-NPY'	'Sp1-malic_enzyme'	1	0
'Sp1-GPC_(2)'	'Sp1-TPI_(4)'	0	0
'Sp1-junD'	'Sp1-junD'	1	1
'Sp1-gamma-globin_(3)'	'Sp1-gamma-globin_(3)'	1	1
'Sp1-Ku80_(1)'	'Sp1-Ku80_(1)'	1	1
'Sp1-COXIV'	'Sp1-p62'	0	0
'SP1/AP2-phospholipas'	'Sp1-erk1_(1)'	0	1
'Sp1-VGF_(1)'	'Sp1-erk1_(2)'	0	1
'Sp1-erk1_(1)'	'Sp1-ACCA-2'	1	0
'Sp1-erk1_(2)'		1	0.68
		0.692308	
non_SP1	**non_SP1**		
names	**names**		
'PEBP2_RS'	'LVa_RS'	0	0
'TFIIIC-Xls-5S.2'	'LVb_RS'	0	0
'HC3'	'APRT-mouse_US'	0	0
'PEA3_RS'	'PEA3_RS'	0	1
'Adh1_US2'	'PUT2_UAS.2'	0	0
'bA-globin.1'	'bA-globin.1'	1	1
'hsp70.2'	'GCN4-HIS3.1'	1	0
'IE1.2'	'MLTF-HMGCoAred'	0	0
'LSF-SV40'	'hsp70.2'	1	0

'WAP_US6'	'LSF-SV40'	1	1
'TTR_inverted_repeat'	'WAP_US5'	1	1
'vaccinia-term-sequen'	'TTR_inverted_repeat'	0	1
'zeste-Ubx'	'T3-box'	1	0
'Pu_box'	'zeste-Ubx'	1	1
'KROX24-F'	'Pu_box'	0	1
'GSG_element_(1)'	'HSV_IE_repeat'	1	0
'H-2RIIBP/T3R-alpha-r'	'junB-US2'	0	0
'EGR-2_RS'	'GSG_element_(1)'	0	1
'T-antigen_RS'	'F-ACT1_RS'	1	0
'GSG_element_(2)'	'PuF_RS'	0	0
'betaP-F4'	'SIF_core_RS'	1	0
'erythropoietin-site_'	'T-antigen_RS'	0	1
'MREc_(3)'	'betaP-F1'	0	0
'GR-intron-site-2'	'CAAT_site(1)'	0	0
'UAS1_(5)'	'C/EBP-apoB-intron-en'	0	0
'A4_amyloid_protein-u'	'GAGA-eve_(6)'	0	1
'alphaA-crystallin-un'	'GCF-beta-actin_(1)'	0	1
'GAGA-eve_(6)'	'GCF-consensus'	1	1
'GCF-beta-actin_(1)'	'phyA3-undefined-site'	0	0
'GCF-consensus'	'gamma-globin-undefin'	1	1
'GG-II/GG-I'	'PDR3_CS'	0	1
'gamma-globin-undefin'	'GR/PR-connexin43'	1	0
'PDR3_CS'	'IL6RP-VGF_(2)'	1	0
'AP-2/Sp1-PLG'	'AP-2-cyclinD2_(1)'	0	0
'Ets_site_(1)'	'NF-Kb/Ets1-p62'	0	0
'CreA_site_(1)'	'E2F-muCdc7-4'	1	0
'GC/FAR_site_(1)'	'CreA_site_(1)'	1	1
'GC/FAR_site_(2)'	'GC/FAR_site_(1)'	0	1
'AP-2-EGFR-site-3'	'Mbp1-mdscan-motif-3'	0	0
		0.410256	0.410256

Appendix 4: Cell study data

Zebularine	Rad Dose		Day 0	Day 1	Day 2	Day 3
0	0	Mean	97.00	98.00	98.00	95.33
		SEM	0.00	0.58	0.00	0.88
	0.5	Mean	99.00	97.00	97.00	95.67
		SEM	0.00	0.58	0.58	0.88
	1	Mean	99.00	96.67	97.00	95.33
		SEM	0.00	0.88	0.00	0.88
	2	Mean	99.00	95.67	94.67	94.00
		SEM	0.00	1.20	0.88	0.58
50	0	Mean	97.00	96.33	95.67	97.33
		SEM	0.00	0.33	0.33	0.67
	0.5	Mean	99.00	94.67	97.33	93.33
		SEM	0.00	1.45	0.33	0.67
	1	Mean	97.67	95.33	96.67	95.00
		Mean	0.88	0.67	0.33	1.53
	2	SEM	98.33	92.67	95.00	93.00
		Mean	0.33	1.20	1.00	1.00
100	0	SEM	97.00	95.67	96.33	95.67
		Mean	0.00	0.88	0.33	1.86
	0.5	SEM	99.00	92.33	96.00	92.67
		Mean	0.00	1.20	0.58	0.67
	1	Mean	97.67	94.67	91.33	95.33
		SEM	0.88	0.33	1.20	1.20
	2	Mean	98.33	94.00	95.00	90.67
		SEM	0.33	1.16	0.58	2.34
200	0	Mean	97.00	95.00	95.00	93.67
		SEM	0.00	0.58	0.00	0.33
	0.5	Mean	99.00	91.67	94.67	93.67
		Mean	0.00	0.88	0.67	0.67
	1	SEM	97.67	95.33	93.00	95.00
		Mean	0.88	0.33	1.53	1.16
	2	SEM	98.33	92.00	92.00	89.00
		Mean	0.33	0.58	0.58	1.00
0	0	Mean	99.00	97.33	97.67	94.00
		SEM	0.00	0.33	0.33	0.58
	0.5	Mean	99.00	97.00	97.00	95.67
		SEM	0.00	0.58	0.58	0.88
	1	Mean	99.00	96.67	97.00	95.33
		SEM	0.00	0.88	0.00	0.88
	2	Mean	99.00	95.67	94.67	94.00

		SEM	0.00	1.20	0.88	0.58
0	L0.5	SEM	99.00	95.20	95.79	
		Mean	0.00	1.45	1.40	
	L1	Mean	99.00	95.66	98.05	
		SEM	0.00	0.98	0.50	
	L2	Mean	99.00	95.04	97.10	
		SEM	0.00	0.72	0.53	
50	L0.5	Mean	99.00	95.08	96.39	
		SEM	0.00	0.38	0.53	
	L1	Mean	99.00	96.56	97.62	
		Mean	0.00	0.53	0.21	
	L2	SEM	99.00	94.77	96.76	
		Mean	0.00	0.64	0.54	
100	L0.5	SEM	99.00	95.63	97.52	
		Mean	0.00	0.34	0.58	
	L1	SEM	99.00	93.40	96.34	
		Mean	0.00	1.02	1.14	
	L2	Mean	99.00	90.85	93.19	
		SEM	0.00	1.76	1.75	
200	L0.5	Mean	99.00	90.82	85.93	
		SEM	0.00	1.31	5.86	
	L1	Mean	99.00	87.83	90.83	
		SEM	0.00	1.72	0.43	
	L2	Mean	99.00	81.65	85.79	
		SEM	0.00	0.83	3.14	

Zebularine	**Rad Dose**		**Day 0**	**Day 1**	**Day 2**	**Day 3**
0	0	Mean	47.63	77.50	202.33	274.67
	0	SEM	2.02	3.97	14.13	13.50
	0.5	Mean	47.63	73.17	177.50	253.00
	0.5	SEM	2.02	4.49	7.22	25.09
	1	Mean	47.63	69.50	158.83	230.67
	1	SEM	2.02	2.79	3.34	8.85
	2	Mean	47.63	62.17	127.00	185.33
	2	SEM	2.02	7.74	7.51	8.89
	0	Mean	43.25	80.00	183.00	294.33
	0	SEM	0.14	4.28	10.71	32.70
50	0	Mean	39.83	78.50	130.33	253.33
	0	SEM	3.32	2.31	4.42	17.84
	0.5	Mean	39.83	64.33	124.33	226.67
	0.5	SEM	3.32	5.19	3.59	20.76

	1	Mean	39.83	58.83	116.17	212.67
	1	SEM	3.32	3.82	6.57	16.04
	2	Mean	39.83	61.83	95.67	185.33
	2	SEM	3.32	2.09	2.89	7.52
100	0	Mean	38.33	80.67	131.83	257.33
	0	SEM	1.45	6.29	10.38	12.88
	0.5	Mean	38.33	68.83	109.33	227.00
	0.5	SEM	1.45	4.34	4.75	20.16
	1	Mean	38.33	62.17	97.67	188.67
	1	SEM	1.45	6.17	1.45	11.88
	2	Mean	38.33	64.50	81.83	153.00
	2	SEM	1.45	4.78	2.32	5.69
200	0	Mean	53.00	72.83	124.83	243.00
	0	SEM	4.62	3.61	1.92	14.03
	0.5	Mean	53.00	66.00	98.67	195.67
	0.5	SEM	4.62	2.76	2.19	13.97
	1	Mean	53.00	64.33	86.83	169.67
	1	SEM	4.62	1.92	2.34	11.06
	2	Mean	53.00	54.00	75.17	116.67
	2	SEM	4.62	0.58	4.98	4.92
0	0	Mean	35.00	72.83	159.67	
		SEM	0.00	7.00	14.17	
	0.5	Mean	35.00	60.17	146.50	
		SEM	0.00	7.60	20.72	
	1	Mean	35.00	67.33	138.50	
		SEM	0.00	6.97	12.79	
	2	Mean	35.00	67.83	133.50	
		SEM	0.00	8.77	4.54	
50	0.5	Mean	33.50	60.67	111.17	
		SEM	0.00	5.41	7.94	
	1	Mean	33.50	74.17	137.00	
		SEM	0.00	5.64	3.27	
	2	Mean	33.50	63.83	133.67	
		SEM	0.00	8.25	2.09	
100	0.5	Mean	44.00	57.33	119.50	
		SEM	0.00	12.00	4.50	
	1	Mean	44.00	53.83	98.50	
		SEM	0.00	4.26	12.06	
	2	Mean	44.00	45.67	98.50	
		SEM	0.00	5.43	7.78	
200	0.5	Mean	36.75	57.83	99.67	
		SEM	0.00	7.54	2.67	
	1	Mean	36.75	51.67	90.86	

		SEM	0.00	9.24	20.14	
	2	Mean	36.75	62.67	88.83	
		SEM	0.00	12.50	7.89	

Appendix 4: Raw Real Time Data

Sample_Gene	CT Value	Melt Temp
1_DLC1	31.9	85.5
1_DLC1	31.5	85.5
1_DLC1	31.4	85.5
1_DLC1	29.2	84.5
1_DLC1	29.3	84.5
1_DLC1	29.7	84.5
1_GAPDH	24.6	85
1_GAPDH	25.2	85
1_GAPDH	25.3	85
1_GAPDH	24.4	84.5
1_GAPDH	24.9	85
1_GAPDH	24.7	85.5
3_DLC1	34	83
3_DLC1	33.5	83
3_DLC1	33.7	83
3_GAPDH	26.9	85
3_GAPDH	27.4	85.5
3_GAPDH	27.1	85.5
10_DLC1	30.6	83
10_DLC1	31	82.5
10_DLC1	30.4	82.5
10_GAPDH	28.3	86.5
10_GAPDH	28.3	86.5
10_GAPDH	28.4	86.5
12_DLC1	30.9	85
12_DLC1	31	85.5
12_DLC1	30.8	85
12_GAPDH	22.8	86.5
12_GAPDH	22.6	86.5
12_GAPDH	22.7	86.5
13_DLC1	31.1	83
13_DLC1	31.3	83
13_DLC1	30.8	83
13_GAPDH	25.8	85.5
13_GAPDH	25.6	85.5
13_GAPDH	26	85.5
14_DLC1	26.4	84
14_DLC1	26.6	84
14_DLC1	26.7	84
14_GAPDH	24.3	85.5
14_GAPDH	24.3	85.5
14_GAPDH	24.3	85.5
15_DLC1	23.9	84.5

15_DLC1	24.1	84.5
15_DLC1	24.6	84.5
15_GAPDH	21.4	85
15_GAPDH	21.6	85.5
15_GAPDH	21.6	85.5
16_DLC1	27.4	84.5
16_DLC1	27.6	84.5
16_DLC1	27.9	84.5
16_GAPDH	23.4	85
16_GAPDH	23.8	85.5
16_GAPDH	23.9	85.5
17_DLC1	26.3	83
17_DLC1	25.8	83
17_DLC1	25.7	82.5
17_GAPDH	23.6	86.5
17_GAPDH	23.8	86.5
17_GAPDH	23.7	86.5
18_DLC1	29.9	84.5
18_DLC1	30	84.5
18_DLC1	31.6	84.5
18_GAPDH	25.8	85.5
18_GAPDH	25.9	85.5
18_GAPDH	26	85.5
19_DLC1	25.9	84
19_DLC1	26.3	84
19_DLC1	26.8	83.5
19_GAPDH	22.8	85.5
19_GAPDH	22.7	85.5
19_GAPDH	23	85.5
20_DLC1	28.6	83.5
20_DLC1	28.4	83.5
20_DLC1	28.1	83
20_GAPDH	23.8	86.5
20_GAPDH	23.9	86.5
20_GAPDH	24.5	86.5
21_DLC1	29.8	84.5
21_DLC1	29.8	84.5
21_DLC1	30.4	84.5
21_GAPDH	24	85.5
21_GAPDH	24.1	85.5
21_GAPDH	24.3	85.5
22_DLC1	28.2	83
22_DLC1	28.6	83
22_DLC1	28.3	83
22_DLC1	24.8	84
22_DLC1	25.4	84.5

22_DLC1	24.9	84
22_DLC1	27.6	79.5
22_DLC1	26.5	80
22_DLC1	25.9	79
22_GAPDH	22.8	85.5
22_GAPDH	23	85.5
22_GAPDH	23.3	85.5
22_GAPDH	22.4	85.5
22_GAPDH	22.3	85.5
22_GAPDH	22.7	85.5
22_GAPDH	21.8	84
22_GAPDH	22.2	83
22_GAPDH	21.2	83.5
23_DLC1	27.3	83
23_DLC1	27.1	83.5
23_DLC1	27.2	83.5
23_DLC1	26.5	83.5
23_DLC1	26.4	83.5
23_DLC1	26.5	83.5
23_GAPDH	26.3	86
23_GAPDH	26.6	86
23_GAPDH	26.8	86
23_GAPDH	25.6	86
23_GAPDH	25.4	86.5
23_GAPDH	25.9	86
23_GAPDH	25.1	82.5
23_GAPDH	24.4	82.5
23_GAPDH	24.7	83
23l_DLC1	25.5	79.5
23l_DLC1	25.2	79.5
23l_DLC1	25.5	78.5
24_DLC1	28.2	76.5
24_DLC1	27.6	79
24_DLC1	27.5	79.5
24_GAPDH	24.9	83
24_GAPDH	24.1	83
24_GAPDH	24.6	83.5
25_DLC1	26.4	78.5
25_DLC1	26.7	79
25_DLC1	27.3	78.5
25_GAPDH	29.1	84
25_GAPDH	27.6	83.5
25_GAPDH	28.5	83.5
26_DLC1	26.4	79.5
26_DLC1	26.1	80
26_DLC1	26.6	79.5

26_GAPDH	23.6	83
26_GAPDH	24.5	83
26_GAPDH	23.8	83.5
27_DLC1	25.8	78.5
27_DLC1	25.8	79
27_DLC1	26.6	78.5
27_GAPDH	23.7	80.5
27_GAPDH	24.5	82.5
27_GAPDH	24.5	83
28_DLC1	24.5	77.5
28_DLC1	24	79
28_DLC1	23.8	79.5
28_GAPDH	21.4	76.5
28_GAPDH	21.4	80
28_GAPDH	21	74.5
29_DLC1	41.8	81.5
29_DLC1	47.5	
29_DLC1	37.2	80
29_GAPDH	23.7	82.5
29_GAPDH	23.9	83
29_GAPDH	24.2	84
3_DLC1	31.8	84.5
3_DLC1	31.4	84
3_DLC1	31.6	84.5
3_GAPDH	26.2	85
3_GAPDH	26.5	85.5
3_GAPDH	26.5	85.5
5_DLC1	33.5	83
5_DLC1	32.7	83
5_DLC1	33.3	85.5
5_DLC1	29.9	84
5_DLC1	30.1	84
5_DLC1	30.3	84
5_GAPDH	26.4	85
5_GAPDH	27	85
5_GAPDH	28.6	85.5
5_GAPDH	26	85
5_GAPDH	26.4	85
5_GAPDH	26.6	85.5
6_DLC1	27.1	83
6_DLC1	27.2	83
6_DLC1	27.2	83
6_GAPDH	23.2	86
6_GAPDH	23.2	86.5
6_GAPDH	23.5	86.5
7_DLC1	30.4	83

7_DLC1	30.4	83
7_DLC1	30.2	83
7_GAPDH	26.8	85.5
7_GAPDH	27.1	85.5
7_GAPDH	27.1	85.5
8_DLC1	25.2	83
8_DLC1	25.5	83
8_DLC1	25.5	83
8_GAPDH	21.4	86
8_GAPDH	21.7	86.5
8_GAPDH	21.9	86.5
9_DLC1	26.5	83
9_DLC1	26.5	83
9_DLC1	33.4	83
9_GAPDH	23.2	86.5
9_GAPDH	22.7	86.5
9_GAPDH	22.7	86.5

Bibliography

1. Hotchkiss RD. Chemical studies on the transforming factor of pneumococci. *Colloques intern centre natl recherche sci Unites biol douees contin genet (Paris)* 1949;8:57-65.

2. Holliday R. Epigenetic inheritance based on DNA methylation. *EXS* 1993;64:452-468.

3. Leu YW, Yan PS, Fan M, et al. Loss of estrogen receptor signaling triggers epigenetic silencing of downstream targets in breast cancer. *Cancer Res* 2004;64(22):8184-8192.

4. Kim TY, Jong HS, Jung Y, et al. DNA hypermethylation in gastric cancer. *Aliment Pharmacol Ther* 2004;20 Suppl 1:131-142.

5. Schulz WA, Hatina J. Epigenetics of prostate cancer: beyond DNA methylation. *J Cell Mol Med* 2006;10(1):100-125.

6. Shamay M, Krithivas A, Zhang J, et al. Recruitment of the de novo DNA methyltransferase Dnmt3a by Kaposi's sarcoma-associated herpesvirus LANA. *Proc Natl Acad Sci U S A* 2006;103(39):14554-14559.

7. Liu H, Wang J, Epner EM. Cyclin D1 activation in B-cell malignancy: association with changes in histone acetylation, DNA methylation, and RNA polymerase II binding to both promoter and distal sequences. *Blood* 2004;104(8):2505-2513.

8. Murai M, Toyota M, Satoh A, et al. Aberrant DNA methylation associated with silencing BNIP3 gene expression in haematopoietic tumours. *Br J Cancer* 2005;92(6):1165-1172.

9. Cui H, Cruz-Correa M, Giardiello FM, et al. Loss of IGF2 imprinting: a potential marker of colorectal cancer risk. *Science* 2003;299(5613):1753-1755.

10. Rollins RA, Haghighi F, Edwards JR, et al. Large-scale structure of genomic methylation patterns. *Genome Res* 2006;16(2):157-163.

11. Singal R, Ginder GD. DNA methylation. *Blood* 1999;93(12):4059-4070.

12. Herman JG, Baylin SB. Gene silencing in cancer in association with promoter hypermethylation. *N Engl J Med* 2003;349(21):2042-2054.

13. Siegfried Z, Eden S, Mendelsohn M, et al. DNA methylation represses transcription in vivo. *Nat Genet* 1999;22(2):203-206.

14. Jones PA, Baylin SB. The epigenomics of cancer. *Cell* 2007;128(4):683-692.

15. Takai D, Jones PA. Comprehensive analysis of CpG islands in human chromosomes 21 and 22. *Proc Natl Acad Sci U S A* 2002;99(6):3740-3745.

16. Bachman KE, Park BH, Rhee I, et al. Histone modifications and silencing prior to DNA methylation of a tumor suppressor gene. *Cancer Cell* 2003;3(1):89-95.

17. Mellor J. It takes a PHD to read the histone code. *Cell* 2006;126(1):22-24.

18. Feinberg AP, Vogelstein B. Hypomethylation of ras oncogenes in primary human cancers. *Biochem Biophys Res Commun* 1983;111(1):47-54.

19. Park J, Brena RM, Gruidl M, et al. CpG island hypermethylation profiling of lung cancer using restriction landmark genomic scanning (RLGS) analysis. *Cancer Biomark* 2005;1(2-3):193-200.

20. Ando Y, Hayashizaki Y. Restriction landmark genomic scanning. *Nat Protoc* 2006;1(6):2774-2783.

21. Fraga MF, Esteller M. DNA methylation: a profile of methods and applications. *Biotechniques* 2002;33(3):632, 634, 636-632, 634, 649.

22. Cottrell SE, Laird PW. Sensitive detection of DNA methylation. *Ann N Y Acad Sci* 2003;983:120-130.

23. Yan PS, Perry MR, Laux DE, et al. CpG island arrays: an application toward deciphering epigenetic signatures of breast cancer. *Clin Cancer Res* 2000;6(4):1432-1438.

24. Houde C, Li Y, Song L, et al. Overexpression of the NOTCH ligand JAG2 in malignant plasma cells from multiple myeloma patients and cell lines. *Blood* 2004;104(12):3697-3704.

25. Dong SM, Sun DI, Benoit NE, et al. Epigenetic inactivation of RASSF1A in head and neck cancer. *Clin Cancer Res* 2003;9(10 Pt 1):3635-3640.

26. Chan MW, Chan LW, Tang NL, et al. Frequent hypermethylation of promoter region of RASSF1A in tumor tissues and voided urine of urinary bladder cancer patients. *Int J Cancer* 2003;104(5):611-616.

27. Al-Kuraya K, Narayanappa R, Siraj AK, et al. High frequency and strong prognostic relevance of O6-methylguanine DNA methyltransferase silencing

in diffuse large B-cell lymphomas from the Middle East. *Hum Pathol* 2006;37(6):742-748.

28. Hegi ME, Diserens AC, Gorlia T, et al. MGMT gene silencing and benefit from temozolomide in glioblastoma. *N Engl J Med* 2005;352(10):997-1003.

29. Donson AM, Addo-Yobo SO, Handler MH, et al. MGMT promoter methylation correlates with survival benefit and sensitivity to temozolomide in pediatric glioblastoma. *Pediatr Blood Cancer* 2007;48(4):403-407.

30. Pelham JT, Irwin PJ, Kay PH. Genomic hypomethylation in neoplastic cells from dogs with malignant lymphoproliferative disorders. *Res Vet Sci* 2003;74(1):101-104.

31. Santi DV, Norment A, Garrett CE. Covalent bond formation between a DNA-cytosine methyltransferase and DNA containing 5-azacytosine. *Proc Natl Acad Sci U S A* 1984;81(22):6993-6997.

32. Issa JP. DNA methylation as a therapeutic target in cancer. *Clin Cancer Res* 2007;13(6):1634-1637.

33. Stresemann C, Brueckner B, Musch T, et al. Functional diversity of DNA methyltransferase inhibitors in human cancer cell lines. *Cancer Res* 2006;66(5):2794-2800.

34. Issa JP, Kantarjian HM, Kirkpatrick P. Azacitidine. *Nat Rev Drug Discov* 2005;4(4):275-276.

35. Shanafelt TD, Lee YK, Call TG, et al. Clinical effects of oral green tea extracts in four patients with low grade B-cell malignancies. *Leuk Res* 2006;30(6):707-712.

36. Brueckner B, Boy RG, Siedlecki P, et al. Epigenetic reactivation of tumor suppressor genes by a novel small-molecule inhibitor of human DNA methyltransferases. *Cancer Res* 2005;65(14):6305-6311.

37. Yuan BZ, Miller MJ, Keck CL, et al. Cloning, characterization, and chromosomal localization of a gene frequently deleted in human liver cancer (DLC-1) homologous to rat RhoGAP. *Cancer Res* 1998;58(10):2196-2199.

38. Wong CM, Lee JM, Ching YP, et al. Genetic and epigenetic alterations of DLC-1 gene in hepatocellular carcinoma. *Cancer Res* 2003;63(22):7646-7651.

39. Yuan BZ, Jefferson AM, Baldwin KT, et al. DLC-1 operates as a tumor suppressor gene in human non-small cell lung carcinomas. *Oncogene* 2004;23(7):1405-1411.

40. Pang JC, Chang Q, Chung YF, et al. Epigenetic inactivation of DLC-1 in supratentorial primitive neuroectodermal tumor. *Hum Pathol* 2005;36(1):36-43.

41. Kim TY, Jong HS, Song SH, et al. Transcriptional silencing of the DLC-1 tumor suppressor gene by epigenetic mechanism in gastric cancer cells. *Oncogene* 2003;22(25):3943-3951.

42. Yuan BZ, Durkin ME, Popescu NC. Promoter hypermethylation of DLC-1, a candidate tumor suppressor gene, in several common human cancers. *Cancer Genet Cytogenet* 2003;140(2):113-117.

43. Ullmannova V, Popescu NC. Expression profile of the tumor suppressor genes DLC-1 and DLC-2 in solid tumors. *Int J Oncol* 2006;29(5):1127-1132.

44. Seng TJ, Low JS, Li H, et al. The major 8p22 tumor suppressor DLC1 is frequently silenced by methylation in both endemic and sporadic nasopharyngeal, esophageal, and cervical carcinomas, and inhibits tumor cell colony formation. *Oncogene* 2007;26(6):934-944.

45. Kim TY, Lee JW, Kim HP, et al. DLC-1, a GTPase-activating protein for Rho, is associated with cell proliferation, morphology, and migration in human hepatocellular carcinoma. *Biochem Biophys Res Commun* 2007;355(1):72-77.

46. Goodison S, Yuan J, Sloan D, et al. The RhoGAP protein DLC-1 functions as a metastasis suppressor in breast cancer cells. *Cancer Res* 2005;65(14):6042-6053.

47. Ullmannova V, Popescu NC. Inhibition of cell proliferation, induction of apoptosis, reactivation of DLC1, and modulation of other gene expression by dietary flavone in breast cancer cell lines. *Cancer Detect Prev* 2007;31(2):110-118.

48. Sahai E, Marshall CJ. RHO-GTPases and cancer. *Nat Rev Cancer* 2002;2(2):133-142.

49. Homma Y, Emori Y. A dual functional signal mediator showing RhoGAP and phospholipase C-delta stimulating activities. *EMBO J* 1995;14(2):286-291.

50. Liao YC, Si L, Vere White RW, et al. The phosphotyrosine-independent interaction of DLC-1 and the SH2 domain of cten regulates focal adhesion localization and growth suppression activity of DLC-1. *J Cell Biol* 2007;176(1):43-49.

51. Wong CM, Yam JW, Ching YP, et al. Rho GTPase-activating protein deleted in liver cancer suppresses cell proliferation and invasion in hepatocellular carcinoma. *Cancer Res* 2005;65(19):8861-8868.

52. Yam JW, Ko FC, Chan CY, et al. Interaction of deleted in liver cancer 1 with tensin2 in caveolae and implications in tumor suppression. *Cancer Res* 2006;66(17):8367-8372.

53. Shi H, Guo J, Duff DJ, et al. Discovery of novel epigenetic markers in non-Hodgkin's lymphoma. *Carcinogenesis* 2006.

54. Wang MX, Shi H.D., Zhao XH, et al. Molecular Detection of Residual Leukemic Cells by a Novel DNA Methylation Biomarker (Abstract #1206). *Mod Pathol* 2007;20(Suppl 2):263A.

55. Hansen K, Khanna C. Spontaneous and genetically engineered animal models; use in preclinical cancer drug development. *Eur J Cancer* 2004;40(6):858-880.

56. Priester WA, McKay FW. The occurrence of tumors in domestic animals. *Natl Cancer Inst Monogr* 1980;(54):1-210.

57. Shaffer AL, Rosenwald A, Staudt LM. Lymphoid malignancies: the dark side of B-cell differentiation. *Nat Rev Immunol* 2002;2(12):920-932.

58. Greenlee PG, Filippa DA, Quimby FW, et al. Lymphomas in dogs. A morphologic, immunologic, and clinical study. *Cancer* 1990;66(3):480-490.

59. Fournel-Fleury C, Magnol JP, Bricaire P, et al. Cytohistological and immunological classification of canine malignant lymphomas: comparison with human non-Hodgkin's lymphomas. *J Comp Pathol* 1997;117(1):35-59.

60. Carter RF, Valli VE, Lumsden JH. The cytology, histology and prevalence of cell types in canine lymphoma classified according to the National Cancer Institute Working Formulation. *Can J Vet Res* 1986;50(2):154-164.

61. Milner RJ, Pearson J, Nesbit JW, et al. Immunophenotypic classification of canine malignant lymphoma on formalin-mixed paraffin wax-embedded tissue by means of CD3 and CD79a cell markers. *Onderstepoort J Vet Res* 1996;63(4):309-313.

62. Valli VE, Vernau W, de Lorimier LP, et al. Canine indolent nodular lymphoma. *Vet Pathol* 2006;43(3):241-256.

63. Engels EA. Infectious agents as causes of non-Hodgkin lymphoma. *Cancer Epidemiol Biomarkers Prev* 2007;16(3):401-404.

64. Teske E, van HP, Rutteman GR, et al. Prognostic factors for treatment of malignant lymphoma in dogs. *J Am Vet Med Assoc* 1994;205(12):1722-1728.

65. Burnett RC, Vernau W, Modiano JF, et al. Diagnosis of canine lymphoid neoplasia using clonal rearrangements of antigen receptor genes. *Vet Pathol* 2003;40(1):32-41.

66. Johnston PB, Bondly C, Micallef IN. Ibritumomab tiuxetan for non-Hodgkin's lymphoma. *Expert Rev Anticancer Ther* 2006;6(6):861-869.

67. Taylor KH, Pena-Hernandez KE, Davis JW, et al. Large-scale CpG methylation analysis identifies novel candidate genes and reveals methylation hotspots in acute lymphoblastic leukemia. *Cancer Res* 2007;67(6):2617-2625.

68. Rahmatpanah FB, Carstens S, Guo J, et al. Differential DNA methylation patterns of small B-cell lymphoma subclasses with different clinical behavior. *Leukemia* 2006.

69. Lattimer JC, Corwin LA, Jr., Stapleton J, et al. Clinical and clinicopathologic effects of samarium-153-EDTMP administered intravenously to normal beagle dogs. *J Nucl Med* 1990;31(5):586-593.

70. Lattimer JC, Corwin LA, Jr., Stapleton J, et al. Clinical and clinicopathologic response of canine bone tumor patients to treatment with samarium-153-EDTMP. *J Nucl Med* 1990;31(8):1316-1325.

71. Rao AV, Akabani G, Rizzieri DA. Radioimmunotherapy for Non-Hodgkin's Lymphoma. *Clin Med Res* 2005;3(3):157-165.

72. Cheson BD. The role of radioimmunotherapy with yttrium-90 ibritumomab tiuxetan in the treatment of non-Hodgkin lymphoma. *BioDrugs* 2005;19(5):309-322.

73. Witzig TE, Gordon LI, Cabanillas F, et al. Randomized controlled trial of yttrium-90-labeled ibritumomab tiuxetan radioimmunotherapy versus rituximab immunotherapy for patients with relapsed or refractory low-grade, follicular, or transformed B-cell non-Hodgkin's lymphoma. *J Clin Oncol* 2002;20(10):2453-2463.

74. Pogribny I, Koturbash I, Tryndyak V, et al. Fractionated low-dose radiation exposure leads to accumulation of DNA damage and profound alterations in DNA and histone methylation in the murine thymus. *Mol Cancer Res* 2005;3(10):553-561.

75. Luong QT, O'Kelly J, Braunstein GD, et al. Antitumor activity of suberoylanilide hydroxamic acid against thyroid cancer cell lines in vitro and in vivo. *Clin Cancer Res* 2006;12(18):5570-5577.

76. Dote H, Cerna D, Burgan WE, et al. Enhancement of in vitro and in vivo tumor cell radiosensitivity by the DNA methylation inhibitor zebularine. *Clin Cancer Res* 2005;11(12):4571-4579.

77. Koturbash I, Pogribny I, Kovalchuk O. Stable loss of global DNA methylation in the radiation-target tissue--a possible mechanism contributing to radiation carcinogenesis? *Biochem Biophys Res Commun* 2005;337(2):526-533.

78. Sharkey RM, Goldenberg DM. Targeted therapy of cancer: new prospects for antibodies and immunoconjugates. *CA Cancer J Clin* 2006;56(4):226-243.

79. Oriuchi N, Higuchi T, Hanaoka H, et al. Current status of cancer therapy with radiolabeled monoclonal antibody. *Ann Nucl Med* 2005;19(5):355-365.

80. Wiseman GA, White CA, Stabin M, et al. Phase I/II 90Y-Zevalin (yttrium-90 ibritumomab tiuxetan, IDEC-Y2B8) radioimmunotherapy dosimetry results in relapsed or refractory non-Hodgkin's lymphoma. *Eur J Nucl Med* 2000;27(7):766-777.

81. Coiffier B. First-line treatment of follicular lymphoma in the era of monoclonal antibodies. *Clin Adv Hematol Oncol* 2005;3(6):484-91, 505.

82. Cilley J, Winter JN. Radioimmunotherapy and autologous stem cell transplantation for the treatment of B-cell lymphomas. *Haematologica* 2006;91(1):114-120.

83. Pohlman B, Sweetenham J, Macklis RM. Review of clinical radioimmunotherapy. *Expert Rev Anticancer Ther* 2006;6(3):445-461.

84. de Herder WW, Kwekkeboom DJ, Valkema R, et al. Neuroendocrine tumors and somatostatin: imaging techniques. *J Endocrinol Invest* 2005;28(11 Suppl):132-136.

85. Rambaldi PF, Cuccurullo V, Briganti V, et al. The present and future role of (111)In pentetreotide in the PET era. *Q J Nucl Med Mol Imaging* 2005;49(3):225-235.

86. Weiner RE, Thakur ML. Radiolabeled peptides in oncology: role in diagnosis and treatment. *BioDrugs* 2005;19(3):145-163.

87. Hall EJ. *Radiobiology for the Radiologist.* 5 ed. Philadelphia: Lippincott Williams and Wilkins, 2000.

88. Ferone D, Semino C, Boschetti M, et al. Initial staging of lymphoma with octreotide and other receptor imaging agents. *Semin Nucl Med* 2005;35(3):176-185.

89. Raderer M, Traub T, Formanek M, et al. Somatostatin-receptor scintigraphy for staging and follow-up of patients with extraintestinal marginal zone B-cell lymphoma of the mucosa associated lymphoid tissue (MALT)-type. *Br J Cancer* 2001;85(10):1462-1466.

90. Cholewinski W, Kowalczyk JR, Stefaniak B, et al. Diagnosis and staging of children's lymphoma using the technetium-labelled somatostatin analogue, 99mTc-depreotide. *Eur J Nucl Med Mol Imaging* 2004;31(6):820-824.

91. Virgolini I, Patri P, Novotny C, et al. Comparative somatostatin receptor scintigraphy using in-111-DOTA-lanreotide and in-111-DOTA-Tyr^3-octreotide versus F-18-FDG-PET for evaluation of somatostatin receptor-mediated radionuclide therapy. *Ann Oncol* 2001;12 Suppl 2:S41-S45.

92. Lugtenburg PJ, Lowenberg B, Valkema R, et al. Somatostatin receptor scintigraphy in the initial staging of low-grade non-Hodgkin's lymphomas. *J Nucl Med* 2001;42(2):222-229.

93. Lugtenburg PJ, Krenning EP, Valkema R, et al. Somatostatin receptor scintigraphy useful in stage I-II Hodgkin's disease: more extended disease identified. *Br J Haematol* 2001;112(4):936-944.

94. Jia F, Figueroa SD, Hunter CJ, et al. Molecular Imaging of *bcl-2* Expression in Chronic Lymphocytic Leukemia Using In-111-Labeled PNA-Peptide Conjugates. Anonymous. *J Nucl Med* 2006; 47, 94P.

95. Jia F, Balaji BS, Figueroa SD, et al. Molecular imaging of *bcl-2* expression in small lymphocytic lymphoma using Cu-64-labeled, amino acid-modified PNA-peptide conjugates. Anonymous. *J Nucl Med* 2007; 48, 21P.

96. Robben J, Claude RJ, Pollak Y, et al. Biodistribution of [^{111}In-DTPA-D-Phe^1]-octreotide in dogs: uptake in the stomach and intestines but not in the spleen points towards interspecies differences. *Nucl Med Biol* 2003;30(3):225-232.

97. Altschul M, Simpson KW, Dykes NL, et al. Evaluation of somatostatin analogues for the detection and treatment of gastrinoma in a dog. *J Small Anim Pract* 1997;38(7):286-291.

98. Garden OA, Reubi JC, Dykes NL, et al. Somatostatin receptor imaging in vivo by planar scintigraphy facilitates the diagnosis of canine insulinomas. *J Vet Intern Med* 2005;19(2):168-176.

99. Lester NV, Newell SM, Hill RC, et al. Scintigraphic diagnosis of insulinoma in a dog. *Vet Radiol Ultrasound* 1999;40(2):174-178.

100. Mohsin H, Sivaguru G, Jia F, et al. Comparison of Pretarget and Conventional CC49 Radioimmunotherapy Using ^{149}Pm, ^{166}Ho and ^{177}Lu. *J Labelled Cpd Radiopharm* 2005;48:S21.

101. Esser JP, Krenning EP, Teunissen JJ, et al. Comparison of [^{177}Lu-DOTA0,Tyr^{3}]octreotate and [^{177}Lu-DOTA0,Tyr^{3}]octreotide: which peptide is preferable for PRRT? *Eur J Nucl Med Mol Imaging* 2006;33(11):1346-1351.

102. Kwekkeboom DJ, Bakker WH, Kam BL, et al. Treatment of patients with gastro-entero-pancreatic (GEP) tumours with the novel radiolabelled somatostatin analogue [^{177}Lu-DOTA0,Tyr^{3}]octreotate. *Eur J Nucl Med Mol Imaging* 2003;30(3):417-422.

103. Kwekkeboom DJ, Teunissen JJ, Bakker WH, et al. Radiolabeled somatostatin analog [^{177}Lu-DOTA0,Tyr^{3}]octreotate in patients with endocrine gastroenteropancreatic tumors. *J Clin Oncol* 2005;23(12):2754-2762.

104. van Essen M., Krenning EP, Kooij PP, et al. Effects of therapy with [^{177}Lu-DOTA0, Tyr^{3}]octreotate in patients with paraganglioma, meningioma, small cell lung carcinoma, and melanoma. *J Nucl Med* 2006;47(10):1599-1606.

105. Bakker WH, Breeman WA, Kwekkeboom DJ, et al. Practical aspects of peptide receptor radionuclide therapy with [^{177}Lu][DOTA0, Tyr^{3}]octreotate. *Q J Nucl Med Mol Imaging* 2006;50(4):265-271.

106. Ketring AR, Erhardt GJ, Embree MF, et al. Production and Supply of High Specific Activity Radioisotopes for Radiotherapy Applications. *Alasbimn* 2003; 5, AJ19-2.

107. Li Y, Wheeler DL, Alters W, et al. Early epidermal destruction with subsequent epidermal hyperplasia is a unique feature of the papilloma-independent squamous cell carcinoma phenotype in PKCepsilon overexpressing transgenic mice. *Toxicol Pathol* 2005;33(6):684-694.

108. Nakai S, Sugitani Y, Sato H, et al. Crucial roles of Brn1 in distal tubule formation and function in mouse kidney. *Development* 2003;130(19):4751-4759.

109. Porter FD, Drago J, Xu Y, et al. Lhx2, a LIM homeobox gene, is required for eye, forebrain, and definitive erythrocyte development. *Development* 1997;124(15):2935-2944.

110. McCaw DL, Chan AS, Stegner AL, et al. Proteomics of canine lymphoma identifies potential cancer-specific protein markers. *Clin Cancer Res* 2007;13(8):2496-2503.

111. van Baren MJ, Brent MR. Iterative gene prediction and pseudogene removal improves genome annotation. *Genome Res* 2006;16(5):678-685.

112. Ho SM, Tang WY, Belmonte de FJ, et al. Developmental exposure to estradiol and bisphenol A increases susceptibility to prostate carcinogenesis and epigenetically regulates phosphodiesterase type 4 variant 4. *Cancer Res* 2006;66(11):5624-5632.

113. Welshons WV, Thayer KA, Judy BM, et al. Large effects from small exposures. I. Mechanisms for endocrine-disrupting chemicals with estrogenic activity. *Environ Health Perspect* 2003;111(8):994-1006.

114. Mancini DN, Singh SM, Archer TK, et al. Site-specific DNA methylation in the neurofibromatosis (NF1) promoter interferes with binding of CREB and SP1 transcription factors. *Oncogene* 1999;18(28):4108-4119.

115. Christy B, Nathans D. DNA binding site of the growth factor-inducible protein Zif268. *Proc Natl Acad Sci U S A* 1989;86(22):8737-8741.

116. Christy B, Nathans D. Functional serum response elements upstream of the growth factor-inducible gene zif268. *Mol Cell Biol* 1989;9(11):4889-4895.

117. Brown RH, Gross SS, Brent MR. Begin at the beginning: predicting genes with 5' UTRs. *Genome Res* 2005;15(5):742-747.

118. Kreienkamp HJ, Zitzer H, Richter D. Identification of proteins interacting with the rat somatostatin receptor subtype 2. *J Physiol Paris* 2000;94(3-4):193-198.

119. Stocco DM. StARTing to understand cholesterol transfer. *Nat Struct Biol* 2000;7(6):445-447.

120. Corcoran M, Parker A, Orchard J, et al. ZAP-70 methylation status is associated with ZAP-70 expression status in chronic lymphocytic leukemia. *Haematologica* 2005;90(8):1078-1088.

121. Thomas R, Smith KC, Ostrander EA, et al. Chromosome aberrations in canine multicentric lymphomas detected with comparative genomic hybridisation and a panel of single locus probes. *Br J Cancer* 2003;89(8):1530-1537.

122. Kovalchuk O, Burke P, Besplug J, et al. Methylation changes in muscle and liver tissues of male and female mice exposed to acute and chronic low-dose X-ray-irradiation. *Mutat Res* 2004;548(1-2):75-84.

123. Li LC, Dahiya R. MethPrimer: designing primers for methylation PCRs. *Bioinformatics* 2002;18(11):1427-1431.

124. Prestridge DS. Predicting Pol II promoter sequences using transcription factor binding sites. *J Mol Biol* 1995;249(5):923-932.

125. Zdobnov EM, Apweiler R. InterProScan--an integration platform for the signature-recognition methods in InterPro. *Bioinformatics* 2001;17(9):847-848.

126. Guan M, Zhou X, Soulitzis N, et al. Aberrant methylation and deacetylation of deleted in liver cancer-1 gene in prostate cancer: potential clinical applications. *Clin Cancer Res* 2006;12(5):1412-1419.

127. Butcher DT, Mancini-DiNardo DN, Archer TK, et al. DNA binding sites for putative methylation boundaries in the unmethylated region of the BRCA1 promoter. *Int J Cancer* 2004;111(5):669-678.

128. Devereux TR, Horikawa I, Anna CH, et al. DNA methylation analysis of the promoter region of the human telomerase reverse transcriptase (hTERT) gene. *Cancer Res* 1999;59(24):6087-6090.

129. Dessain SK, Yu H, Reddel RR, et al. Methylation of the human telomerase gene CpG island. *Cancer Res* 2000;60(3):537-541.

130. Nomoto K, Maekawa M, Sugano K, et al. Methylation status and expression of human telomerase reverse transcriptase mRNA in relation to hypermethylation of the p16 gene in colorectal cancers as analyzed by bisulfite PCR-SSCP. *Jpn J Clin Oncol* 2002;32(1):3-8.

131. Zinn RL, Pruitt K, Eguchi S, et al. hTERT is expressed in cancer cell lines despite promoter DNA methylation by preservation of unmethylated DNA and active chromatin around the transcription start site. *Cancer Res* 2007;67(1):194-201.

132. Fraga MF, Agrelo R, Esteller M. Cross-talk between aging and cancer: the epigenetic language. *Ann N Y Acad Sci* 2007;1100:60-74.

133. Culmsee K, Simon D, Mischke R, et al. Possibilities of flow cytometric analysis for immunophenotypic characterization of canine lymphoma. *J Vet Med A Physiol Pathol Clin Med* 2001;48(4):199-206.

134. Toyota M, Issa JP. Epigenetic changes in solid and hematopoietic tumors. *Semin Oncol* 2005;32(5):521-530.

135. Cheng JC, Yoo CB, Weisenberger DJ, et al. Preferential response of cancer cells to zebularine. *Cancer Cell* 2004;6(2):151-158.

136. Cheng JC, Matsen CB, Gonzales FA, et al. Inhibition of DNA methylation and reactivation of silenced genes by zebularine. *J Natl Cancer Inst* 2003;95(5):399-409.

137. Holleran JL, Parise RA, Joseph E, et al. Plasma pharmacokinetics, oral bioavailability, and interspecies scaling of the DNA methyltransferase inhibitor, zebularine. *Clin Cancer Res* 2005;11(10):3862-3868.

138. Williams LE, Johnson JL, Hauck ML, et al. Chemotherapy followed by half-body radiation therapy for canine lymphoma. *J Vet Intern Med* 2004;18(5):703-709.

139. Rodel S, Engert A, Diehl V, et al. Combination chemotherapy with adriamycin, cyclophosphamide, vincristine, methotrexate, etoposide and dexamethasone (ACOMED) followed by involved field radiotherapy induces high remission rates and durable long-term survival in patients with aggressive malignant non-Hodgkin's lymphomas: long-term follow-up of a pilot study. *Leuk Lymphoma* 2005;46(12):1729-1734.

140. Macklis RM, Beresford BA, Humm JL. Radiobiologic studies of low-dose-rate 90Y-lymphoma therapy. *Cancer* 1994;73(3 Suppl):966-973.

141. Valkema R, Pauwels S, Kvols LK, et al. Survival and response after peptide receptor radionuclide therapy with [^{90}Y-DOTA0,Tyr^{3}]octreotide in patients with advanced gastroenteropancreatic neuroendocrine tumors. *Semin Nucl Med* 2006;36(2):147-156.

142. Stacchini A, Aragno M, Vallario A, et al. MEC1 and MEC2: two new cell lines derived from B-chronic lymphocytic leukaemia in prolymphocytoid transformation. *Leuk Res* 1999;23(2):127-136.

143. Balch C, Yan P, Craft T, et al. Antimitogenic and chemosensitizing effects of the methylation inhibitor zebularine in ovarian cancer. *Mol Cancer Ther* 2005;4(10):1505-1514.

144. Egger G, Aparicio AM, Escobar SG, et al. Inhibition of histone deacetylation does not block resilencing of p16 after 5-aza-2'-deoxycytidine treatment. *Cancer Res* 2007;67(1):346-353.

145. Lattuada D, Casnici C, Crotta K, et al. Inhibitory effect of pasireotide and octreotide on lymphocyte activation. *J Neuroimmunol* 2007;182(1-2):153-159.

146. Boultwood J, Wainscoat JS. Gene silencing by DNA methylation in haematological malignancies. *Br J Haematol* 2007.

147. Katzenellenbogen RA, Baylin SB, Herman JG. Hypermethylation of the DAP-kinase CpG island is a common alteration in B-cell malignancies. *Blood* 1999;93(12):4347-4353.

148. LeBlanc AK, LaDue TA, Turrel JM, et al. Unexpected toxicity following use of gemcitabine as a radiosensitizer in head and neck carcinomas: a

veterinary radiation therapy oncology group pilot study. *Vet Radiol Ultrasound* 2004;45(5):466-470.

149. Lewis JS, Laforest R, Lewis MR, et al. Comparative dosimetry of copper-64 and yttrium-90-labeled somatostatin analogs in a tumor-bearing rat model. *Cancer Biother Radiopharm* 2000;15(6):593-604.

150. deJong M., Breeman WA, Valkema R, et al. Combination radionuclide therapy using ^{177}Lu- and ^{90}Y-labeled somatostatin analogs. *J Nucl Med* 2005;46 Suppl 1:13S-17S.

151. Smith CJ, Sieckman GL, Owen NK, et al. Radiochemical investigations of gastrin-releasing peptide receptor-specific [(99m)Tc(X)(CO)3-Dpr-Ser-Ser-Ser-Gln-Trp-Ala-Val-Gly-His-Leu-Met-(NH2)] in PC-3, tumor-bearing, rodent models: syntheses, radiolabeling, and in vitro/in vivo studies where Dpr = 2,3-diaminopropionic acid and X = H2O or P(CH2OH)3. *Cancer Res* 2003;63(14):4082-4088.

152. Miller WH, Hartmann-Siantar C, Fisher D, et al. Evaluation of beta-absorbed fractions in a mouse model for ^{90}Y, ^{188}Re, ^{166}Ho, ^{149}Pm, ^{64}Cu, and ^{177}Lu radionuclides. *Cancer Biother Radiopharm* 2005;20(4):436-449.

153. Kelly WK, Richon VM, O'Connor O, et al. Phase I clinical trial of histone deacetylase inhibitor: suberoylanilide hydroxamic acid administered intravenously. *Clin Cancer Res* 2003;9(10 Pt 1):3578-3588.

154. Li S, Kurtaran A, Li M, et al. ^{111}In-DOTA-dPhe^{1}-Tyr^{3}-octreotide, ^{111}In-DOTA-lanreotide and 67Ga citrate scintigraphy for visualisation of extranodal marginal zone B-cell lymphoma of the MALT type: a comparative study. *Eur J Nucl Med Mol Imaging* 2003;30(8):1087-1095.

155. Mealey KL, Northrup NC, Bentjen SA. Increased toxicity of P-glycoprotein-substrate chemotherapeutic agents in a dog with the MDR1 deletion mutation associated with ivermectin sensitivity. *J Am Vet Med Assoc* 2003;223(10):1453.

156. Mironova N, Shklyaeva O, Andreeva E, et al. Animal model of drug-resistant tumor progression. *Ann N Y Acad Sci* 2006;1091:490-500.

Vita

Jeffrey Bryan was born in 1968 in Vallejo, CA. His elementary education took place in Novato, CA, and he attended high school at St. Ignatius College Preparatory in San Francisco, CA. He began working in veterinary hospitals at the age of 16 in San Francisco. He attended the University of California at Davis for undergraduate studies, during which he married Peggy Herrell in 1988. He attended veterinary school at UC Davis, receiving his Doctorate of Veterinary Medicine in 1993. Jeffrey and Peggy moved to San Francisco where he started work at the Irving Street Veterinary Hospital, and began their family. Jeffrey has five children with Peggy. They are Christina, Claire, Darius, Ruth, and Bobby. Jeffrey completed Master's Degree in Biomedical Sciences at the University of Missouri-Columbia with an emphasis on radiopharmaceutical science in 2004. He completed his residency and board-certification by the American College of Veterinary Internal Medicine at the University of Missouri-Columbia in 2005. In July of 2007, he will begin work at Washington State University as an Assistant Professor of Oncology. He spends as much time on a bicycle as possible.